Flood Control 2015
Delft, The Netherlands
www.floodcontrol2015.com

PILOT PROJECT: RSDYK2008

STRENGTH OF PEAT DYKES EVALUATED BY REMOTE SENSING

GEBIEDSDEKKENDE DIJKSTERKTE BEPALING MET REMOTE SENSING

PROGRAM FLOOD CONTROL 2015

15 DECEMBER 2008

Hack HRGK[1], Van der Meijde M[1], Van der Schrier JS[3], Awaju JH[1], Rupke J[6], Barritt S[1], Van 'T Hof J[4], Maccabiani J[2], Maresch S[1], Calero DP[4], Reymer A[4], Schweckendiek T[2], Stoop J[7], Wilbrinck H[1], Zomer W[5]

[1] International Institute for Geo-Information Science and Earth Observation (ITC), Enschede, The Netherlands
[2] Deltares, Delft, The Netherlands
[3] Royal Haskoning, Nijmegen, The Netherlands
[4] TNO Science & Industry , Delft, The Netherlands
[5] Stichting IJkdijk, Groningen, The Netherlands
[6] Gemeente Reeuwijk, Reeuwijk, The Netherlands
[7] Hoogheemraadschap van Rijnland, Leiden, The Netherlands

SUMMARY

In the context of the FloodControl 2015 project this pilot project RSDYK2008 is done to establish the possible correlations between terrestrial remote sensing techniques, geological information of the surrounding subsurface, geophysical details of a dyke and the quality of peat dykes. The pilot project was done at three sites in Reeuwijk, The Netherlands.

Spatial and temporal variations in the radiation temperatures measured by remote sensing have been established at all sites. These thermal responses of the dykes are mainly related to the seasonal variation and to the distribution in the moisture content of the topsoil. The thermal images acquired during the dry period (August) show a positive relationship with the images of October and a negative relation with the images of December. The multi-temporal near infrared images of the same sites do not show any obvious relationship.

The subsurface geology and stratigraphic profile have been obtained from interpolated pseudo-sections of the 2-D and 3D electrical imaging surveys and from boreholes and Dutch Penetration testing (CPT). The lateral and vertical variations as well as the heterogeneity of the dyke material is very obvious and a clear relation between resistivity imaging and boreholes and CPT testing is established.

Soil moisture is one of the most important parameter affecting surface stability in soil structures. This is because in peat soil, the effective stresses and shear strength are directly related to water content, and even pre-failure deformations are largely controlled by the moisture content. Since the distribution of water content and total unit weight vary in both vertical and horizontal layer in the peat units in the dykes.

The problems as “kwel” and possibly subsidence in the “problem” dyke site Tempeldijk-South are identified by nearly all investigation methods, however, it is often only by knowing from another investigation method that the problem could be pinpointed.

Main conclusions of this pilot project are:

- The comparison of the reference site (Tempeldijk-North) with Tempeldijk-South (a known “problem” location) shows that in all surface and subsurface investigations the Tempeldijk-South surface and subsurface structure are more irregular which are due to or indicate “problems’ such as “kwel” and subsidence.
- The thermal infrared images of Tempeldijk-South showed a layered structure which is reflecting the subsurface structure of the dyke. The layered structure was detectible likely because excess water was present in some of the layers.
- Visual images showed differences in vegetation cover at locations where excess water is likely present.
- The gamma ray survey shows a pattern that is likely related to the real subsurface structure.
- The data from the Algemeen Hoogtebestand Nederland may show patterns indicating deficiencies in a dyke.

Recommendations

Thermal infrared in combination with near infrared imaging and in particular hyper spectral imaging should be able to accurately locate problem areas in dykes. The near-infrared or hyper-spectral imaging will likely be a supporting tool to be used to compensate the thermal infrared interpretation for vegetation, and environment and climate changes. The hyper-spectral method could not be fully evaluated but is possibly a better means for investigation than near-infrared. A combination with Lidar data would probably be adventurous, even the data of the Algemeen Hoogtebestand Nederland may already give sufficient accurate data for dyke investigations. It is recommended that the ideas developed in this pilot project are fully worked out and investigated in detail to develop a

methodology that will be able to detect dyke deficiencies more efficiently, accurately, and cheaper than possible by visual inspection only.

KEY WORDS

Key words: dyke, peat, thermal, infrared, radiation, reflectance, resistivity, Reeuwijk, RSDYK

LIST OF ACRONYMS

ADC	Agricultural digital camera
NAP	National mean sea level reference
NIR	Near infrared
TIR	Thermal infrared
TAW	Technical Advisory Board for Water Barriers

ACKNOWLEDGEMENTS

The project could not have been done without the assistance of the Hoogheemraadschap Rijnland and the City Council of Reeuwijk. The owners of the land at the three test sites are acknowledged for their cooperation.

TABLE OF CONTENTS

1 INTRODUCTION

1.1 Flood Control 2015

Dykes are a flooding protection mechanism in the Netherlands and some other counties. According to Van Baars (2005), the primary (3200km) and secondary (14000km) dykes in the Netherlands protect more than 50% of the country from flooding. To maintain the groundwater level and drain the precipitation of the lower lands, water is pumped from the ditches to the canals and from the canals into the sea. Many of the secondary dykes are so-called “peat dykes”. These dykes consist of peat that has not been excavated while the surrounding peat was excavated. The peat was excavated for fuel starting from the early middle ages.

The peat and clay dykes act as a flooding tempering means in case a large flooding of the Western part of the Netherlands occurs. The flooding is unlikely to be stopped by these dykes but the lowering of the flooding rate may give opportunities to use dykes and the roads that are often on top.

Due to the shear large number of dyke length it is impossible to do a thorough investigation over the full length. Presently the quality of the dykes is established by visual inspection and only at locations where the quality is visually deemed to be low; a further investigation to the quality of the dyke is done. Apart from the fact that a visual inspection is slow and may be biased and subjective, a more important problem is that a dyke may in different seasons behave qualitative differently, even on different days depending on the weather. The visual inspection is generally restricted to a once a year or may be a couple of times more in case the safety of the dyke is not trusted, but certainly not on a basis that can ascertain that a dyke is stable in all environmental conditions.

Remote sensing from the air allows for a far faster means of inspection. However, although it has been thought for a long time that remote sensing may be an attractive option it has never been systematically studied. Therefore this pilot project has been initiated to establish whether remote sensing is a possible option for dyke quality assessment before and during flooding situations.

Within the context of the Flood Control 2015 project (FC2015 project) the secondary peat dykes have a specific function. Secondary dykes may reduce the flooding rate in the Westen part of the Netherlands when the main dykes against the sea and main rivers have failed. Important is then how long these dykes may still be able to function. Obviously in a time of a major flooding in the Western part of the Netherlands no time will be available to start an investigation to the quality of the dykes. The quality of the dykes has therefore to be established beforehand.

1.2 Remote sensing

Any vegetation present around the dykes is likely to be influenced by changes in groundwater table or moisture content of the material and vice versa. The health of the vegetation can be affected as the groundwater table becomes too shallow or too deep. The most likely changes are expected to occur in the chlorophyll concentrations in the vegetation which are an indicator of the health state (Van der Meijde et al., 2004). Adams (Adams et al., 1999) showed that in stressed vegetation the absorption efficiency of the chlorophyll decreases and the IR reflectance decreases due to changes in the cell structure of the plant. This leads to a reduction in reflectance in the IR simultaneous with an increase in reflectance in the red.

The spatial distribution of surface temperature around the dyke can be related to the moisture content of the soil. The temperature variation in the subsurface depends on its thermal diffusivity which itself is also a function of water content. The effective soil water content is maximal at the beginning of the spring and then decreases until the end of summer (Behaegel et al., 2006). Soil

thermal properties are strongly influenced by the soil volumetric water content, volume fraction of solids and volume fraction of air.

Hence, if the stability of peat and to a certain extend also clay dykes depend on the moisture content, and the health of the vegetation on a dyke is dependent on the moisture content, and it is possible to establish the health of the vegetation by remote sensing, it should then be possible to establish a relation between remotely sensed images and the quality of the peat and probably clay dykes. In the context of the FloodControl 2015 project this pilot project is done to establish the possible correlations between terrestrial remote sensing techniques, geological information of the surrounding subsurface, geophysical details of a dyke and the quality of peat dykes. The pilot project was done at three sites in Reeuwijk, The Netherlands.

1.3 Pilot project objectives

The main objective of this pilot project is to indicate possible relationships between terrestrial remote sensing, geological information of the surrounding subsurface, and weak areas in dykes mainly consisting of peat. Geophysics, boreholes and Dutch Cone Penetration (CPT) tests have been done to investigate the subsurface of the dyke.

1.3.1 SPECIFIC OBJECTIVES

The project addresses the following specific objectives:

- Identify the spatial and temporal variations of the thermal radiation of the dyke materials as well as reflectance features of the grass using thermal infrared (TIR) and near infrared (NIR).
- Determine the variation in the composition of a dyke, the soil moisture condition and the material properties using two and three-dimensional (2D and 3D) electrical imaging surveys, boreholes and CPTs.
- Indicate possible relationships between the thermal infrared, near infrared, and visual remote sensing and the subsurface model of the dyke and possible weak areas of the dyke.

1.4 Research methodology

This pilot project comprises pre-field, field data collection and post field data analysis works. A literature review has been made on terrestrial remote sensing techniques (TIR and NIR) and physical parameters of peat dykes such as moisture content, permeability, porosity, bulk density, organic content and consolidation. Information about the geological setting of the study area also gathered from previous works of different researchers who worked in the study area.

During the field data collection, field images of TIR, NIR and visual were acquired using ground based sensors in three dyke sites. This was done in three different season's summer, autumn and winter. In addition, 2-D and 3D electrical imaging surveys were conducted on two dyke sites. In the summer boreholes and Dutch cone penetration tests were done for referencing the geophysical subsurface model.

Figure 1-1 shows a summarized schematic workflow that has been used to achieve the objectives of the project.

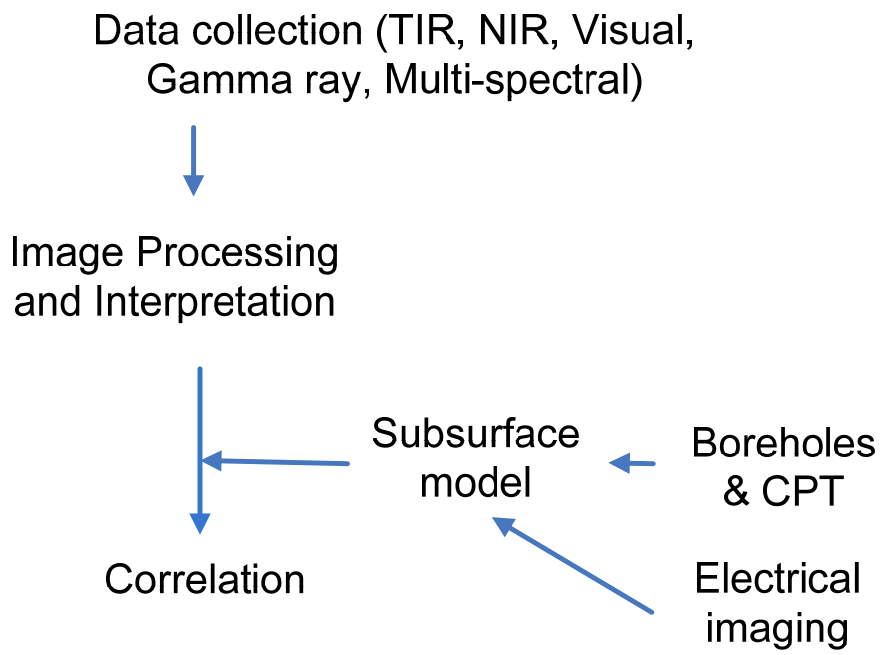

Figure 1-1: Schematic work flow diagram.

1.5 Project partners

The partners in the project and the persons involved in the project are listed in Appendix A.

1.6 Activities

The activities during the project are listed in Appendix B.

2 LIRETURTURE REVIEW

A brief literature review is incorporated in appendix C. The literature review gives an overview of the characteristics of peat and remote sensing characteristics of peat and vegetation as commonly found on dykes. The conclusions of the literature review are many but can be summarized as follows:

- Remote sensing should give good opportunities to evaluate the homogeneity of the surface cover of dykes during various seasons,
- the surface cover is coupled by the presence of water to the deeper materials in the dyke,
- the presence of water is often a good indicator of the possible problems with a dyke, such as excess water ("kwel"), unwanted water flows, or may indicate a situation that the dyke is jeopardized by a shortage of water, e.g. the materials in the dyke are dried out (for example, the "Wilnes" case),
- surface deviations of the dyke are easily detected, and
- remote sensing is a far faster method of investigation of dykes than traditional visual investigations.

3 TEST SITES

3.1 Locations

Reeuwijk is located in a polder area in the province of Zuid Holland, in the central western part of The Netherlands. Maps and aerial photographs of the area and locations of the test sites are included in appendix D. In the area extensive excavation of peat has taken place since the early Middle Ages. Three test sites were selected (Figure 3-1). In this report describing the results of a pilot project, only the test site with problems, “Tempeldijk-South”, is fully evaluated.

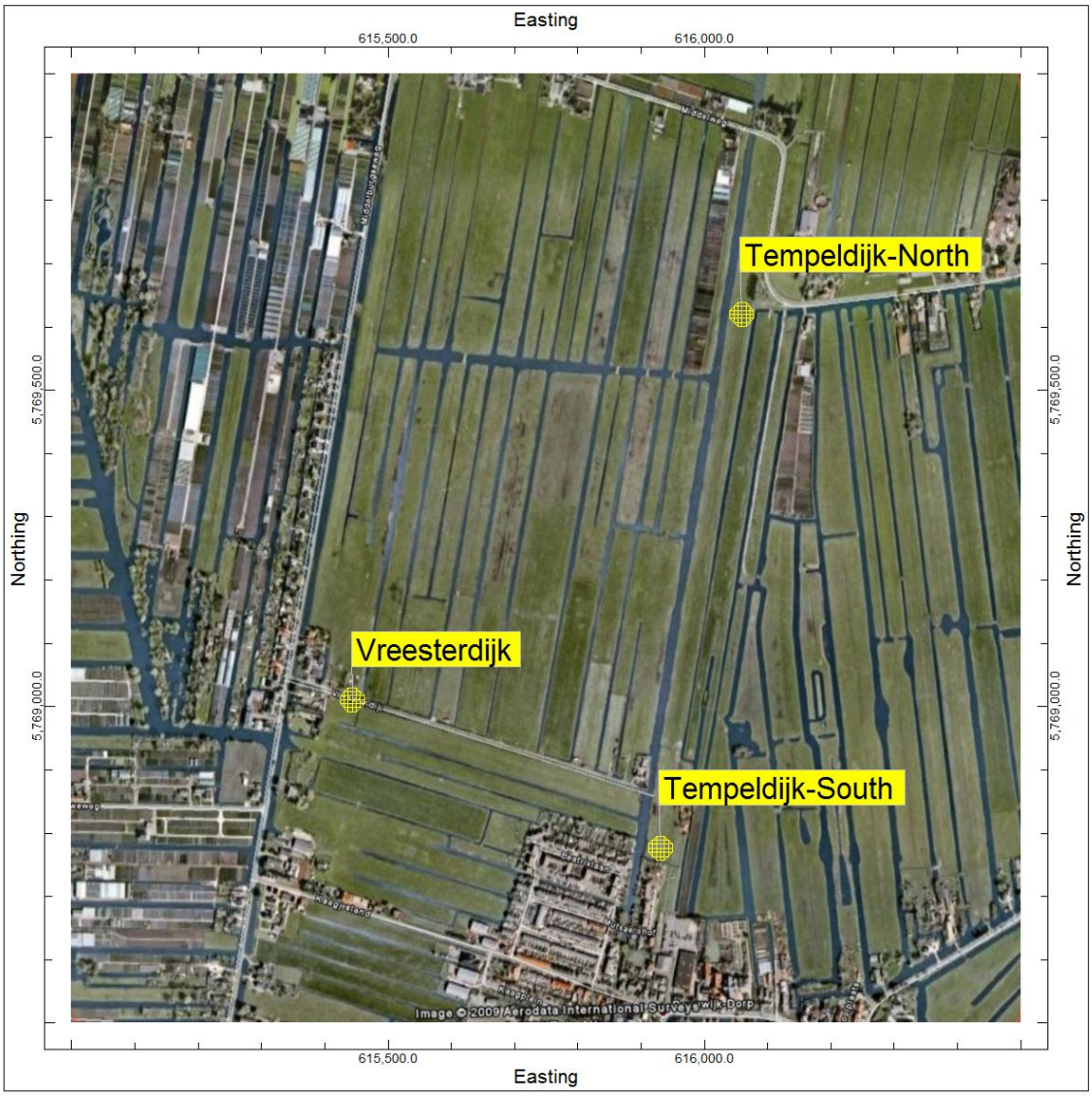

Figure 3-1. Location test sides. The urban area in the bottom middle is Reeuwijk-Dorp. (photo Google Earth, 2008. Grid: UTM (WGS84, zone 31 NH)

3.1.1 VREESTERDIJK

The Vreesterdijk is located in the area where peat has been excavated and consists of a road on an embankment of non-excavated peat. The structure of the dyke is not known in detail, but is assumed to consist of in-situ peat in the lower part. Likely, the dyke has been covered by road pavement

materials many times (probably for hundreds of years) and is covered by a bitumen layer at present. The extent in depth of the layers is unknown. The dyke does not function as boundary for a water canal, but as a local division dyke (dam) in the excavated area, and as an access road to a farm.

3.1.2 TEMPELDIJK

The Tempeldijk is the boundary between a high-laying in-situ peat deposit area where the peat has not been excavated and a low-laying area where the peat layer has been excavated. The dyke functions as a dyke (e.g. dam – "boezem kade") for a de-watering canal. Two test sites were selected; one on both ends, e.g. Tempeldijk-North and Tempeldijk-South (originally these were named Tempeldijk-1 and Tempeldijk-2. As this caused confusion names have changed to the more location specific names of Tempeldijk-North and Tempeldijk-South).

3.1.3 TEMPELDIJK-NORTH

Tempeldijk-North location is chosen as reference. The dyke seems to function without known problems. Also on the surface of the dyke no features have been distinguished that may indicate seepage ('kwel'), subsidence', or otherwise features that could be an indication of "problems".

3.1.4 TEMPELDIJK-SOUTH

Tempeldijk-South location is reported to have problems due to seepage ("kwel") and possibly subsidence. For a more detailed description of Tempeldijk-South is referred to chapter 4.

3.2 Geological environment and topography

Geologically the study area is a deltaic environment. The area is rather flat with an average elevation of –1.6 m NAP (National Mean Sea-Level Reference) with man-made dykes and cannels. Polders resulting from reclamation after peat extraction have elevations around –5.0 m N.A.P.

3.3 Climate

According to Köppen's classification, The Netherlands has a moderate sea climate with rain almost throughout the whole year. In general, the winters are mild having an average mean temperature of 1.7^{o} C. The mean temperature may be below zero in the coldest month. In summer five months have a mean temperature over 10^{o} C with a maximum temperature of 17^{o} C in July. The precipitation is evenly distributed over the year with a yearly average of 760 mm (Ten Cate, 1982). In Spring precipitation is low which causes a deficit in surface water due to evaporation.

3.4 Geological setting

The information about the geological setting of the test sites is summarized from previous works of researchers who worked in the area, from regional studies, and from the general geological history of the Netherlands. A summary is included in appendix E. The geological lithology of the area resulted from sedimentation in the Holocene period. During the Holocene, the area was located in the perimarine zone, where the deposits were formed under the influence of sea level fluctuations and sea level rising from the west interacting with river input from the east. This resulted in extensive areas where for a longer time stagnant water and swamps allowed the development of large and thick peat layers. Occasionally marine or river influence caused the deposition of clay and sand layers and lenses.

4 TEMPELDIJK-SOUTH LOCATION

4.1 Introduction

The test site location Tempeldijk-South measures about 100 by 50 m along the Tempeldijk (Figure 4-1). The test location is the west site of the dyke. The top of the dyke is at about -2 m while the bottom of the dyke is at about -5 m. The area is covered with grass that is regularly cut in summer. The first layer of material to a depth of around 0.3 m is a man-made cover of clay with peat (oral information, Rupke, 2008, and confirmed by boreholes). In the canal and at the foot of the dyke at the western site of the dyke “kwel” occurs. Possible a part of the dyke has (slightly) subsided as indicated by the elevation contour lines between p1 and ph1 (Figure 4-1). The elevations are based on the data of the “Actueel Hoogtebestand Nederland”.

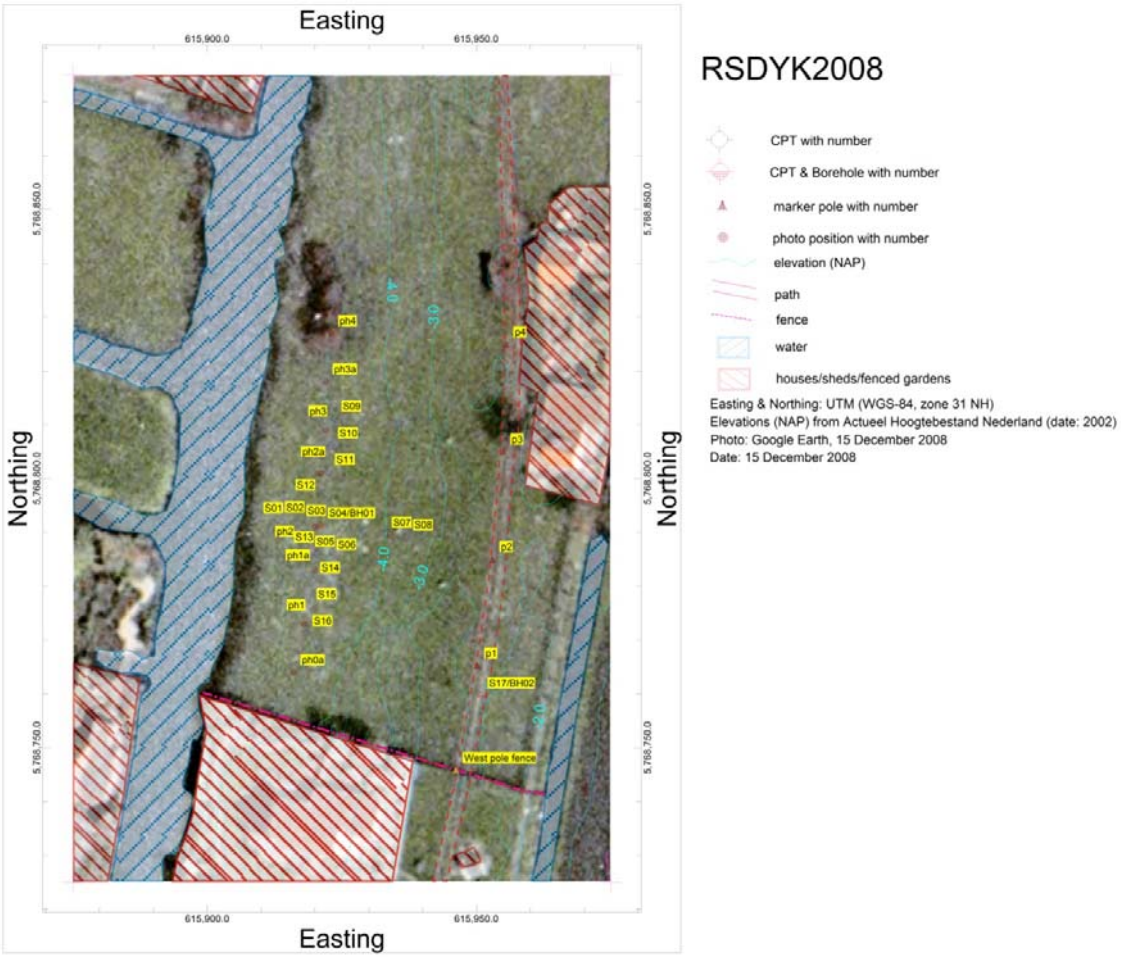

Figure 4-1. Tempeldijk-South test site area Boreholes and CPT

At the location of Tempeldijk-South two boreholes and 17 CPTs (Dutch Cone Penetration tests) with pore water pressure measurement have been made. The locations, and borehole, including photo logs, and CPT logs are included in appendix E. Direct besides a borehole also a CPT test has been made to facilitate interpretation of the CPT. The boreholes are made with a so-called “Delft Continuous Soil Sampler” (a type of triple-tube core sampler). Borehole logs have been made by visual description of the borehole cores.

4.2 Subsurface modeling

4.2.1 INTRODUCTION

The borehole and CPT logs obtained at Tempeldijk-South have been included in a three-dimensional geological model. Sections are included in appendix F. The interpretation has been done starting with the description of the boreholes coupled to the nearby CPT. In-between the CPTs the lithology identification has been done loosely following the standards commonly used in The Netherlands and international standards (Abu-Farsakh et al., 2008, Robertson, 1990) for CPT interpretation. Interpretation of soil lithology based on CPT data only and in particular details in peat and peat containing layers is notoriously difficult. Variations in type of plants remains or the competence of plant remains give changes in CPT values which are difficult to correlate to the visual description of the peat layers. For the purpose of this investigation especially the horizontal and vertical changes in lithology are likely very important. The differentiation of the lithology based on CPT values therefore has been done in as much detail as possible.

4.2.2 GENERALIZED SUBSURFACE CONDITIONS

The subsurface from the surface downwards can be generalized for the Tempeldijk-South location. The lithology names refer to the names used in the sections and 3D model in appendix G. The generalized composition of the dyke is:

- From the top a layer of clayey peat is present with a thickness of about 0.3 m in the East on top of the dyke reducing in thickness towards the west, the bottom of the dyke (PEATS). This layer is likely a man-made top layer.
- A sequence of peat and silty or clayey peat layers with some thin silt and clay layers is present between the man-made top layer and a depth of about – 5 m. In western directions these layers truncate against the man-made top layer (PEAT7, CLAY5, PEAT6, SILT3, and PEAT5).
- A fairly consistent clay clayey peat layer (CLAY4) is present at -5 m.
- Between about -5 and -9.5 to -10.5 a sequence of peat and silty or clayey peat layers with some thin silt and clay layers is present.
- At about -9.5 to -10.5 m an undulating sand layer sequence starts (SAND2).

4.3 Electrical resistivity

4.3.1 INTRODUCTION

The purpose of the electrical imaging survey is to determine the subsurface resistivity distribution of the sites. The resistivity of the subsurface materials is determined largely by the water content and secondary by the resistivity of the subsurface materials and the resistivity of the water. 2D and 3D resistivity surveys have been done. The 2D survey has mainly been used for determining the best array setup (appendices H and J).

4.3.2 2D RESISTIVITY

A 2-D electrical imaging survey is usually carried out using a large number of electrodes connected to a multi-core cable. The typical setup for a 2-D survey with a number of electrodes along a straight line attached to a multi-core cable is illustrated in Figure 4-2. A computer operated “Sting R1/IP” has been used as measuring device. It is a single channel automatic resistivity imaging device with a multi-electrode system. It has a built-in set of command files for different electrode arrays. Typically, 28 electrodes are laid out in two strings of 14 electrodes, with electrodes connected by a multi core cable to a switching box and resistance meter (Figure 4-3). The electrode spacing has been 1 m.

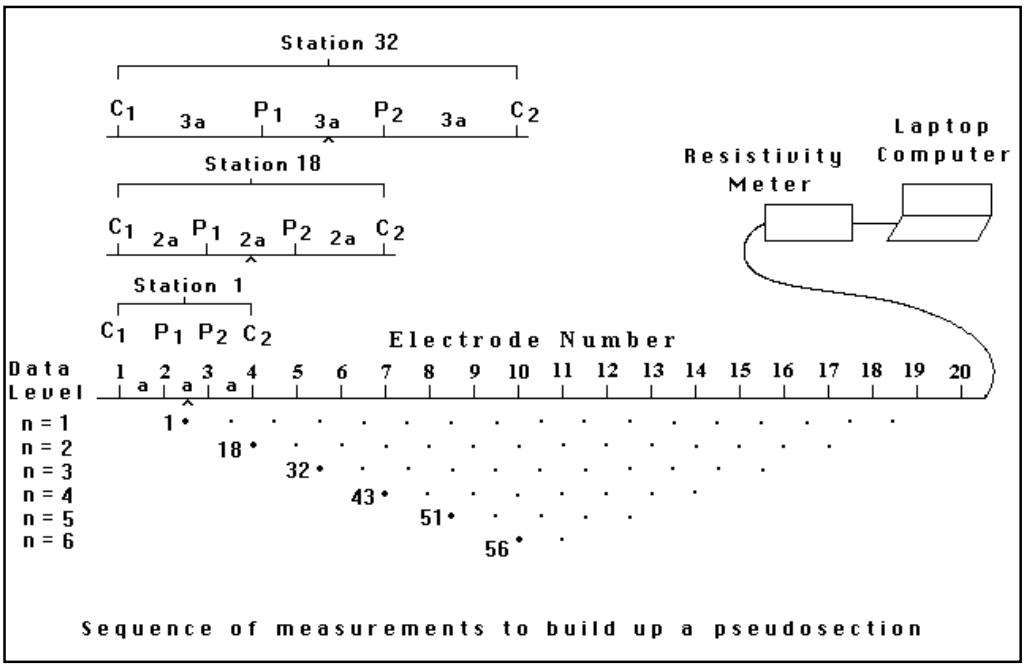

Figure 4-2: The electrode arrangement for a 2-D electrical imaging survey and the sequence of measurements used to build up a pseudo-section (Loke M.H., 2000).

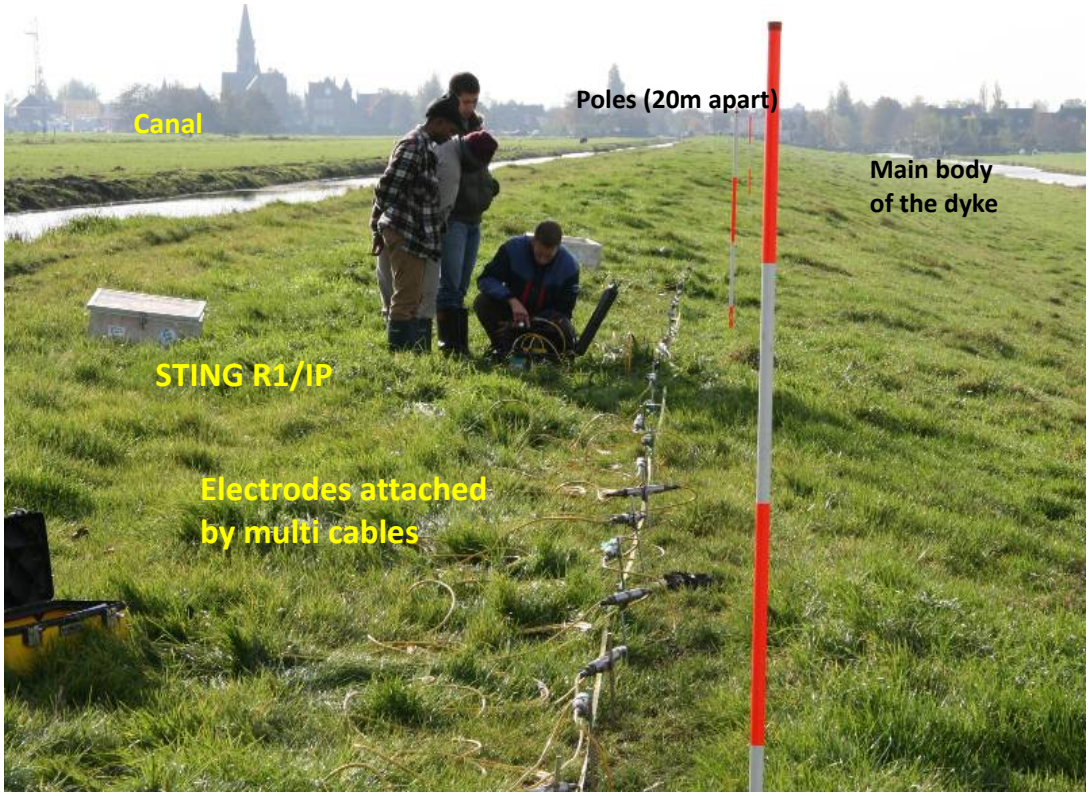

Figure 4-3: A 2-D electrical imaging survey on the Tempeldijk-North. The equipment consists of a Sting R1/IP and 28 electrodes having a 1 m spacing laid out in two strings of 14 electrodes.

4.3.3 ADVANTAGES AND DISADVANTAGES OF THE THREE ARRAYS

In 2-D imaging surveys, the electrode setups “Schlumberger”, “Wenner” and “dipole-dipole” are the electrode arrays that are the most commonly used. The choice of the “best” array for a field survey depends on the type of structure to be mapped, the sensitivity of the resistivity meter and the background noise level. The Wenner array is relatively sensitive to vertical changes (i.e. horizontal structures) in the subsurface resistivity below the centre of the array. However, it is less sensitive to horizontal changes (i.e. narrow vertical structures) in the subsurface resistivity. The dipole-dipole array is most sensitive to resistivity changes between the electrodes in each dipole pair and the sensitivity contour pattern is almost vertical. This array is therefore very sensitive to horizontal changes in resistivity, but relatively insensitive to vertical changes in the resistivity. Unlike the above arrays, the Schlumberger array is moderately sensitive to both horizontal and vertical structures. In areas where both types of geological structures are expected, this array might be a good compromise between the Wenner and the dipole-dipole array.

4.3.4 3D RESISTIVITY SURVEY

A full three-dimensional resistivity survey has been done on the location Tempeldijk-South. The results are included in appendix G.

4.3.5 CORRELATION BETWEEN 3D RESISTIVITY SURVEY AND SUBSURFACE MODEL AT TEMPELDIJK-SOUTH

The resistivity imaging of the subsurface at Tempeldijk-South can fairly accurately be related to the subsurface lithology model. The low resistivity vales correlate to peat layers and in particular to more silty or sandy peat layers. In the top part of the dyke (e.g. above -5 m) the low resistivity values correlate with a silt or silty peat layer (refer to appendix H, figures H-4 and H-5) in which the silt layer is indicated with SILT3.

5 IMAGING

5.1 Visual, Thermal InfraRed (TIR) and Near-InfraRed (NIR)

In appendix I are included the analysis of the remote sensing images.

5.2 Gamma Ray survey

In appendix K the results of the gamma ray survey are included.

5.3 Hyper Spectral Survey

In appendix L are included the analysis of the hyper spectral survey.

6 DISCUSSION, CONCLUSION AND RECOMMENDATION

6.1 Discussion

The soil moisture content is one of the most important parameter affecting surface stability in soil structures and hence in the typical peat dykes found in the western part of the Netherlands. In peat, the effective stresses and shear strength that are determining the stability are directly related to the water content. Since the distribution of water content and also the properties of the materials in dykes vary both vertically and horizontally, the stability of the peat dykes is also highly variable vertically and horizontally. This highly variable nature and the enormous length of so-called peat dykes make that assessment of the stability on a regular basis is a costly affair. Therefore, any means that would be able to assess the stability or even to indicate only changes in the stability that are cheaper than the presently used visual inspections are worthwhile to be investigated on their merits. Remote sensing is thought to be a possible assessment method, and therefore is in this research is investigated how far remote sensing techniques could determine variations in water and soil properties of the dykes.

6.1.1 VISUAL

The visual images show obviously mainly that surface and thus the surface vegetation cover of the dyke. The vegetation cover, however, may show also differences in vegetation cover, such as the presence of small yellow flowers in part of the foot of the dyke (Tempeldijk-South, appendix I, Figure 6). It is remarkable that this location more or less coincides with the location where possible excess water flows out of the dyke. It is not unlikely that locations that are wetter also have a vegetation cover that is different from those covering more dry areas.

6.1.2 ELEVATION DATA

Although not intended to be investigated in this pilot study, the data from the Algemeen Hoogtebestand Nederland may show deficiencies in a dyke. The data determined by Lidar surveys is accurate enough to determine surface patterns with high detail. The Tempeldijk-South location shows a pattern that may indicate a deficiency (subsidence) at a location where also the layers in the subsurface (determined from the three-dimensional resistivity survey and 3D subsurface model) show variations in elevation. Visually any deficiency in the surface of the dyke has not been noted.

6.1.3 THERMAL INFRARED (TIR)

The geotechnical properties of peat differ from those of clay in many aspects. Compared to clay, peat has a much higher porosity and ability to hold water under natural (unloaded) conditions. This was clearly indicated from their ability to absorb and emit electromagnetic energy. Apart from the emissivity property of the material composition, the emissivity of an object is highly depending on the moisture content. Water has very dark to medium gray tones in day TIR images and moderately light tones in night TIR images, compared with the soil. This simply means that water is cooler in the day and warmer in the night than most other materials present. This response is due in part to a rather high thermal inertia, relative to typical land surfaces, as controlled largely by water's high specific heat. After prolonged period of rainfall, in this research thus mainly in the autumn and winter, when the topsoil water content is high, the heat capacity of the topsoil is also high and as a result, more energy is needed to increase its temperature. In consequence, the surface temperature response to solar radiation and air temperature is slower and weaker. However, after a long period without rain the water content of the soil is less, and surface temperatures responds quicker to solar radiation and air temperatures. This feature is shown by the multi-temporal TIR images of Tempeldijk-South. During the summer following the reduction of the moisture content due to

evaporation and evapo-transpiration from the topsoil, the peat layer becomes dry and has higher temperatures where as during the winter it becomes wet and has low temperatures.

Since the dykes are covered with grass, the radiation temperature values are the resultant of the emitted temperatures from the topsoil of the dyke material and the grass. It is difficult to establish how much of this resulted from the grass compared to that from the topsoil. The variation in the radiation temperature of the grass is mainly related to the accumulation of the rainfall water. Fallen debris from the grass (dead leafs), the water content in the soil, the apparent roughness, and the position with respect to the sun also influence the radiation. The radiation temperature variation of the dyke materials is mainly related to the seasonal variability of water content in the soil water content and therefore can probably be related to the geotechnical properties of the dyke materials.

6.1.4 RESISTIVITY SURVEYS

The results of the 2-D electrical imaging surveys identify the stratigraphic profile of the two sites on the Tempeldijk. The interpolated pseudo-sections reveal the geological formation of the dyke. The boundary between the clay layer and the peat layer was clearly determined. Also lateral variations were established that may indicate heterogeneity of these layers, however, also variation in water content may be present. In the lower parts also more salt containing water from the sub-surface seepage from deeper layers may be present which is shown by low resistivity values.

6.2 Conclusions Pilot study

Main conclusions of this pilot study are:

- The comparison of the reference site (Tempeldijk-North) with Tempeldijk-South (a known “problem” location) shows that in all surface and subsurface investigations the Tempeldijk-South surface and subsurface structure are more irregular which are due to or indicate “problems’ such as “kwel” and subsidence.
- Visual images showed differences in vegetation cover at locations where excess water is likely present.
- The gamma ray survey shows a pattern that is likely related to the real subsurface structure, but further investigations are required to determine the exact nature of this relation.
- The 3D subsurface model and 3D resistivity model correlate.
- The data from the Algemeen Hoogtebestand Nederland may show patterns indicating deficiencies in a dyke. The data determined by Lidar surveys is accurate enough to determine surface patterns with high detail.

A quantitative analysis was used to evaluate the relationship between the TIR and the NIR images. Scatter plots were made between the radiation temperature and reflectance DN-values. Most of the plots illustrate a very weak relationship. Some of the influencing factors are:

6.3 Recommendations

- Thermal emissivity is highly dependent on the moisture content of a soil and thus the emissivity of this moisture content can vary with diurnal period. Therefore, it is important to acquire thermal images in different hours of the day in order to see the variation in the emissivity of the dyke materials and to indicate the distribution of moisture content of the topsoil.
- Two objects might have the same T_{kin} (kinetic temperature) but have different T_{rad} (radiation temperature) because of differences in their emissivity and their emissivity can be influenced by external factors such as moisture content, color, and surface roughness. In situ measurement of the surface temperature of the dyke materials using digital thermometers is very important to understand the degree of the influence from these factors and to calibrate the results of the thermal images.

- Local meteorological variables have to be measured simultaneously with the TIR imaging in order to characterize the conditions of the sensor-ground surface continuum. These included air temperature and the global radiation reaching the surface.
- The remotely sensed imaging should have to be acquired perpendicular to the study interest, by increasing the platform above the ground. This will help to minimize the scattering effect in the reflection for the near infrared imaging.
- Vegetation stress can possibly be detected better using hyper spectral remote sensing. Using spectroscopy it will be easier to differentiate the stressed grass from the healthy grass based on their variation in the reflectance spectral signature. Therefore, it might be better to use hyper spectral spectroscopy in the future study.

APPENDIX A

RSDYK2008 - PARTIES AND PERSONS INVOLVED IN THE PROJECT

The project was executed by the following parties:

- International Institute for Geo-Information Science and Earth Observation (ITC) (project leader)
- Deltares
- Haskoning
- TNO Science & Industry
- Stichting IJkdijk
- Gemeente Reeuwijk
- Hoogheemraadschap van Rijnland

The persons involved in the project are:

- Yonnas Haddish Awaju, MSc (ITC)
- Dr. Sally Barritt (ITC)
- Dr. Robert Hack (ITC) (project leader)
- Jaap van 't Hof (Monitoring Systems TNO Science & Industry)
- Ir. Jos Maccabiani (Deltares)
- Sabine Maresch, MSc. (ITC)
- Dr. Mark van der Meijde (ITC)
- Daniel Perez Calero (Monitoring Systems TNO Science & Industry)
- Dr. Arthur Reymer (Monitoring Systems TNO Science & Industry)
- Dr. Jan Rupke (Gemeente Reeuwijk)
- Ir. Joost van der Schrier (Haskoning)
- Timo Schweckendiek (Deltares)
- Jaap Stoop (Hoogheemraadschap van Rijnland)
- Henk Wilbrinck (ITC)
- Wouter Zomer, Ing (Stichting IJkdijk
-

APPENDIX B

RSDYK2008 – ACTIVITIES

Table 1 shows an overview of the activities in this project.

Table 1. Overview activities.

15 Aug 2007	fieldwork Reeuwijk - visual, TIR and NIR images
15 Aug 2007	fieldwork Reeuwijk – 2D resistivity survey
31 Oct 2007	fieldwork Reeuwijk - visual, TIR and NIR images
13 Dec 2007	fieldwork Reeuwijk - visual, TIR and NIR images
13 Dec 2007	meeting City Council Reeuwijk
19 Dec 2007	meeting on location, Reeuwijk
9 Jan 2008	meeting Delft
15 Jan 2008	meeting Delft
7 Feb 2008	workshop FC2015
20 Feb 2008	meeting Delft
6 Mar 2008	conference “Waterkeringen”, Amersfoort
7 Mar 2008	meeting Delft
13 Mar 2008	meeting Delft
19 Mar 2008	meeting Reeuwijk
2-4 Jun 2008	fieldwork Reeuwijk – visual, TIR and NIR images
2-4 Jun 2008	fieldwork Reeuwijk – 3D resistivity survey
4 Jun 2008	fieldwork Reeuwijk - gamma ray survey
4 Jun 2008	fieldwork Reeuwijk - hyper spectral survey
5 Jun 2008	meeting HH Rijnland, Leiden
30-31 Jul 2008	fieldwork Reeuwijk – visual, TIR and NIR images
25 Aug 2008	fieldwork Reeuwijk – boreholes and CPT

APPENDIX C

RSDYK2008 - LITERATURE REVIEW

Contents

1 GENERAL CHARACTERISTICS OF PEAT

1.1 Introduction

Continues detection and monitoring of peat dykes is very important to secure their stability and protect the major impact on the environment and casualties (McCahon et al., 1987). Previous studies show that, there is still lack in detailed understanding of peat mass movements (Carling, 1986a; Dykes and Kirk, 2001). However, the hydrological and geotechnical conditions are the main issues of peat dykes. These conditions are usually affected by seasonal variations, which can be considered as a main cause of failure in many engineering structures (Tallis et al., 1997; Evans et al., 1999).

1.2 Peat as dyke foundation

Ward has been described the risk of a peat layer under a dyke (Ward 1948 and Ward 1955). He indicated that dykes founded on very weak peat might collapse within a short period after construction. Instability can occur in peat dykes even if they are on the top of an impervious material like clay (Carling, 1986a). This is because peat dykes can have less weight than the resultant water force especially when the crest of the dyke dries out (Van Baars, 2005). This resultant force can be affected by a rise of water level in the canals, ditch or streams.

1.3 Differential settlement

In countries with large peat deposits at surface such as Canada and Ireland, where peat covers as much as 16-18% of the area, construction activities face a serious problem to engineers with respect to the differential settlement and deformation. This is also a well-known problem in the test site area, Reeuwijk, The Netherlands.

1.4 Water content and homogeneity

The distribution of water content and total unit weight vary in both vertical and horizontal directions in peat layers. Saiyid (Saiyid Hassan, 1994); Dalton (1954) and Radforth (1964) postulated that, the retention of water in peat may be recognized as free water in large cavities, capillary water in narrower cavities and water bound (physically, chemically…). This indicated that any variability in the water content would affect the stability of peat structures.

In peat, the effective stresses and shear strength that are determining the stability are directly related to the water content. The water content of the topsoil varies with respect to the seasonal variations. Following the reduction of the water content of the topsoil during the dry conditions in the summer can result in drying and shrinkage of the peat layer. This will cause new cracking, reactivation of old cracks, and opening of peat fuel cuttings (Long, 2006). During the intense rainfall, water can rapidly percolate to the base of the peat through the new and old cracks. Therefore, any increase in stability due to lowering of the water content is likely to have been offset by the reduction in unit weight of the peat by drying. Pore pressures in the peat would have increased significantly, reducing the effective stresses and the resistance to sliding. It is also possible to speculate that repeated drying and wetting cycles caused shrinkage and swelling movements in the peat (Warburton et al., 2004). The soil moisture content is also a key parameter in computing the surface energy balance and important in many applications including hydrology, agriculture and meteorology (Petrone et al., 2004). Other factors like specific gravity, organic content, heterogeneity in soil texture, vegetation, land use, topography and surface temperature also affect the stability of peat dykes (Tansey, 1999; Li and Islam, 1999).

2 REMOTE SENSING

Remote sensing in all ranges of the electro-magnetic spectrum has many applications in geotechnical investigations (Figure 1). It is also used for mapping the top soil moisture over a varying landscape (Famiglietti et al., 1999; Li and Islam, 1999) and in identifying engineering structures. Rijswaterstaat, The Netherlands, has made an inventory of the possibilities of remote sensing applications for the purpose of dyke quality assessment (Swart, 2007). In this publication the possible options for using remote sensing are described based on a literature review.

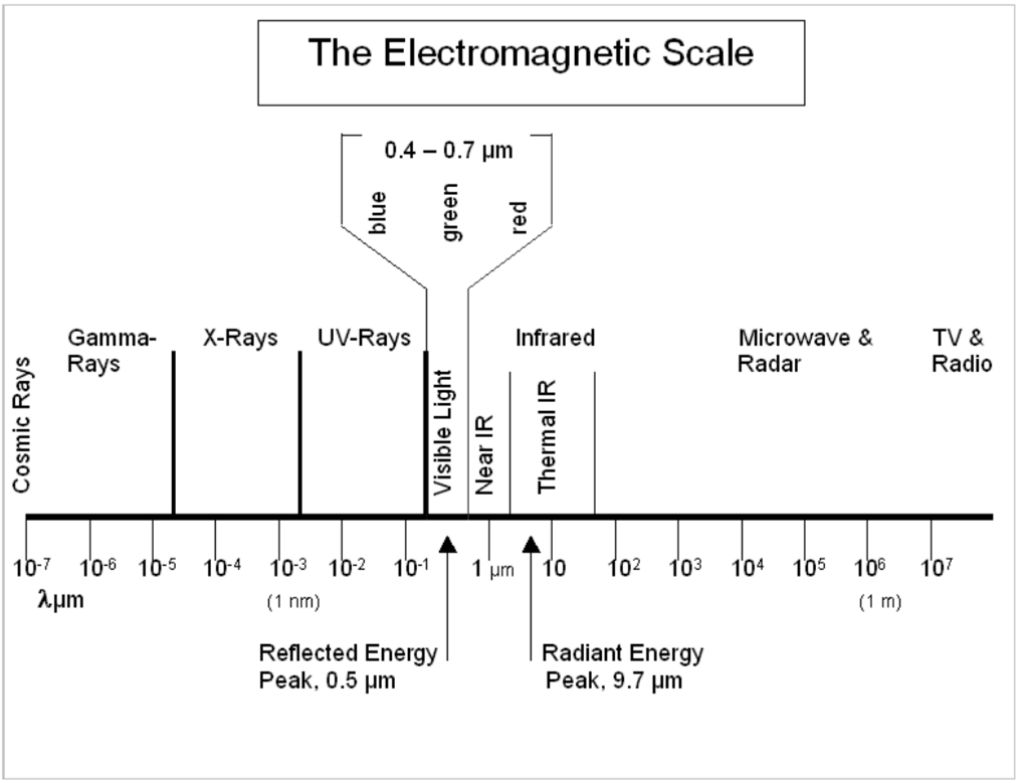

Figure 1. The electro-magnetic spectrum.

2.1 Thermal infrared

Thermal remote sensing is widely used for many applications including coal fire detection (Yang. 1995), dam leakage monitoring etc. Thermal remote sensing is based on the infrared range of the electro-magnetic spectrum. According to Planck's Radiation law, all objects above 0°K emit thermal electromagnetic energy in the 3.0 –14 µm wavelength region. The emissive power of a black body at any wavelength and temperature, as well as the amount of emitted energy per wavelength depends on the object's temperature. Different materials can have widely different values within the range of 0 to 1. The range of emissivity for ground components in situ of soil, vegetation and rocks, varies at a given wavelength according to their physical properties and water content (Fuchs and Tanner, 1966, Van de Griend et al., 1991, Blumberg, D.G et.al., 2000 and 2001).

Planck's law gives the spectral radiance of electromagnetic radiation at all wavelengths from a black body at temperature T as a function of wavelength λ:

$$M_{\lambda,T} \equiv C_1 \frac{C_1}{\lambda^5 \left(e^{\frac{C_2}{\lambda T}} - 1 \right)} \quad [1]$$

In which $M_{\lambda,T}$ is the spectral radiance in (Wm^3), λ is the wavelength in (m), T is the temperature of the blackbody in (K), C_1 is the first radiation constant, 3.74151. 10-16 (Wm^2) and C_2 is the second radiation constant, 0.01438377 (mK).

The emissivity power increases with temperature at each wavelength and the position of the maximum emissive power shifts towards the shorter wavelengths. Relatively more energy is emitted at shorter wavelength (Figure 2).

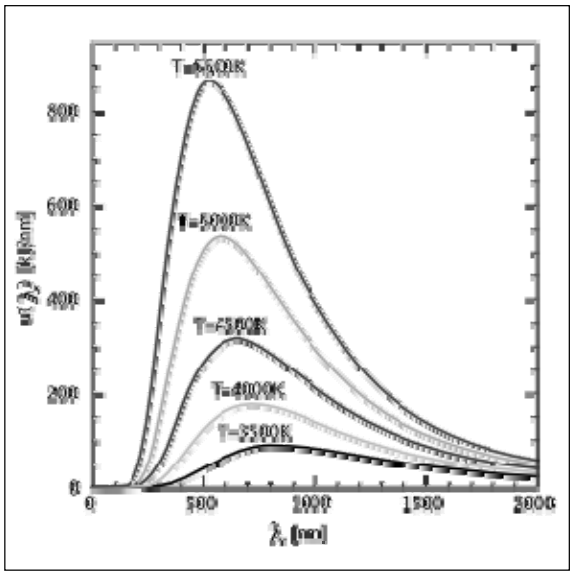

Figure 2. The blackbody curve at 3500, 4000, 4500, 5000 and 5500k

Many researchers (Idso et al., 1975; Reginato et al., 1976; Price, 1980) assessed and mapped soil moisture by thermal infrared using radar microwave technology, satellite images and/or airborne sensors for studying bio-physical processes on a micro-scale. Jackson (2002) showed the difficulties for retrieval of soil moisture due to the influence of surface variables like vegetation cover. Recent studies use terrestrial thermal remote sensing for detection purposes. Thermo tracer (TH9100) is one of the high sensitive radiometric cameras that measures the infrared radiation emitted from objects. Preliminary analyses using this thermal camera show a significant relationship between infrared-based temperature and surface soil moisture. At a small scale, the thermal infrared images by a thermo tracer is shown to be useful to map areas characterized by different soil moisture content (P.Mora, et al., 2007).

2.2 Reflectance features of vegetation

Changes in vegetation can affect the surrounding engineering structures and local groundwater level (Fredlund, 2001). A difference in the reflectance of grass, which covers a peat dyke, might relate to the soil moisture variation of the material. Remote sensing allows the detection of hazardous gas leakage of pipelines from the reflectance spectral signature of stressed vegetation (Van der Werff et al., 2007). The health of plants is reflected in its chlorophyll content (Van der Meijde et al., 2004). Adams demonstrated that healthy vegetation shows high reflectance in the green and NIR region (Figure 3). However, the chlorophyll of stressed or dry vegetation decreases its absorption efficiency and increase in reflectance in the red (Gausman 1974, Tucker 1979,

Adams M.L. et al., 1999). Environmental factors such as soil, geomorphology and vegetation apparent roughness influence the reflectance values. Variations in climatic factors, in particular precipitation and temperature, have therefore a strong influence on variation in the reflectance.

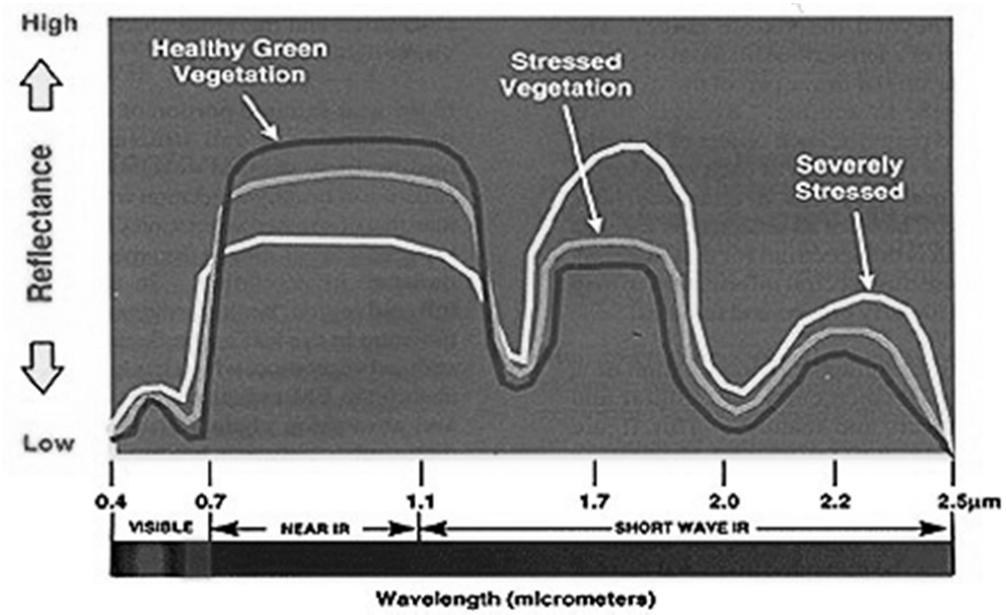

Figure 3. This general diagram shows the stress indicated by a progressive decrease in Near-IR reflectance accompanied by a reversal in Short-Wave IR reflectance

3 REFERENCES

For the references is referred to appendix N.

APPENDIX D

RSDYK2008 - LOCATION TEST SITES

Maps and aerial and satellite photos of the test site area and the locations of the test sites.

Figure 1. Location Reeuwijk (map: Routenet-Routeplan, http://www.routenet.nl ; 16 Feb 2009).

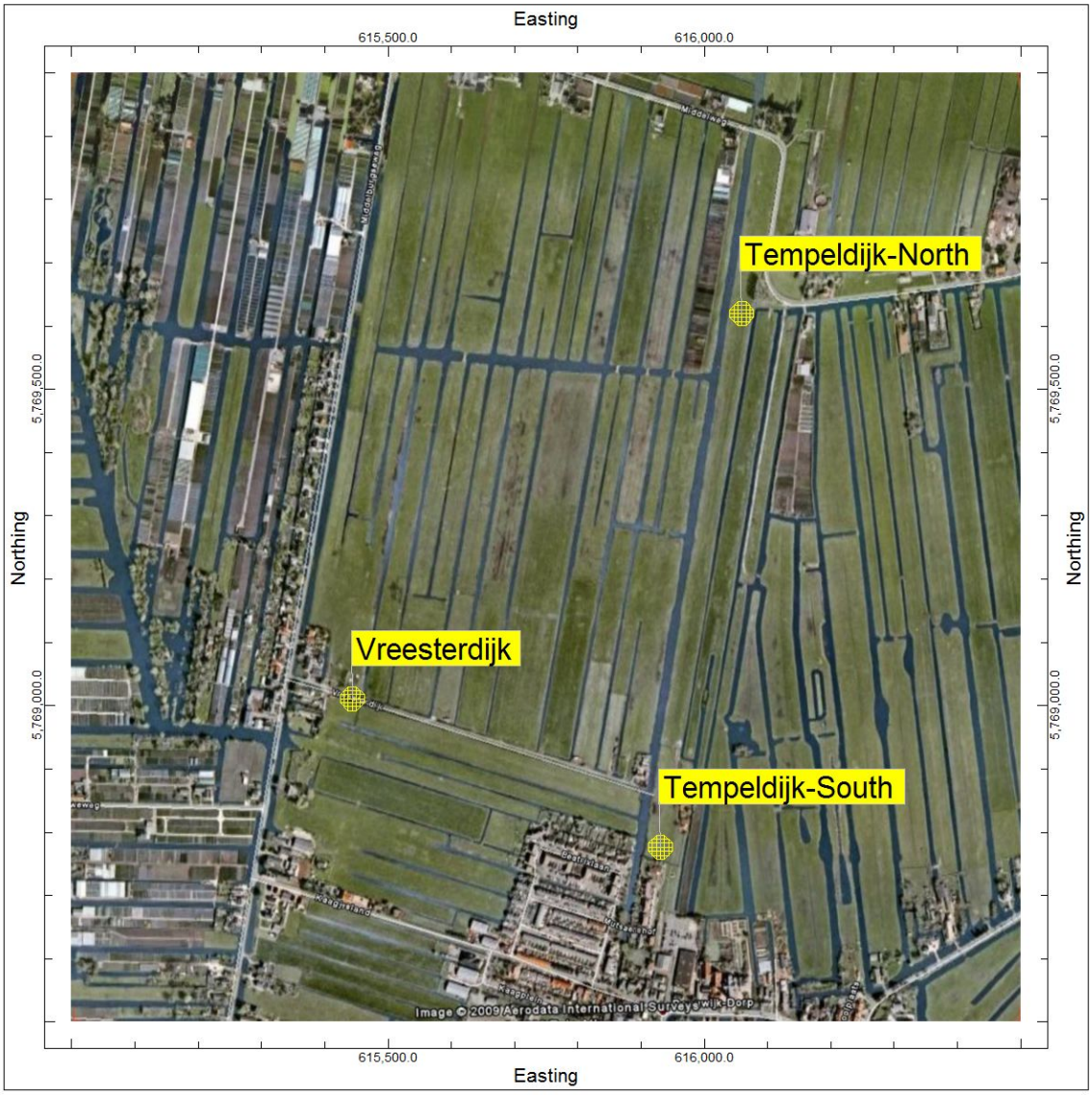

Figure2. Test sites in Reeuwijk (photo Google Earth, 17 Feb 2009). (Reeuwijk-Dorp is just south of Tempeldijk-South test location)

APPENDIX E

RSDYK2008 – GEOLOGY

1 GEOLOGICAL SETTING

The information about the geological setting of the test sites is summarized from previous works of researchers who worked in the area, from regional studies, and from the general geological history of the Netherlands.

1.1 Regional Geologic history

According to Van Staalduinen, at the end of the early Tertiary, the North Sea Basin developed in northwestern Europe and the later territory of the Netherlands was located at the southern tip of the basin. During the Tertiary and the Quaternary, the basin subsided gradually due to the continuous filling up with sediments (Van Staalduinen et al., 1979; Ten Cate, 1982).

According to Ten Cate (1982), the configuration of the coastline of the Netherlands was determined by the tectonically active area of the Central Graben and Lower Rhine embayment in the southeast in the latest part of the Tertiary. The river Rhine had its course towards the northwest and built a delta in the Central Graben area. In the northeast, delta where built on by North German on ancient Baltic rivers. This indicates that the large part of the deposits has been laid down in a coastal area at the end of the Tertiary. These deposits are referred deposition either in a shallow sea not deeper than ten meters, or in coastal swamps, lagoons and lower river courses. However, at present they are found at considerable depth below sea level, sometimes as low as 400 to 600m. Variations in intensity of tectonic movement, changes in river courses and climatic changes with glacial and interglacial periods have determined the geological genesis of the subsiding basin in the Netherlands during the Quaternary (Ten Cate, 1982).

During the Saalian glaciation (Figure 3.2) the inland ice covered Northern Europe again, as in several glacial periods before Quaternary, but this time it included the northern half of the Netherlands. This event had a profound influence on both the sedimentation pattern and the morphology of the landscape. The rivers Rhine and Meuse were forced into westerly courses. The ice sheet that pushed by pre-glacial and river sediments formed the hills in the central and eastern part of the country.

The Saalian glaciation was followed by the melting of the inland ice during the Eemian interglacial and at the end of the Weichselian (remained in the Per-glacial zone without inland ice) resulted in a rise of sea level and the sea penetrating far more to the east. According to Ten Cate, during the sea level rising at the end of the Weichselian, there were three zones of sedimentation: a littoral sandy zone of coastal barriers and dunes, a clayey zone of tidal flats, salt marshes and brackish lagoons and, at a greater distance from the sea, a zone of peat formation in a fresh water environment. These zones were shifted towards the east as the sea gradually flooded the former dry North Sea floor.

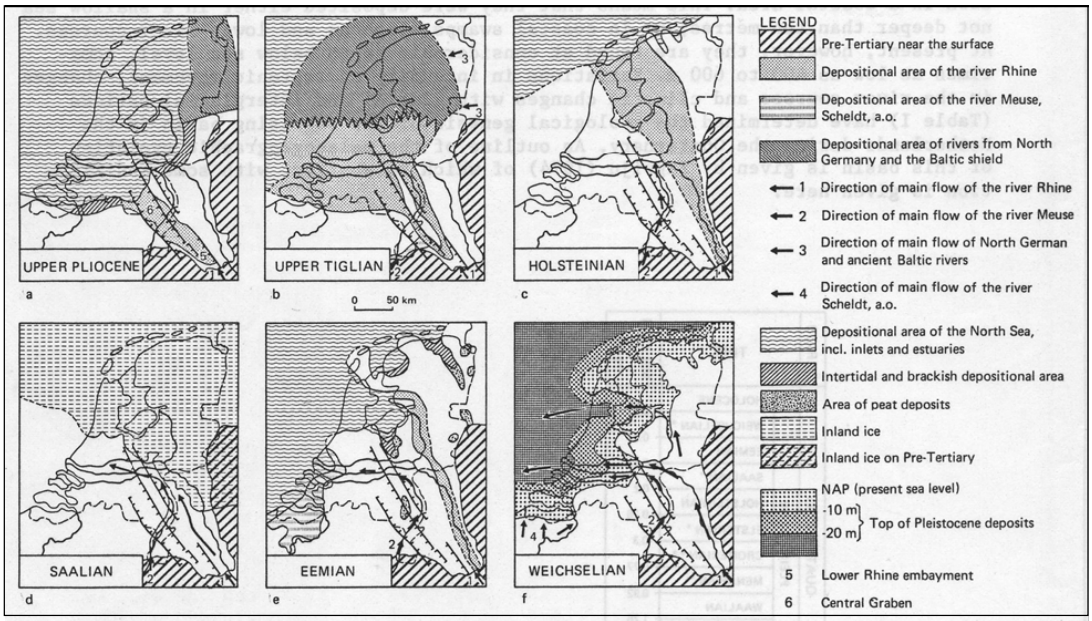

Figure 1. Palaeogeographic map of the Netherlands during the Upper Tertiary and the Quaternary (Ten Cate, 1982)

1.2 Holocene geology of the study area

The regional geological setting of the study area was formed largely in the quaternary by the direct and indirect activities of the river and the sea (Ten Cate, 1982). The Dutch coastal area was drowning due to the melting of the Weichselian glacial ice sheet. The melting of this glacial ice in combination with the tectonic movements resulted in sea level rising. The western Netherlands was gently westward slopping plain at the end of the Pleistocene. This indicates that the geology of the western Netherlands is greatly influenced by the Holocene deposits (Figure 3.3).

At the start of the Holocene, climate change causes a very rapidly sea level rise accompanied by a rise of regional groundwater table. As the result of the rise of the water table, peat growth took place in various places (Ten Cate, 1982). Sedimentation in the Holocene period started with the formation of peat (basal peat). The battle between the land and the water increased as the sea level continued to rise rapidly. As the result, the coastline moved further inward and reached the Dutch territory in about 8000 BP (Bijlsm, 1982). The Palaeo-geographical map above shows that the marine sediments deposited in the coastal area while the fluvial sediments was deposited in the perimarine area (Figure 3.3a). According to Bijlsma, the rate of sea level rise reduced to 27cm/100years during 5000BP (Bijlsma, 1982) and the extension of marine deposit reduced significantly (Figure 3.3b). The sea level rise rate was extremely slow in about 3700BP and more stable river pattern was formed; however, the groundwater level was still high to develop a thick peat layer over the marine and fluvial deposits (Figure 3.3c). This peat forming process continued until 700BP in the central part of the Netherlands (Figure 3.3d). When the peat layer was inundated and/or eroded by the water, the marine or fluvial sediments deposited over it (Figure 3.3e).

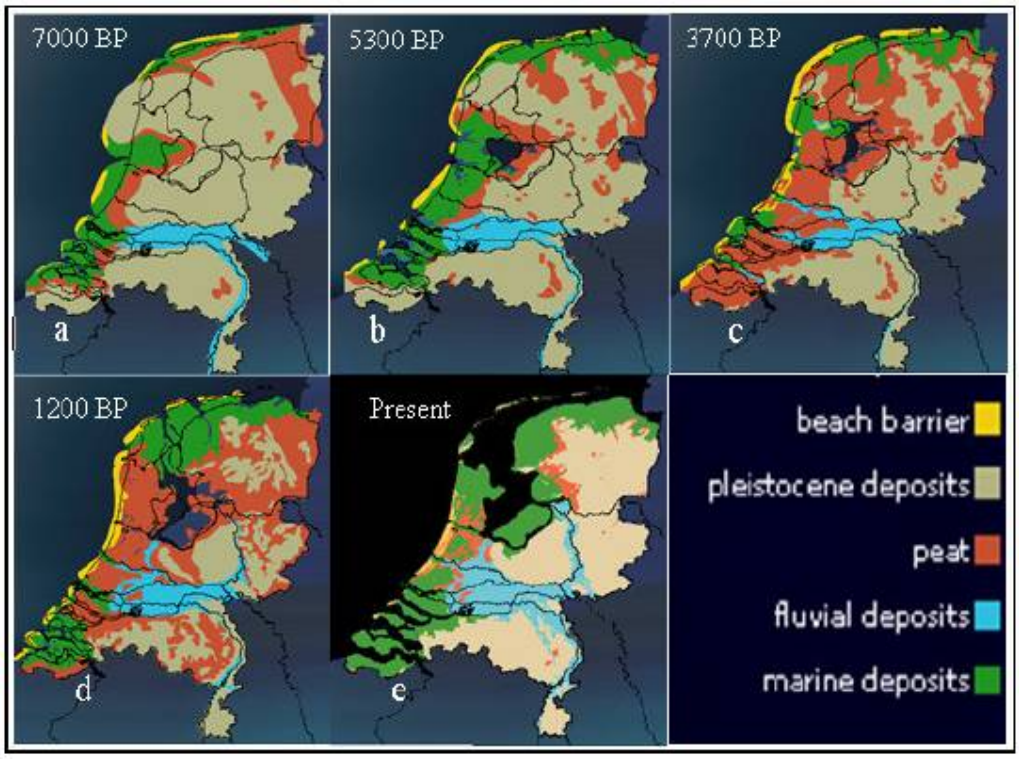

Figure 2. Palaeogeographic map of the Netherlands during the Holocene period (source: took from Mahabubur 2007)

During this Holocene period, the area was located in the perimarine zone, where the deposits were formed under the influence of the sea level rising interacting with river input from the east. Specifically the study area is located on the Holocene deposits of The Netherlands, which are dominated by the thick layers of peat and clay. According to Bosch and Kok, these deposits have two main origins; namely marine and fluvial deposits. In the Netherlands, the Holocene fluvial deposits are named as Gorkum and Tiel depending on their correlation to Calais and Dunkirk marine deposits (Bosch and Kok, 1994).

The marine (Calais and Dunkirk) deposits were formed in a tidal flat depositional environment, normally a plain gently dipping towards the seacoasts with marked tidal rhythms. The deposits comprise very silty and moderately silty, massive clays coarsening upward (Bosch and Kok, 1994). According to the classification made by Reineck and Singh based on the sedimentation process, the fluvial deposits of the area are grouped into three main groups (Reineck and Singh, 1973):

- The channel deposits: are sediment deposits formed mainly from the activity of river channels. It comprises channel lag, point bar deposits, channel bar deposits and channel fill deposits of sand.
- Bank deposits: are riverbank sediments, which are deposited during the flood period. Levee deposits and crevasse splay deposits of sand and clay are included in these deposits.
- Flood basin deposits: are essentially fine-grained sediment deposits formed during heavy floods when river water flows over the levees into the flood basin. They include flood basin deposits and marsh deposits.

The Holocene deposits of the study area belong to Westland and Kreftenheye Formation and both formations being mainly formed by river deposits (Bosch & Kok, 1994).

Different layers are distinguished within the westland formation. This formation overlies the Kreftenheye Formation comprises the fluvial sediments (Gorkum and Tiel deposits) together with the clastic marine deposits and intercalated peat layers (Bosch & Kok, 1994). In the Reeuwijk, area the formation consists predominantly of complex alternations of floodplain clay deposits

with Holland peat. Lenses of sandy clay levee and sand channel deposits occasionally interrupt these deposits. Abrupt changes of the soil type in short distances complicate the geology of the area in general.

The Kreftenheye deposits mainly consist of gray, coarse sand and gravel with plant remains. The silt-less sand contains calcareous material. Locally the sand is intercalated with organic clay layers. The lower boundary is located at approximately 20 m below NAP; however, it may reach 10m deeper at channel infill locations (Bosch & Kok, 1994).

The Geological Map of Reeuwijk (1:50000) (Bosch & Kok, 1994) is shown in Figure 1.

Legend (Holocene deposits):

G0: Holland peat

rC2: Holland peat on an alternation of Gorkum (flood-plain and levee deposits) and Holland peat on Gorkum deposits (channel deposits)

rG2: Holland peat on an alternation of Gorkum deposits (flood-plain and levee deposits) and Holland peat

C2: Holland peat on Callais III Deposits (tidal flat deposits) on an alternation of Holland peat and Gorkum deposits

C2..: Holland peat on Callais III Deposits (tidal flat deposits) on Gorkum deposits (channel deposits)

rC0: Holland peat on Gorkum deposits (channel deposits)

rBd2g: Tiel deposits (channel deposits) on an alternation of Holland peat and Gorkum deposits (flood-plain and levee deposits)

rD0g: Tiel deposits (channel deposits, locally covered by levee deposits)

rA0k: Tiel deposits (flood-plain deposits) on Holland peat on Gorkum deposits (channel deposits)

rD0k: Tiel deposits (flood-plain deposits on channel deposits)

C0: Tiel deposits (flood-plain deposits)

rD1k: Tiel deposits (flood-plain deposits) on Gorkum deposits (flood-plain and levee deposits) on Gorkum deposits (Channel deposits)

rF2k: Tiel deposits (flood-plain deposits) on an alternation of Holland peat and Gorkum deposits (flood-plain and levee deposits)

rA2k: Tiel deposits (flood-plain deposits) on an alternation of Holland peat and Gorkum deposits (flood-plain and levee deposits) on Gorkum deposits (channel deposits)

rF0k: Tiel deposits (flood-plain deposits) on Holland peat

F3k: Tiel deposits (flood-plain deposits) on an alternation of Holland peat and Gorkum deposits (flood-plain and levee deposits)

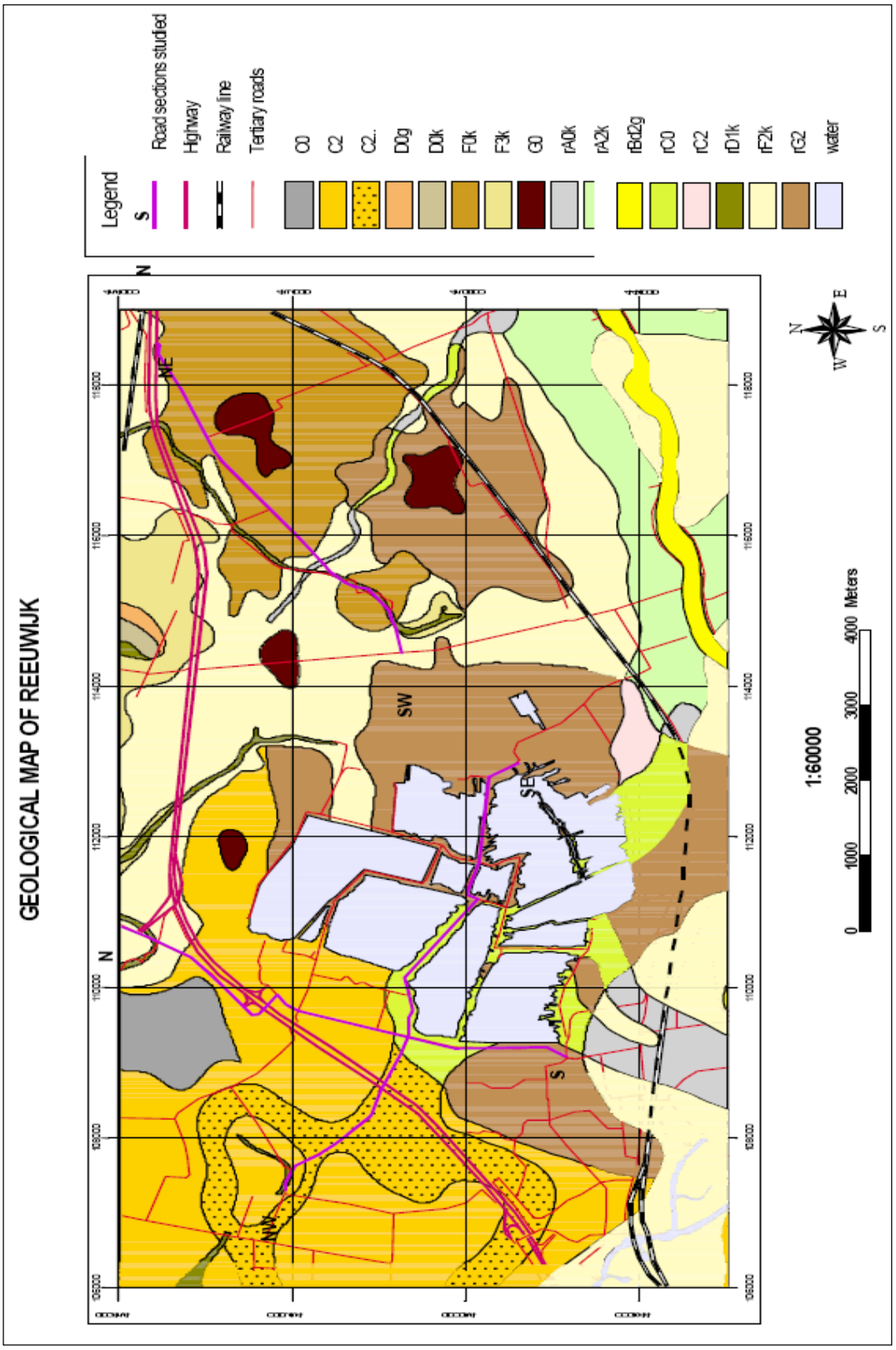

Figure 1. Geological map of the area around Reeuwijk (after Bosch and Kok, 1994) (Legend see page before).

APPENDIX F

RSDYK2008 - BOREHOLES AND DUTCH CONE PENETRATION (CPT) TESTS

A total of 2 boreholes made with a "Delft Continuous Soil Sampler" (a type of triple-tube sampler) and 17 Dutch cone penetrometer tests (CPT) with pore water pressure measurement have been made at the Reeuwijk Tempeldijk-South location (behind Aldi Supermarket).

Table 1. Coordinates of boreholes and Dutch Cone Penetrometer tests (CPT).

	RD		UTM(ETRS89) (31)		NAP
Naam	X coor	Y-coor	Easting	Northing	Elevation (m)
BH01 (S04)	107238.38	452370.59	615921.089	5768791.26	-4.58
BH02 (S17)	107267.02	452338.03	615950.779	5768759.67	-2.01
S01	107226.43	452371.91	615909.104	5768792.19	-5.06
S02	107230.42	452371.91	615913.091	5768792.32	-4.85
S03	107234.39	452371.18	615917.083	5768791.72	-4.69
S04	107238.38	452370.59	615921.089	5768791.26	-4.58
S05	107242.25	452369.91	615924.979	5768790.71	-4.39
S06	107246.2	452369.18	615928.95	5768790.11	-4.23
S07	107250.23	452368.51	615932.999	5768789.57	-4.03
S08	107254.09	452367.9	615936.877	5768789.09	-3.64
S09	107241.57	452390.37	615923.627	5768811.13	-4.77
S10	107240.77	452385.44	615922.99	5768806.18	-4.66
S11	107240.01	452380.53	615922.392	5768801.25	-4.54
S12	107239.33	452376.64	615921.84	5768797.34	-4.52
S13	107237.42	452365.41	615920.3	5768786.06	-4.52
S14	107236.65	452360.55	615919.69	5768781.17	-4.49
S15	107235.8	452355.61	615919.003	5768776.21	-4.5
S16	107234.9	452350.69	615918.266	5768771.26	-4.56
S17	107267.02	452338.03	615950.779	5768759.67	-2.01

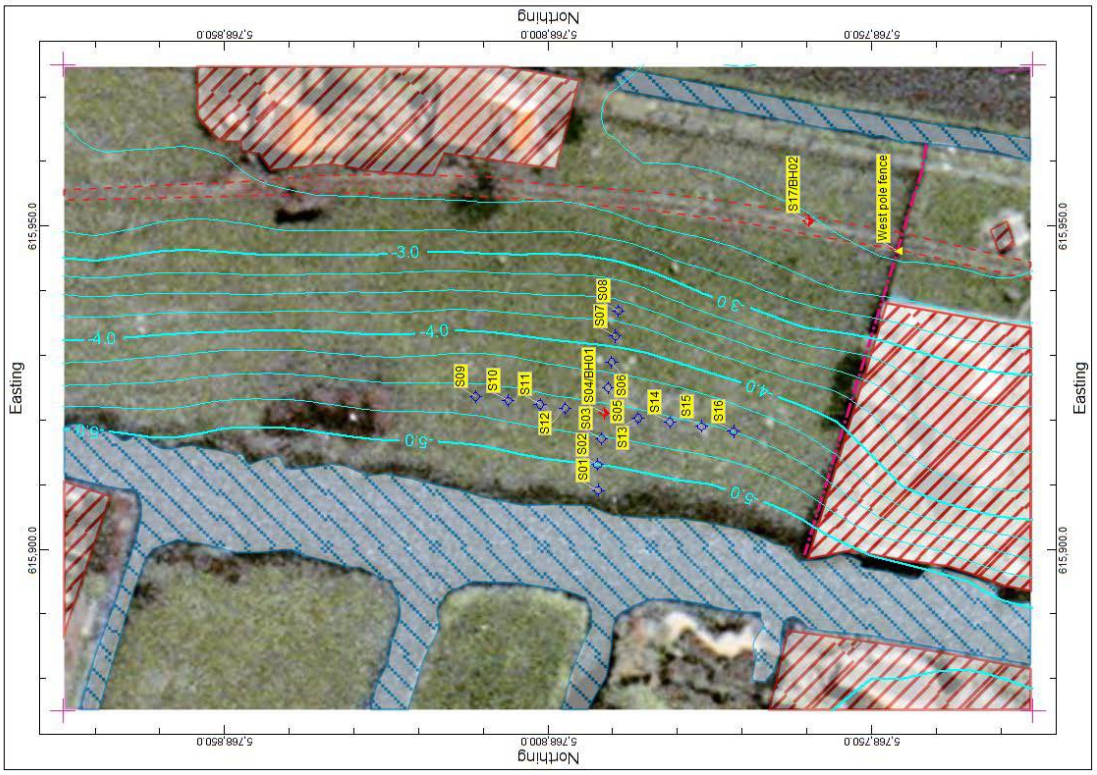

Figure 1. Locations boreholes and Dutch Cone penetrometer (CPT) tests.

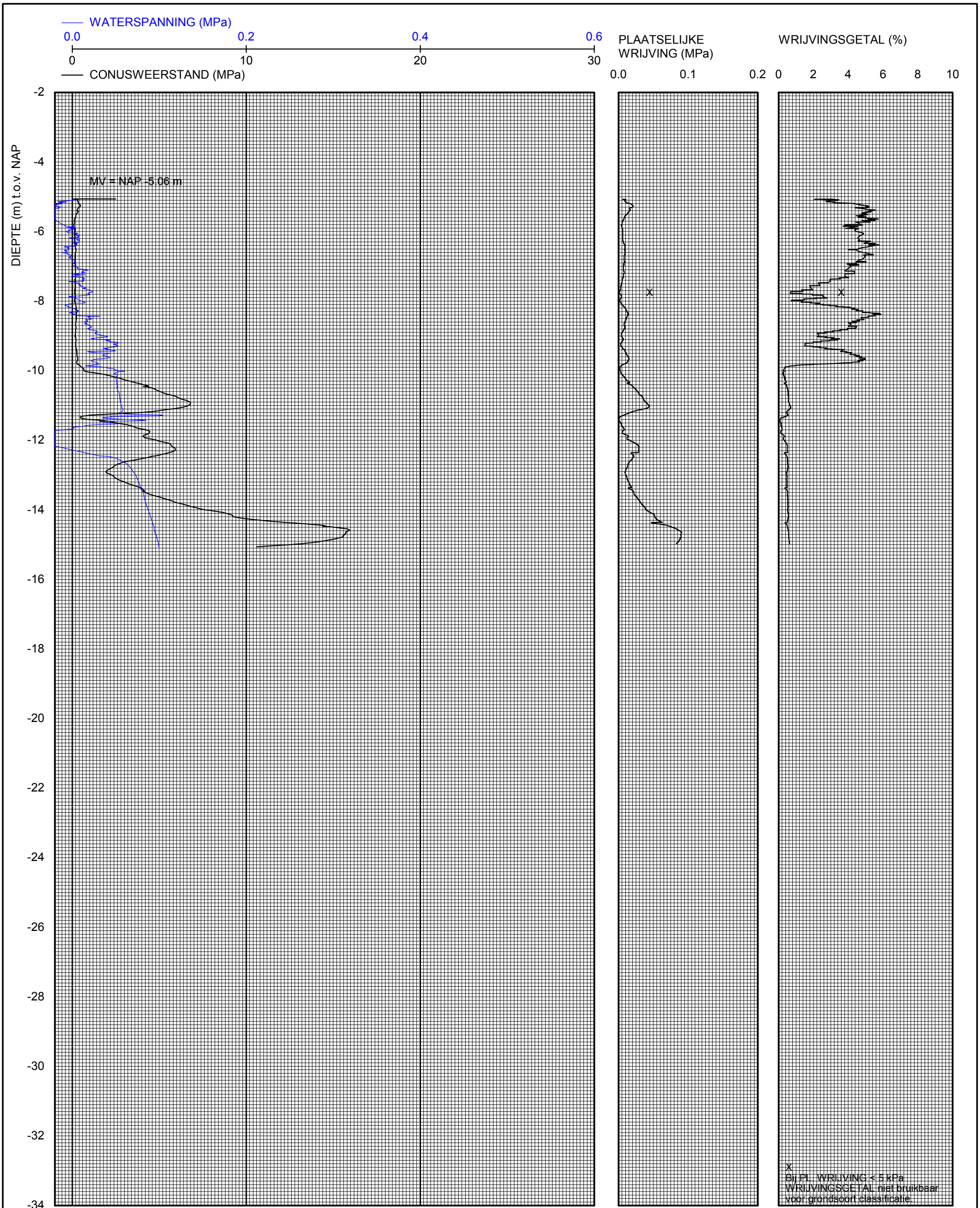

1

Deltares Deltares
Stieltjesweg 2
2628 CK Delft
Telefoon +31-15-2693500
Telefax +31-15-2610821

datum 2008-08-25
get. Lws
gez.
form. A3

Grondonderzoek Reeuwijk FC 2015
Reeuwijk
SONDERING S01

CO-432500/360
BIJL. CS1

Piezosondering uitgevoerd volgens NEN5140 klasse 2
Conus nr. CKR10/1-273, voorzien van electrische opnemers voor conusweerstand, plaatselijke wrijving, waterspanning en conushelling.

Geodetische bijzonderheden:
MV = NAP -5.06 m
X = 107226.43 m
Y = 452371.91 m

Meetbereiken:
Conusweerstand: 50 MPa
Plaatselijke wrijving: 0.7 MPa
Waterspanning: 1 MPa
Conushelling: 350 mRad

*) Vrijgegeven door Vin op 2008-09-03 11:09

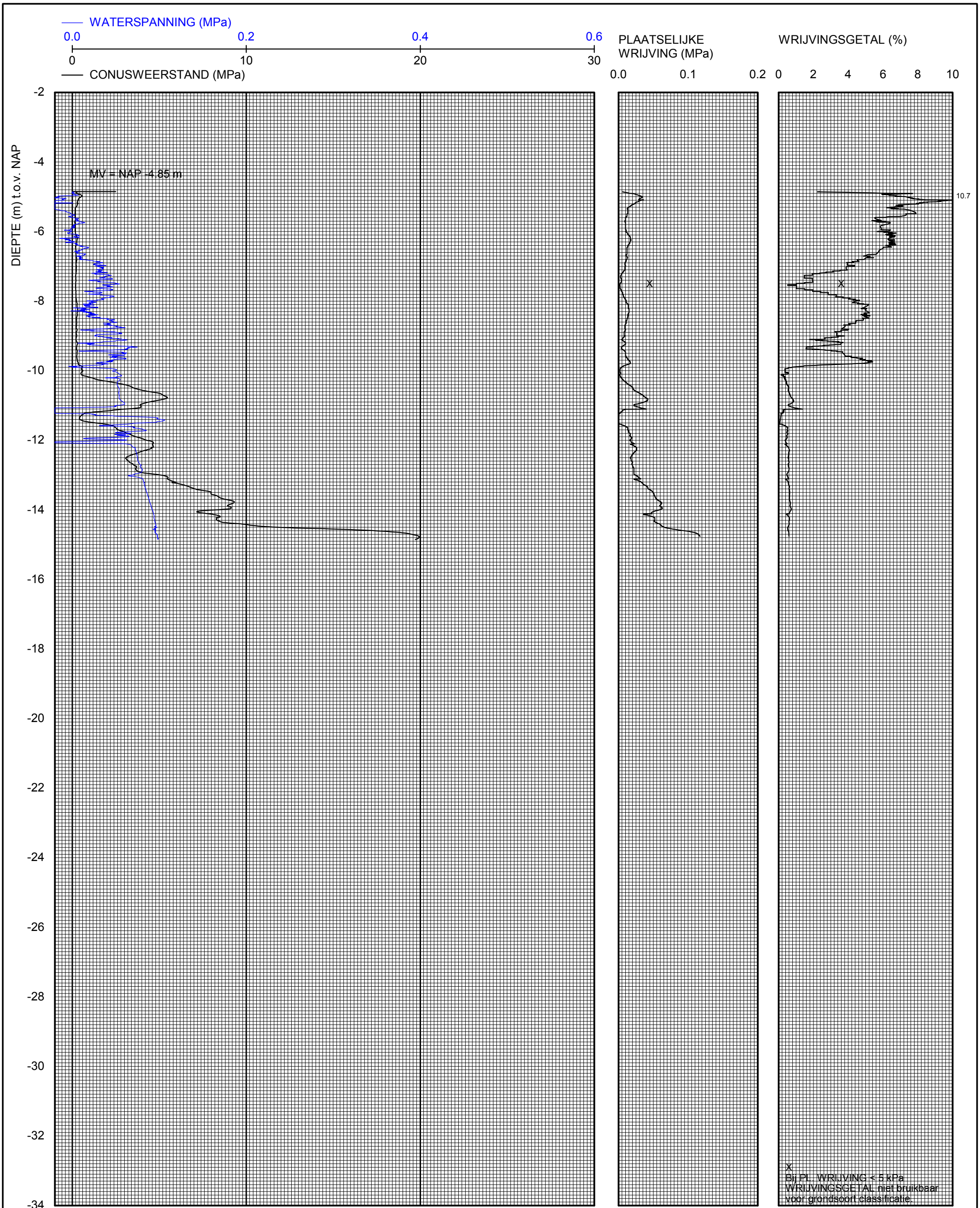

2

Deltares Deltares	Stieltjesweg 2 2628 CK Delft	Telefoon +31-15-2693500 Telefax +31-15-2610821	datum 2008-08-25	get. Lws	Piezosondering uitgevoerd volgens NEN5140 klasse 2 Conus nr. CKR10/1-273, voorzien van electrische opnemers voor conusweerstand, plaatselijke wrijving, waterspanning en conushelling
Grondonderzoek Reeuwijk FC 2015 Reeuwijk SONDERING S02			CO-432500/360 BIJL. CS2	gez. form. A3	Geodetische bijzonderheden: MV = NAP -4.85 m X = 107230.42 m Y = 452371.91 m Meetbereiken: Conusweerstand: 50 MPa Plaatselijke wrijving: 0.7 MPa Waterspanning: 1 MPa Conushelling: 350 mRad

*) Vrijgegeven door Vin op 2008-09-03 11:09

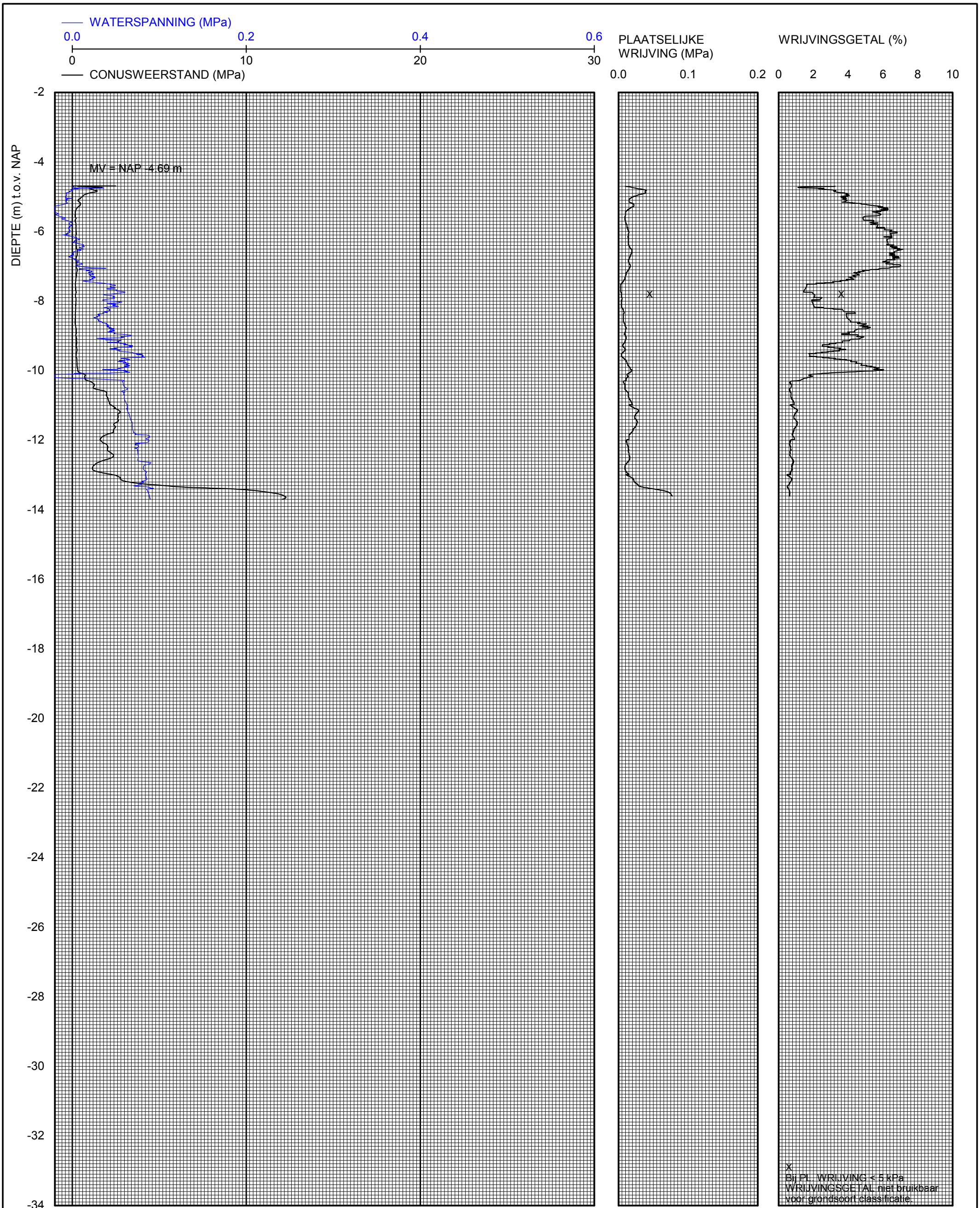

Deltares Deltares	Stieltjesweg 2 2628 CK Delft	Telefoon +31-15-2693500 Telefax +31-15-2610821	datum 2008-08-25	get. Lws	Piezosondering uitgevoerd volgens NEN5140 klasse 2 Conus nr. CKR10/1-273, voorzien van electrische opnemers voor conusweerstand, plaatselijke wrijving, waterspanning en conushelling
Grondonderzoek Reeuwijk FC 2015 Reeuwijk SONDERING S03			CO-432500/360 BIJL. CS3	gez. form. A3	Geodetische bijzonderheden: MV = NAP -4.69 m X = 107234.39 m Y = 452371.18 m Meetbereiken: Conusweerstand: 50 MPa Plaatselijke wrijving: 0.7 MPa Waterspanning: 1 MPa Conushelling: 350 mRad

*) Vrijgegeven door Vin op 2008-09-03 11:10

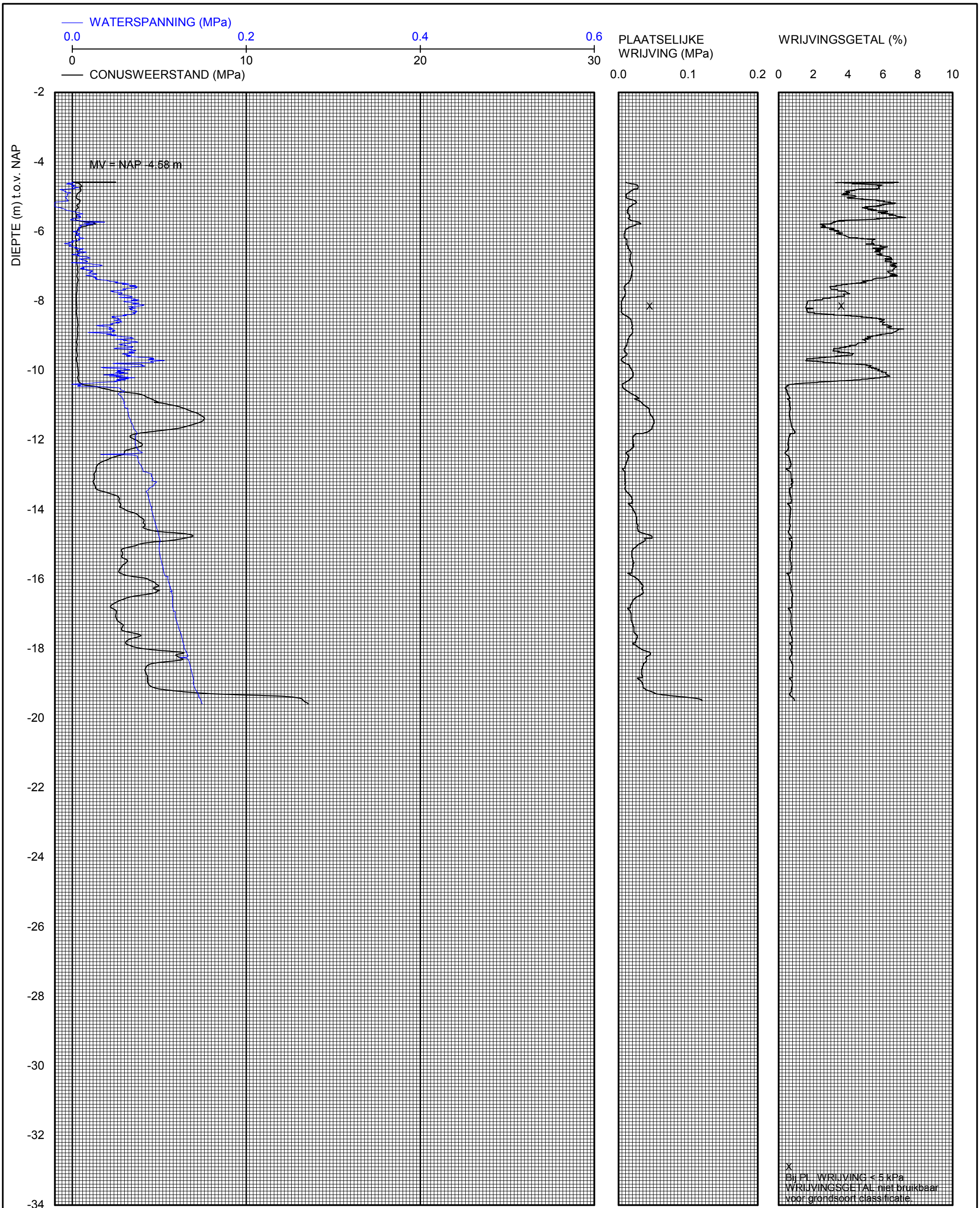

4

Deltares Deltares	Stieltjesweg 2 2628 CK Delft	Telefoon +31-15-2693500 Telefax +31-15-2610821	datum 2008-08-25	get. Lws	Piezosondering uitgevoerd volgens NEN5140 klasse 2 Conus nr. CKR10/1-273, voorzien van electrische opnemers voor conusweerstand, plaatselijke wrijving, waterspanning en conushelling
Grondonderzoek Reeuwijk FC 2015 Reeuwijk			CO-432500/360	gez.	Geodetische bijzonderheden: MV = NAP -4.58 m X = 107238.38 m Y = 452370.59 m
SONDERING S04			BIJL. CS4	form. A3	Meetbereiken: Conusweerstand: 50 MPa Plaatselijke wrijving: 0.7 MPa Waterspanning: 1 MPa Conushelling: 350 mRad

*) Vrijgegeven door Vin op 2008-09-03 11:10

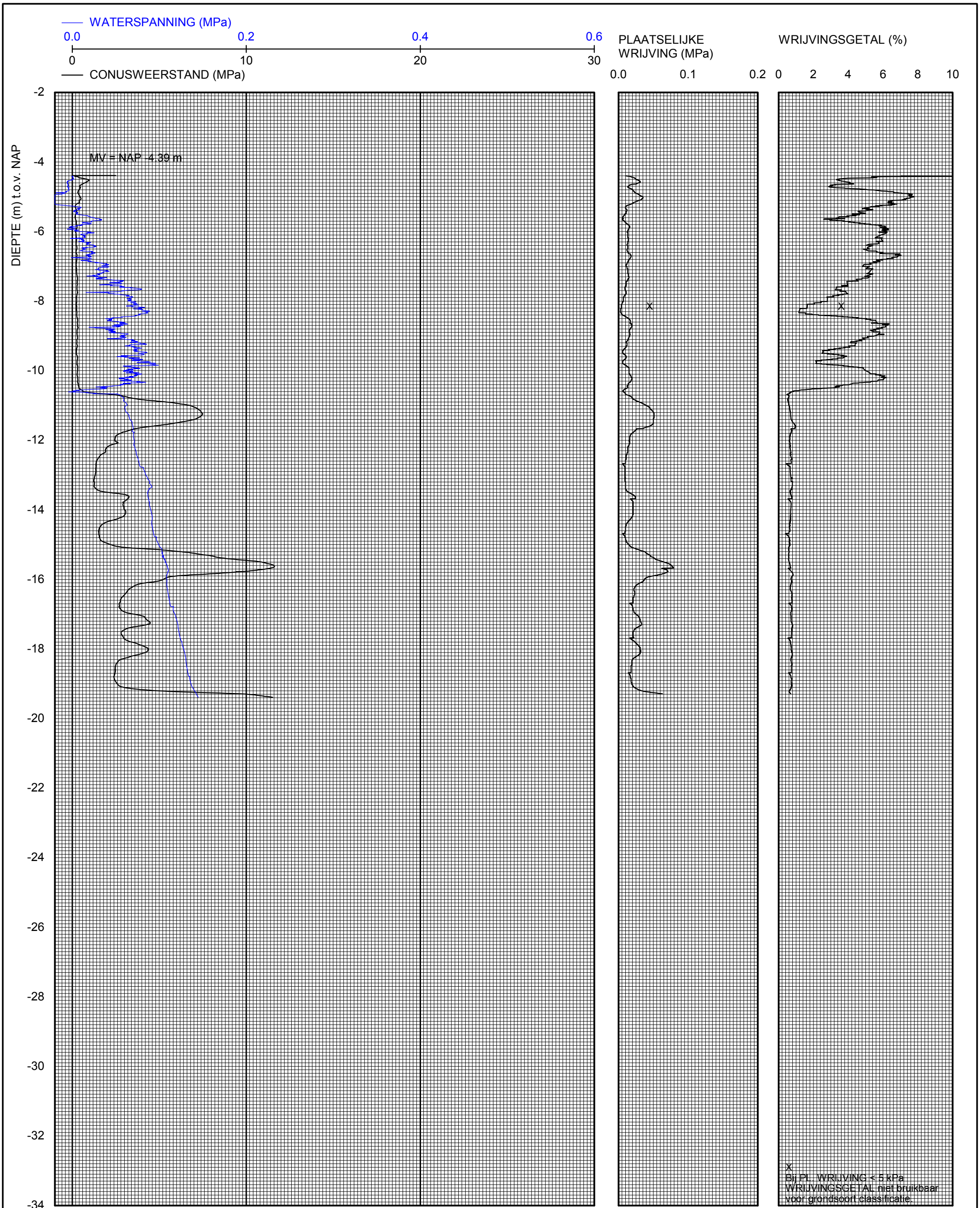

11

Deltares Deltares	Stieltjesweg 2 2628 CK Delft	Telefoon +31-15-2693500 Telefax +31-15-2610821	datum 2008-08-25	get. Lws	Piezosondering uitgevoerd volgens NEN5140 klasse 2 Conus nr. CKR10/1-273, voorzien van electrische opnemers voor conusweerstand, plaatselijke wrijving, waterspanning en conushelling
Grondonderzoek Reeuwijk FC 2015 Reeuwijk SONDERING S05			CO-432500/360 BIJL. CS5	gez. form. A3	Geodetische bijzonderheden: MV = NAP -4.39 m X = 107242.25 m Y = 452369.91 m Meetbereiken: Conusweerstand: 50 MPa Plaatselijke wrijving: 0.7 MPa Waterspanning: 1 MPa Conushelling: 350 mRad

*) Vrijgegeven door Vin op 2008-09-03 11:14

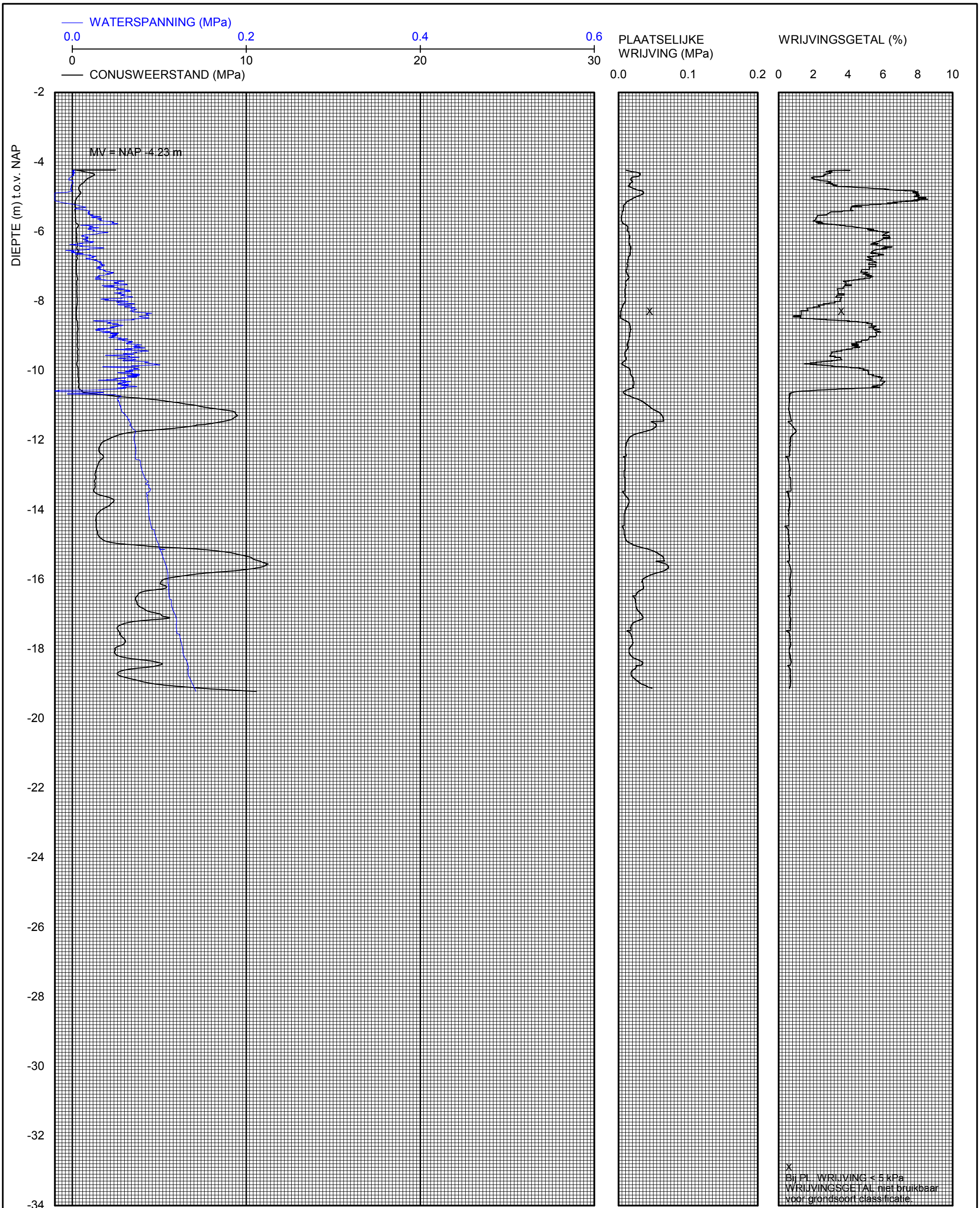

5

Deltares Deltares
Stieltjesweg 2
2628 CK Delft
Telefoon +31-15-2693500
Telefax +31-15-2610821

datum 2008-08-25
get. Lws
gez.
form. A3

Grondonderzoek Reeuwijk FC 2015
Reeuwijk
SONDERING S06

CO-432500/360
BIJL. CS6

Piezosondering uitgevoerd volgens NEN5140 klasse 2
Conus nr. CKR10/1-273, voorzien van electrische opnemers voor conusweerstand, plaatselijke wrijving, waterspanning en conushelling.

Geodetische bijzonderheden:
MV = NAP -4.23 m
X = 107246.20 m
Y = 452369.18 m

Meetbereiken:
Conusweerstand: 50 MPa
Plaatselijke wrijving: 0.7 MPa
Waterspanning: 1 MPa
Conushelling: 350 mRad

*) Vrijgegeven door Vin op 2008-09-03 11:11

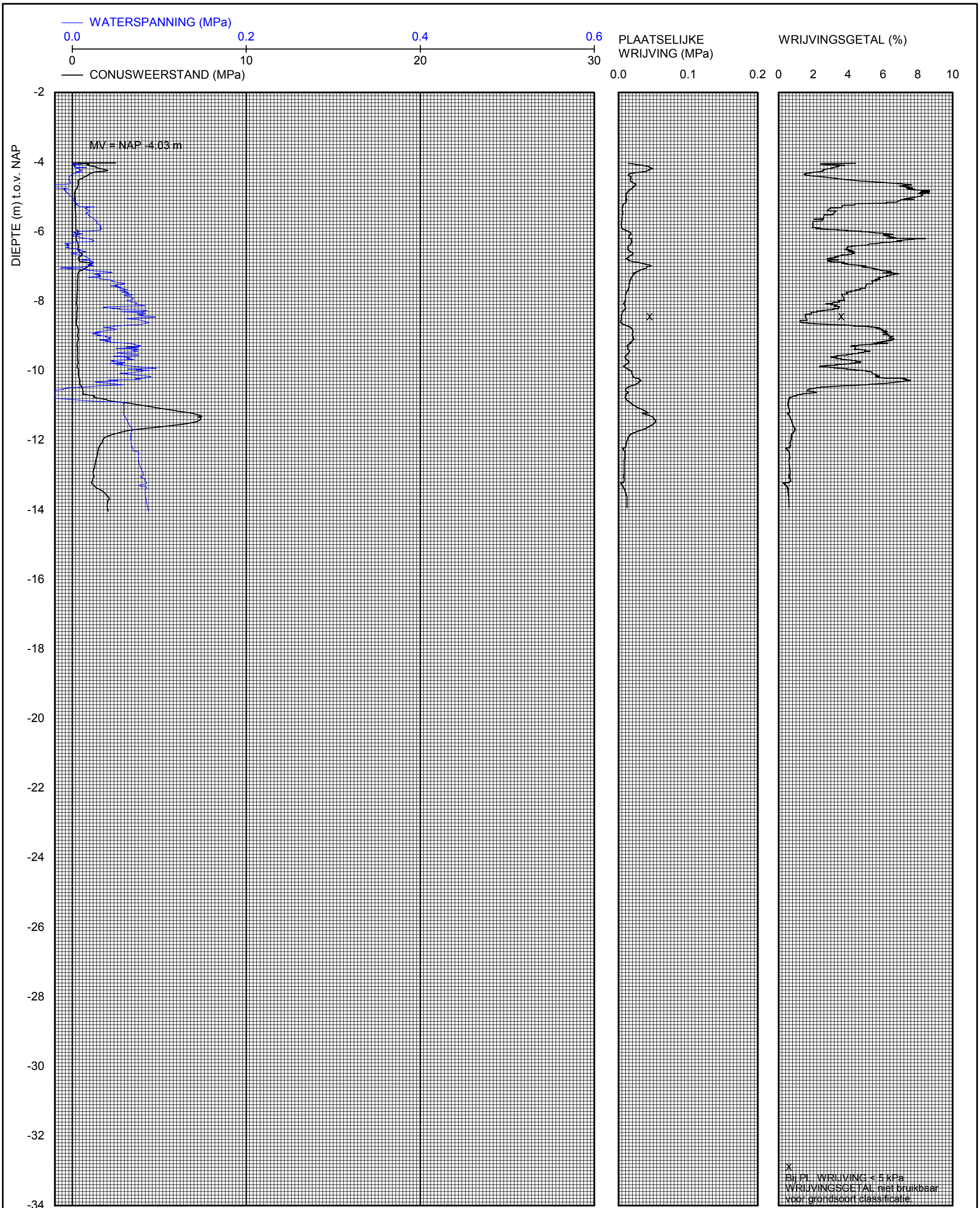

6

Deltares Deltares
Stieltjesweg 2
2628 CK Delft
Telefoon +31-15-2693500
Telefax +31-15-2610821

datum 2008-08-25
get. Lws
gez.
form. A3

Grondonderzoek Reeuwijk FC 2015
Reeuwijk
SONDERING S07

CO-432500/360
BIJL. CS7

Piezosondering uitgevoerd volgens NEN5140 klasse 2
Conus nr. CKR10/1-273, voorzien van electrische opnemers voor conusweerstand, plaatselijke wrijving, waterspanning en conushelling.

Geodetische bijzonderheden:
MV = NAP -4.03 m
X = 107250.23 m
Y = 452368.51 m

Meetbereiken:
Conusweerstand: 50 MPa
Plaatselijke wrijving: 0.7 MPa
Waterspanning: 1 MPa
Conushelling: 350 mRad

*) Vrijgegeven door Vin op 2008-09-03 11:12

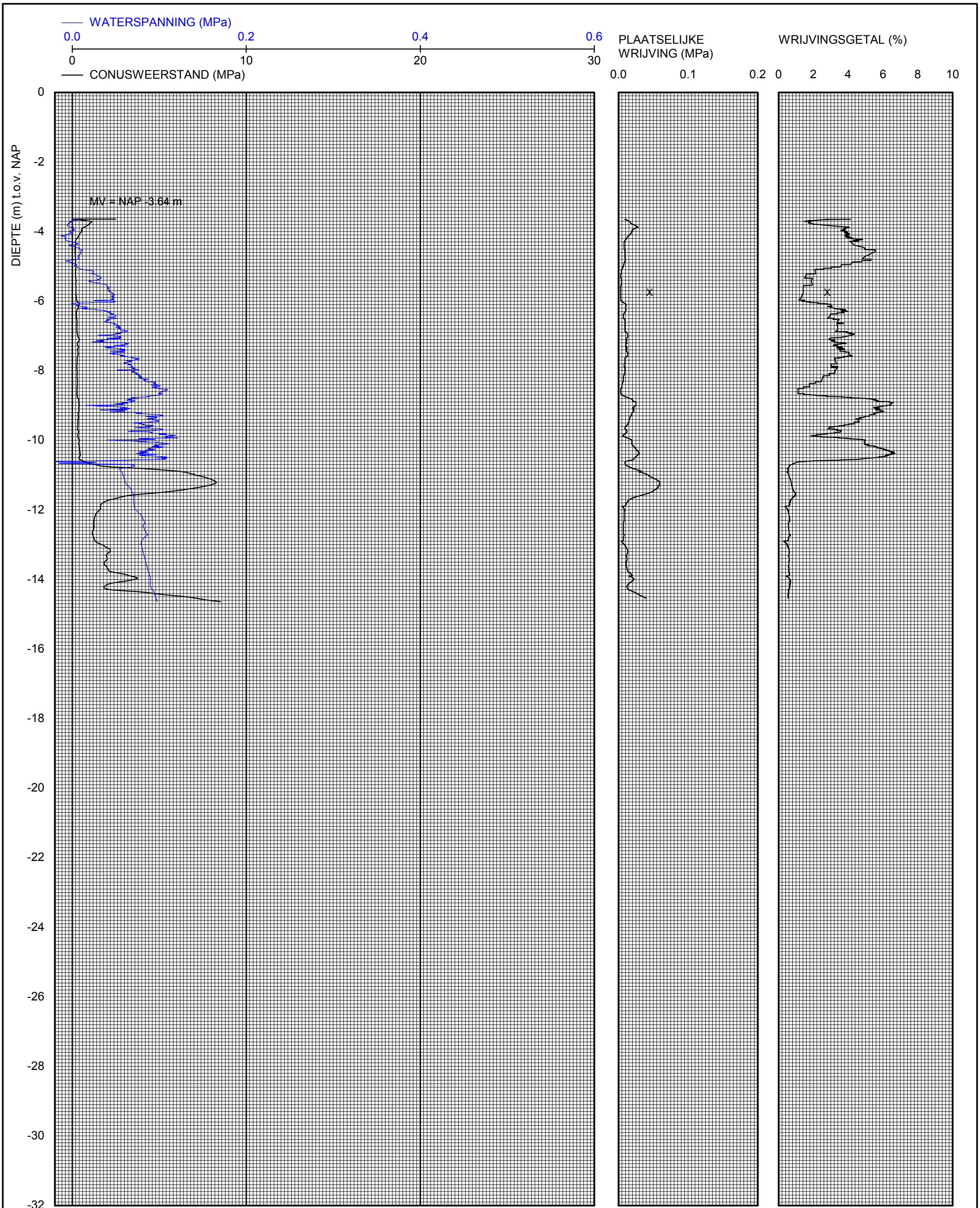

7

Deltares Deltares	Stieltjesweg 2 2628 CK Delft	Telefoon +31-15-2693500 Telefax +31-15-2610821	datum 2008-08-25	get. Lws	Piezosondering uitgevoerd volgens NEN5140 klasse 2 Conus nr. CKR10/1-273, voorzien van electrische opnemers voor conusweerstand, plaatselijke wrijving, waterspanning en conushelling
Grondonderzoek Reeuwijk FC 2015 Reeuwijk SONDERING S08			CO-432500/360 BIJL. CS8	gez. form. A3	Geodetische bijzonderheden: MV = NAP -3.64 m X = 107254.09 m Y = 452367.90 m Meetbereiken: Conusweerstand: 50 MPa Plaatselijke wrijving: 0.7 MPa Waterspanning: 1 MPa Conushelling: 350 mRad

*) Vrijgegeven door Vin op 2008-09-03 11:13

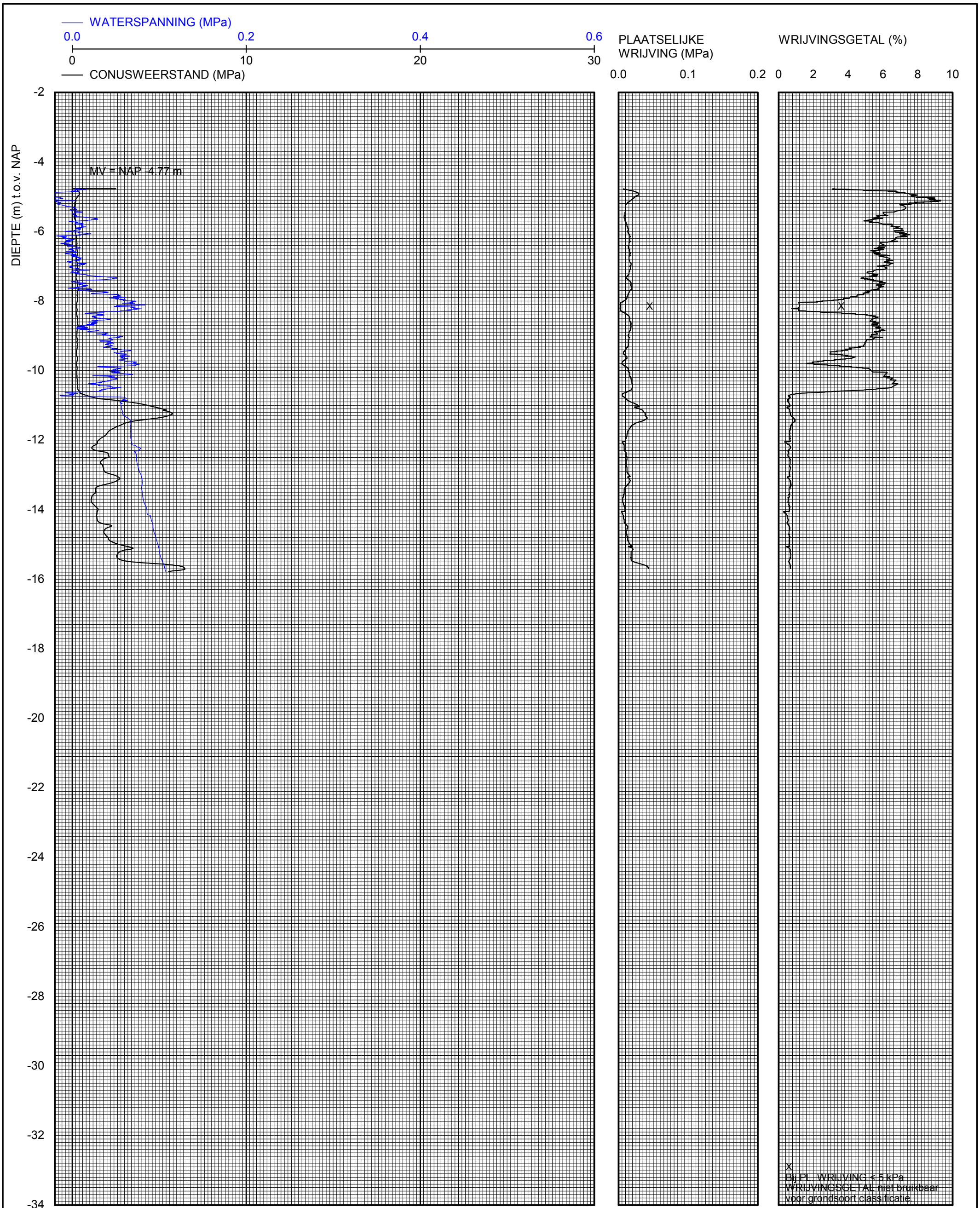

8

Deltares Deltares Stieltjesweg 2 2628 CK Delft Telefoon +31-15-2693500 Telefax +31-15-2610821	datum 2008-08-25	get. Lws	Piezosondering uitgevoerd volgens NEN5140 klasse 2 Conus nr. CKR10/1-273, voorzien van electrische opnemers voor conusweerstand, plaatselijke wrijving, waterspanning en conushelling	
Grondonderzoek Reeuwijk FC 2015 Reeuwijk	CO-432500/360	gez.	Geodetische bijzonderheden: MV = NAP -4.77 m X = 107241.57 m Y = 452390.37 m	Meetbereiken: Conusweerstand: 50 MPa Plaatselijke wrijving: 0.7 MPa Waterspanning: 1 MPa Conushelling: 350 mRad
SONDERING S09	BIJL. CS9	form. A3		

*) Vrijgegeven door Vin op 2008-09-03 11:13

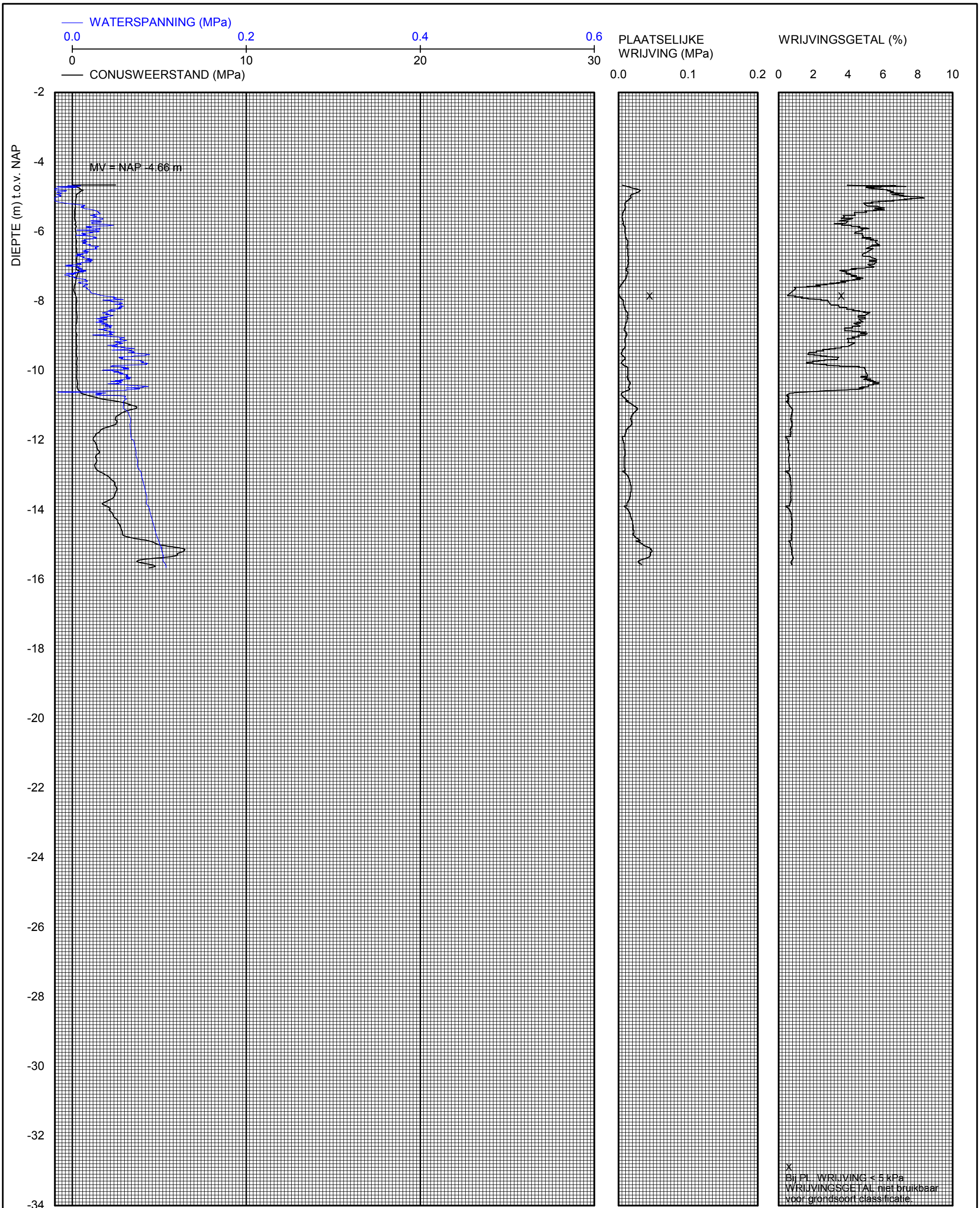

9

Deltares Deltares Stieltjesweg 2 2628 CK Delft Telefoon +31-15-2693500 Telefax +31-15-2610821	datum 2008-08-26	get. Lws	Piezosondering uitgevoerd volgens NEN5140 klasse 2 Conus nr. CKR10/1-273, voorzien van electrische opnemers voor conusweerstand, plaatselijke wrijving, waterspanning en conushelling
Grondonderzoek Reeuwijk FC 2015 Reeuwijk	CO-432500/360	gez.	Geodetische bijzonderheden: MV = NAP -4.66 m X = 107240.77 m Y = 452385.44 m
SONDERING S10	BIJL. CS10	form. A3	Meetbereiken: Conusweerstand: 50 MPa Plaatselijke wrijving: 0.7 MPa Waterspanning: 1 MPa Conushelling: 350 mRad

*) Vrijgegeven door Vin op 2008-09-03 11:13

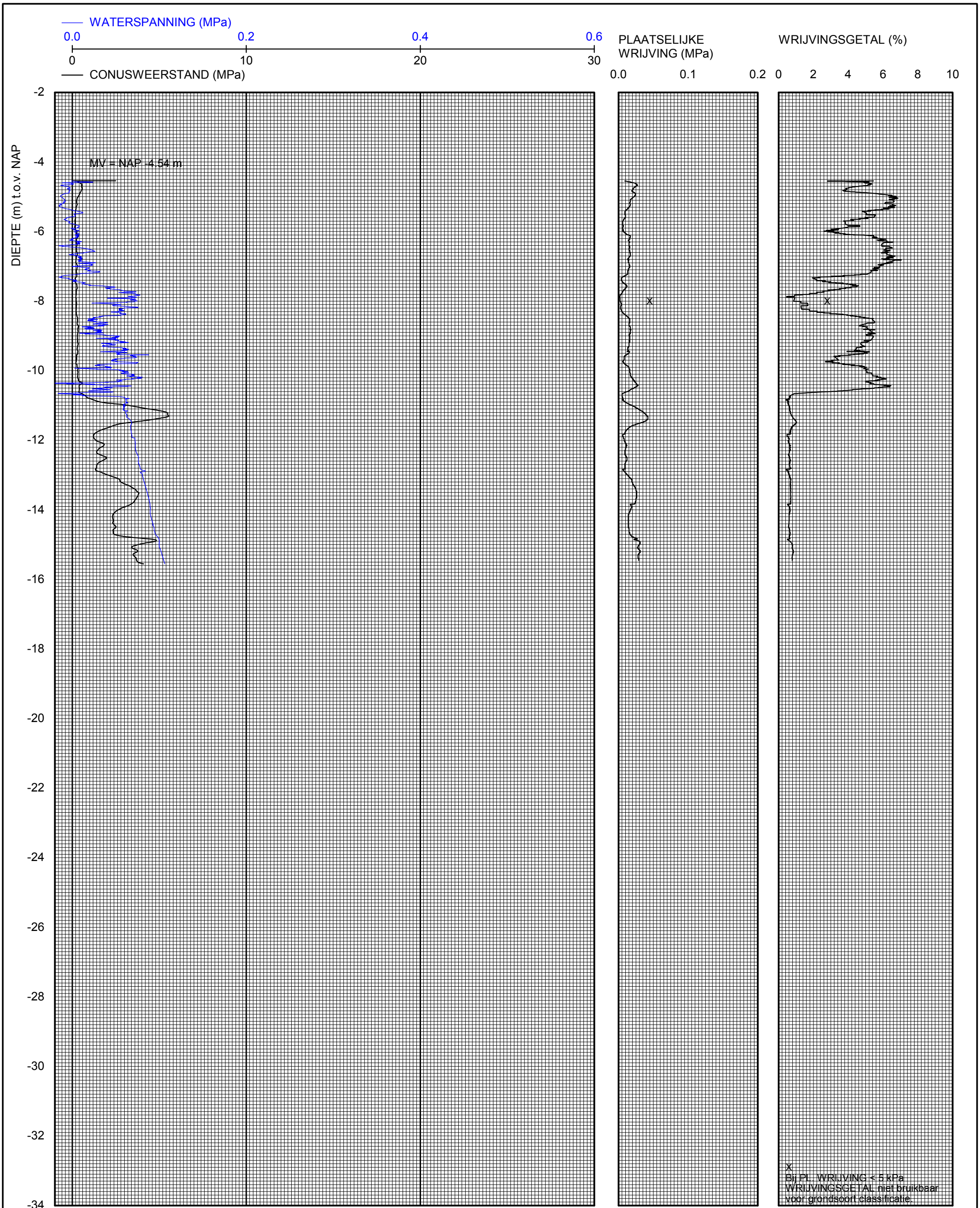

10

Deltares Deltares	Stieltjesweg 2 2628 CK Delft	Telefoon +31-15-2693500 Telefax +31-15-2610821	datum 2008-08-26	get. Lws	Piezosondering uitgevoerd volgens NEN5140 klasse 2 Conus nr. CKR10/1-273, voorzien van electrische opnemers voor conusweerstand, plaatselijke wrijving, waterspanning en conushelling
Grondonderzoek Reeuwijk FC 2015 Reeuwijk SONDERING S11			CO-432500/360 BIJL. CS11	gez. form. A3	Geodetische bijzonderheden: MV = NAP -4.54 m X = 107240.01 m Y = 452380.53 m Meetbereiken: Conusweerstand: 50 MPa Plaatselijke wrijving: 0.7 MPa Waterspanning: 1 MPa Conushelling: 350 mRad

*) Vrijgegeven door Vin op 2008-09-03 11:14

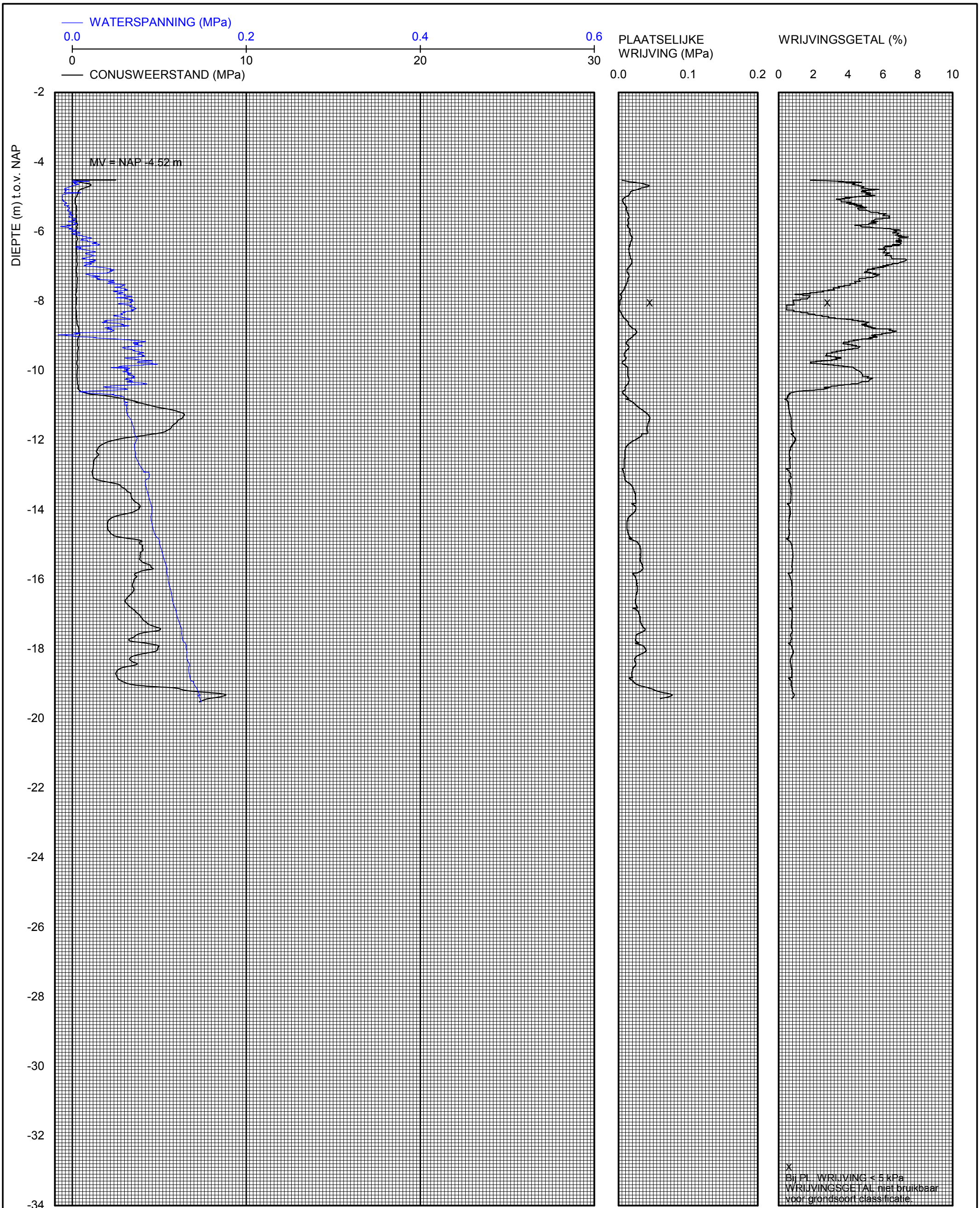

12

Deltares Deltares	Stieltjesweg 2 2628 CK Delft	Telefoon +31-15-2693500 Telefax +31-15-2610821	datum 2008-08-26	get. Lws	Piezosondering uitgevoerd volgens NEN5140 klasse 2 Conus nr. CKR10/1-273, voorzien van electrische opnemers voor conusweerstand, plaatselijke wrijving, waterspanning en conushelling
Grondonderzoek Reeuwijk FC 2015 Reeuwijk			CO-432500/360	gez.	Geodetische bijzonderheden: MV = NAP -4.52 m X = 107239.33 m Y = 452376.64 m
SONDERING S12			BIJL. CS12	form. A3	Meetbereiken: Conusweerstand: 50 MPa Plaatselijke wrijving: 0.7 MPa Waterspanning: 1 MPa Conushelling: 350 mRad

*) Vrijgegeven door Vin op 2008-09-03 11:14

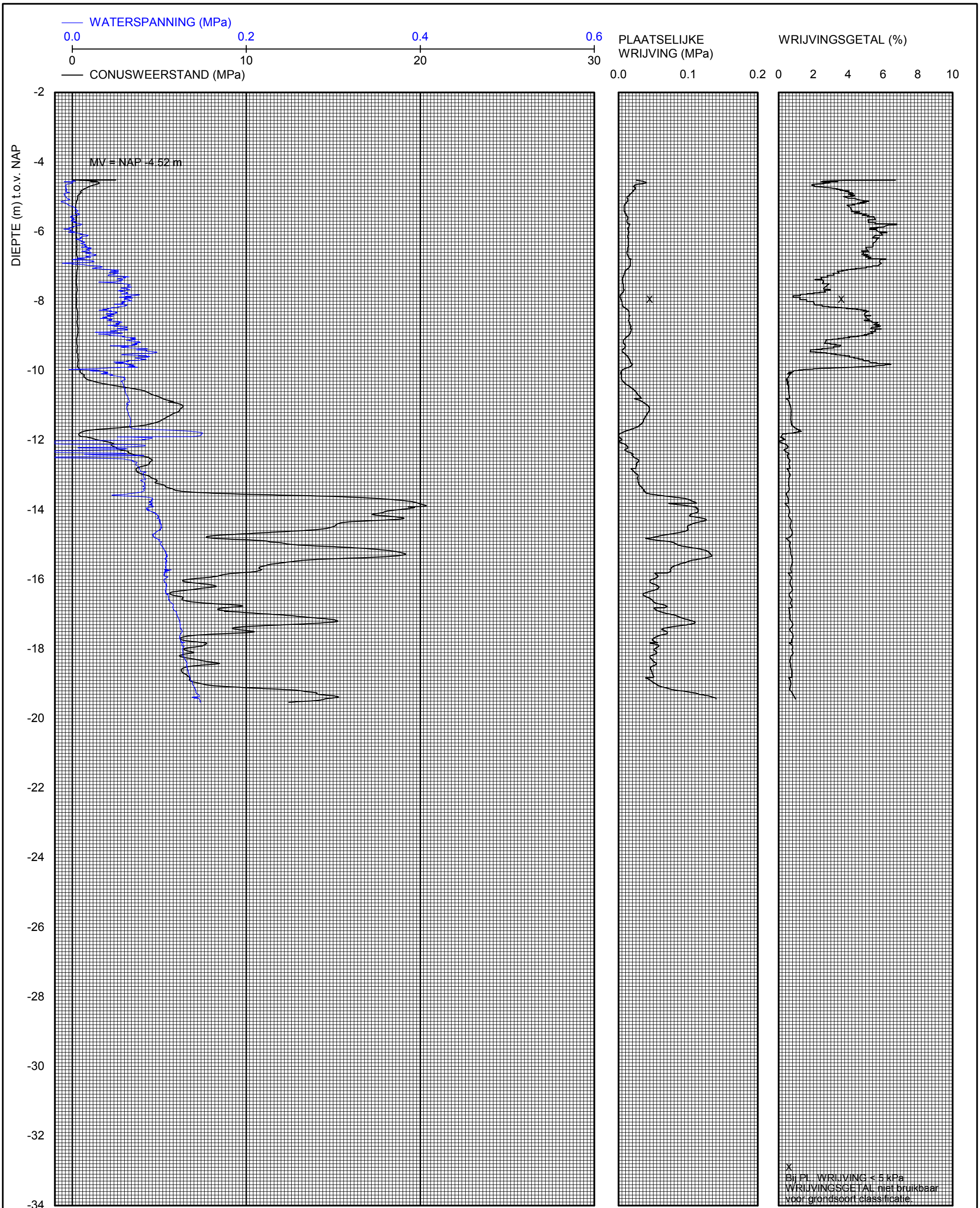

13

Deltares Deltares
Stieltjesweg 2
2628 CK Delft
Telefoon +31-15-2693500
Telefax +31-15-2610821

datum 2008-08-26	get. Lws	Piezosondering uitgevoerd volgens NEN5140 klasse 2 Conus nr. CKR10/1-273, voorzien van electrische opnemers voor conusweerstand, plaatselijke wrijving, waterspanning en conushelling
CO-432500/360	gez.	Geodetische bijzonderheden: MV = NAP -4.52 m X = 107237.42 m Y = 452365.41 m
BIJL. CS13	form. A3	Meetbereiken: Conusweerstand: 50 MPa Plaatselijke wrijving: 0.7 MPa Waterspanning: 1 MPa Conushelling: 350 mRad

Grondonderzoek Reeuwijk FC 2015
Reeuwijk
SONDERING S13

*) Vrijgegeven door Vin op 2008-09-03 11:15

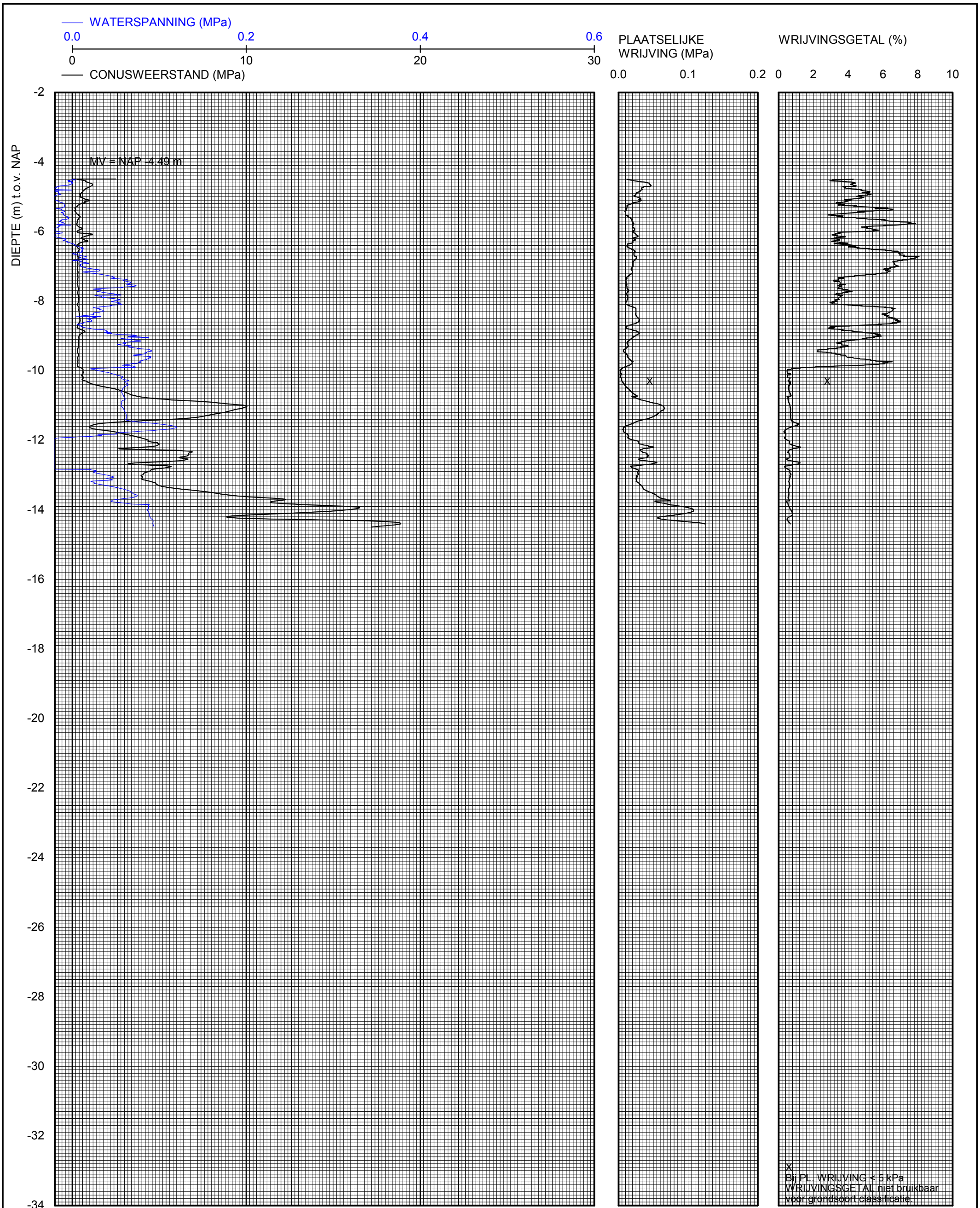

14

Deltares Deltares	Stieltjesweg 2 2628 CK Delft	Telefoon +31-15-2693500 Telefax +31-15-2610821	datum 2008-08-26	get. Lws
Grondonderzoek Reeuwijk FC 2015 Reeuwijk			CO-432500/360	gez.
SONDERING S14			BIJL. CS14	form. A3

Piezosondering uitgevoerd volgens NEN5140 klasse 2
Conus nr. CKR10/1-273, voorzien van electrische opnemers voor conusweerstand, plaatselijke wrijving, waterspanning en conushelling.

Geodetische bijzonderheden:
MV = NAP -4.49 m
X = 107236.65 m
Y = 452360.55 m

Meetbereiken:
Conusweerstand: 50 MPa
Plaatselijke wrijving: 0.7 MPa
Waterspanning: 1 MPa
Conushelling: 350 mRad

*) Vrijgegeven door Vin op 2008-09-03 11:15

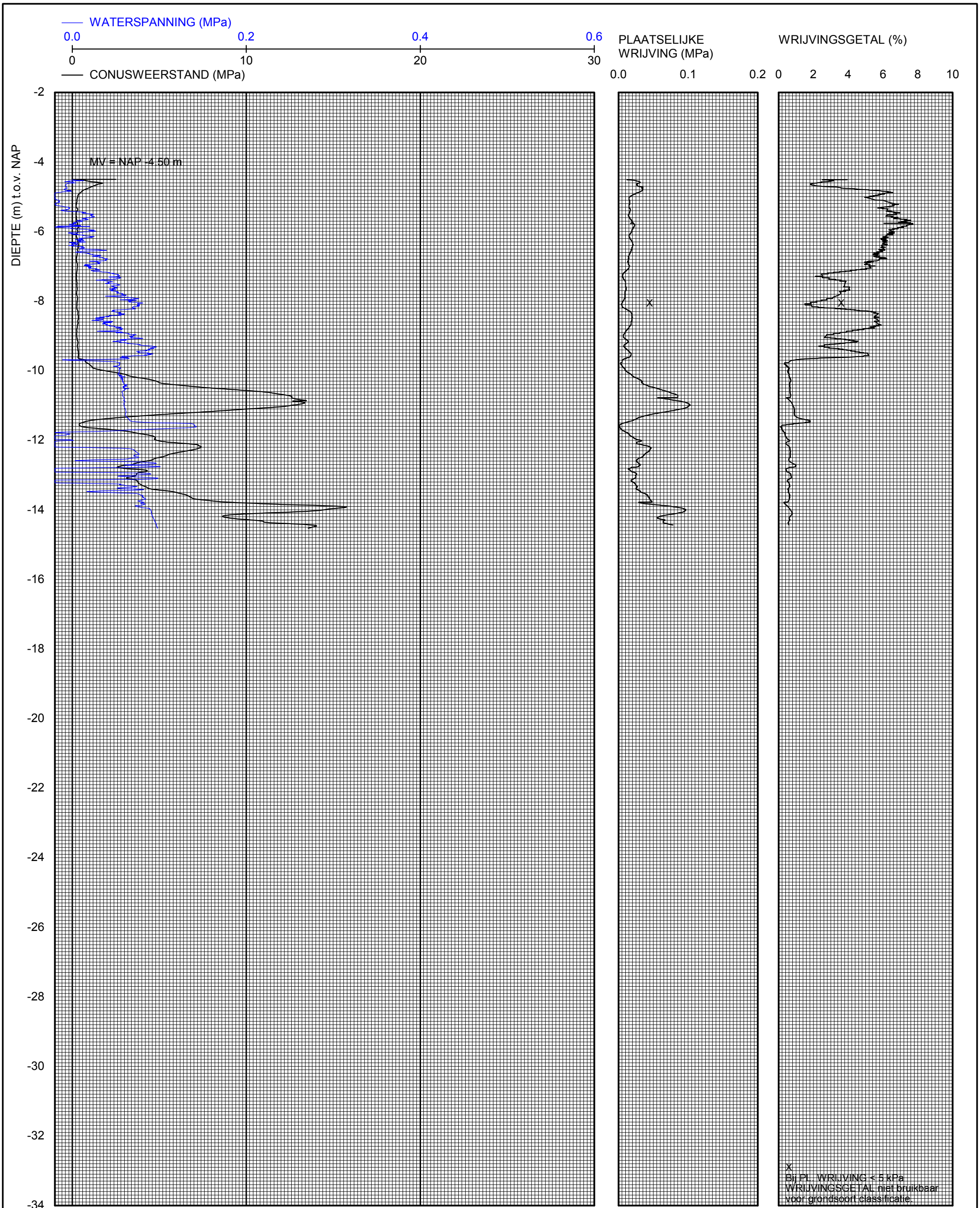

15

Deltares Deltares Stieltjesweg 2 2628 CK Delft Telefoon +31-15-2693500 Telefax +31-15-2610821	datum 2008-08-26	get. Lws	Piezosondering uitgevoerd volgens NEN5140 klasse 2 Conus nr. CKR10/1-273, voorzien van electrische opnemers voor conusweerstand, plaatselijke wrijving, waterspanning en conushelling	
Grondonderzoek Reeuwijk FC 2015 Reeuwijk	CO-432500/360	gez.	Geodetische bijzonderheden: MV = NAP -4.50 m X = 107235.80 m Y = 452355.61 m	Meetbereiken: Conusweerstand: 50 MPa Plaatselijke wrijving: 0.7 MPa Waterspanning: 1 MPa Conushelling: 350 mRad
SONDERING S15	BIJL. CS15	form. A3		

*) Vrijgegeven door Vin op 2008-09-03 11:15

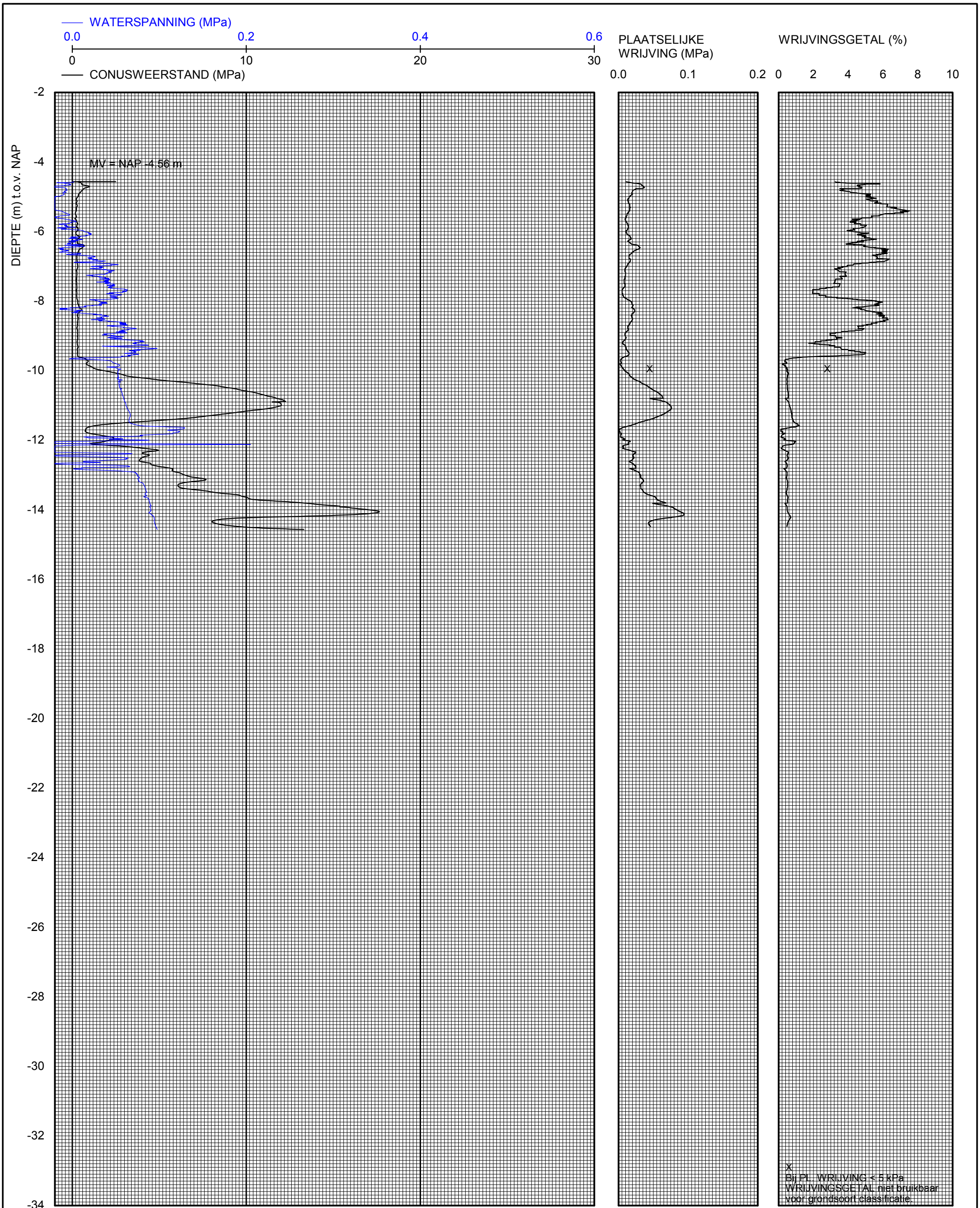

16

Deltares Deltares Stieltjesweg 2 2628 CK Delft Telefoon +31-15-2693500 Telefax +31-15-2610821	datum 2008-08-26	get. Lws	Piezosondering uitgevoerd volgens NEN5140 klasse 2 Conus nr. CKR10/1-273, voorzien van electrische opnemers voor conusweerstand, plaatselijke wrijving, waterspanning en conushelling
Grondonderzoek Reeuwijk FC 2015 Reeuwijk SONDERING S16	CO-432500/360 BIJL. CS16	gez. form. A3	Geodetische bijzonderheden: MV = NAP -4.56 m X = 107234.90 m Y = 452350.69 m Meetbereiken: Conusweerstand: 50 MPa Plaatselijke wrijving: 0.7 MPa Waterspanning: 1 MPa Conushelling: 350 mRad

*) Vrijgegeven door Vin op 2008-09-03 11:16

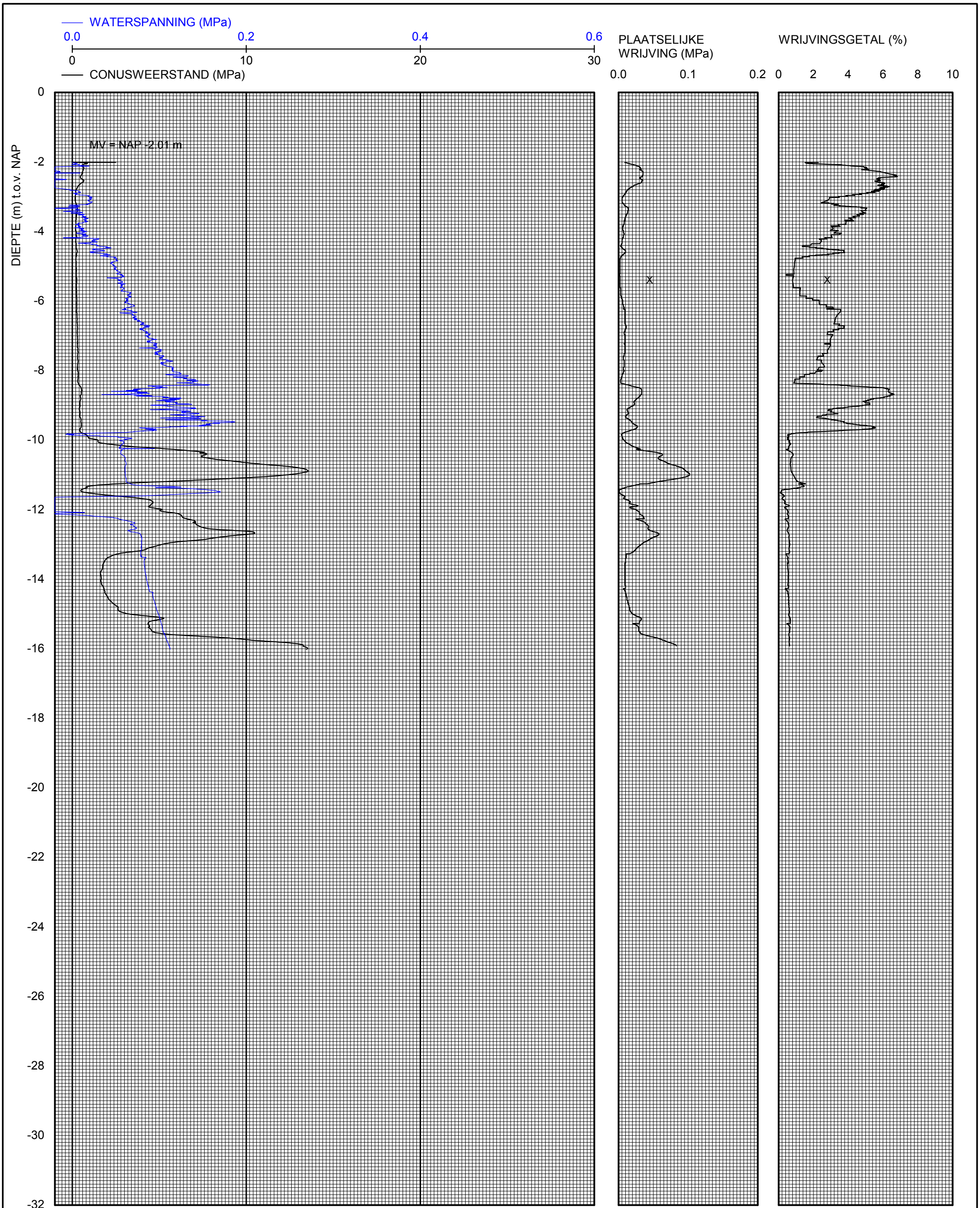

17

Deltares Deltares	Stieltjesweg 2 2628 CK Delft	Telefoon +31-15-2693500 Telefax +31-15-2610821	datum 2008-08-26	get. Lws	Piezosondering uitgevoerd volgens NEN5140 klasse 2 Conus nr. CKR10/1-273, voorzien van electrische opnemers voor conusweerstand, plaatselijke wrijving, waterspanning en conushelling
Grondonderzoek Reeuwijk FC 2015 Reeuwijk SONDERING S17			CO-432500/360 BIJL. CS17	gez. form. A3	Geodetische bijzonderheden: MV = NAP -2.01 m X = 107267.02 m Y = 452338.03 m Meetbereiken: Conusweerstand: 50 MPa Plaatselijke wrijving: 0.7 MPa Waterspanning: 1 MPa Conushelling: 350 mRad

*) Vrijgegeven door Vin op 2008-09-03 11:16

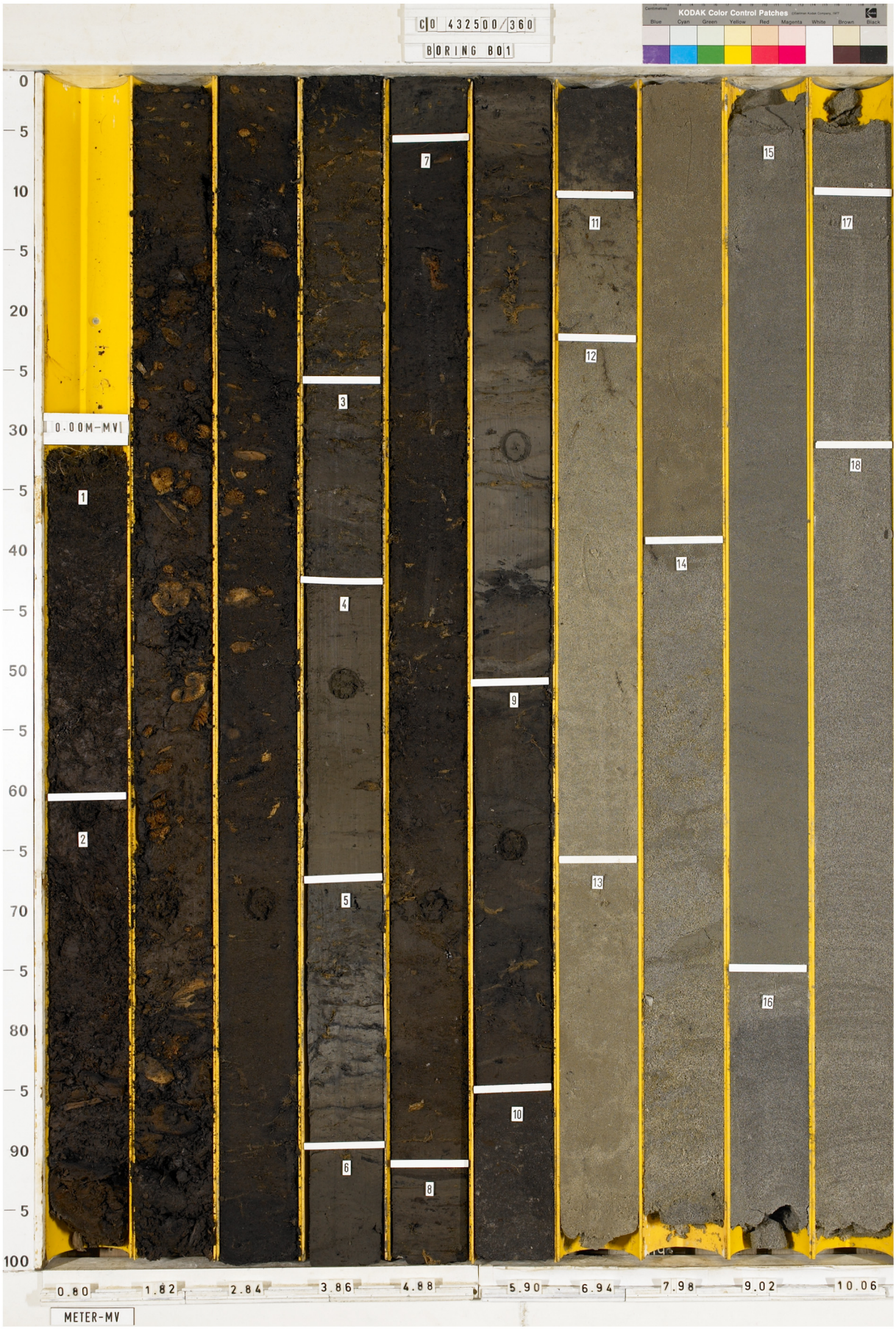

BESCHRIJVING: ZIE GETEKENDE VERSIE VAN BORING	Filenaam: B01bijS04	Gewijzigd: 2008-12-18	Blad 1/2	

Deltares
Postbus 177 2600 MH Delft, Stieltjesweg 2, 2628 CK Delft
Telefoon (0)15 269 35 00 Telefax (0)15 261 08 21
www.deltares.nl info@deltares.nl

datum	get.
2008-12-18	Mar

Grondonderzoek Reeuwijk FC 2015
Reeuwijk

CO-432500/360	gez.

FOTO BORING B01 bij S04 Type: Begemannboring 66 mm

BIJL. BFB1	form. A4

*) Vrijgegeven door Hsd op 2009-01-05 08:44

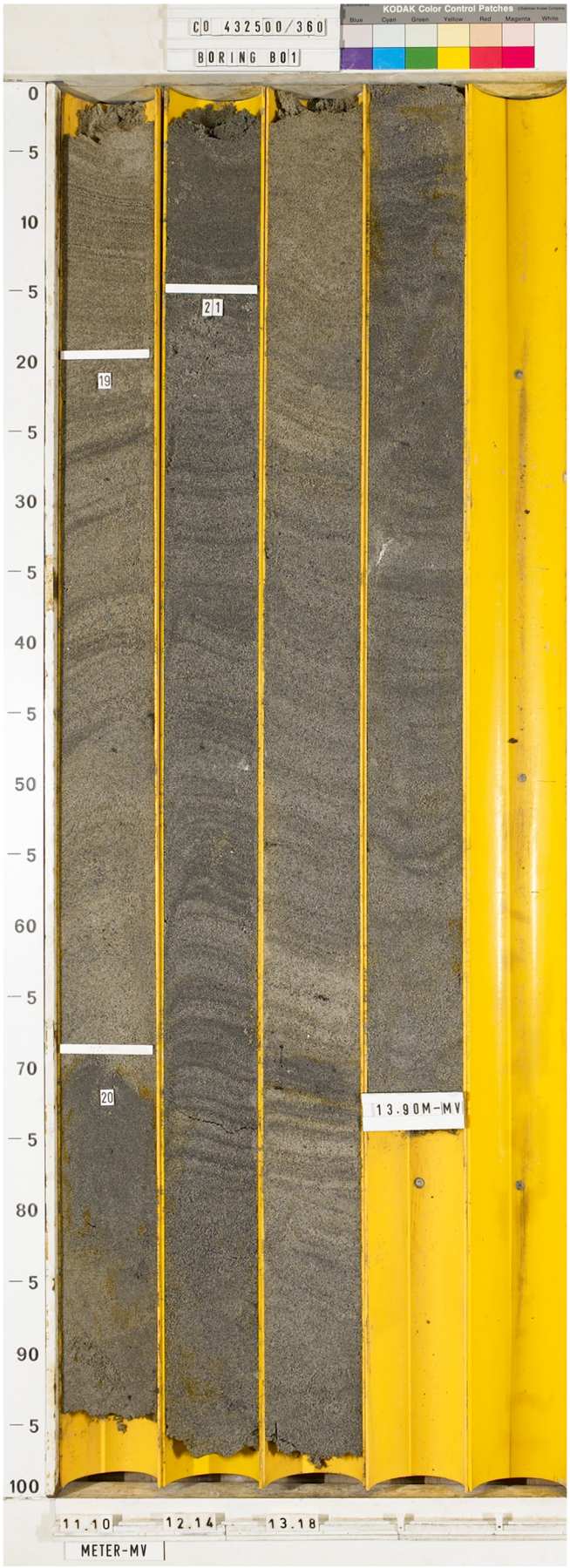

BESCHRIJVING: ZIE GETEKENDE VERSIE VAN BORING	Filenaam: B01bijS04A	Gewijzigd: 2008-12-18	Blad 2/2	

Deltares
Postbus 177 2600 MH Delft, Stieltjesweg 2, 2628 CK Delft
Telefoon (0)15 269 35 00 Telefax (0)15 261 08 21
www.deltares.nl info@deltares.nl

datum 2008-12-18	get. Mar	
Grondonderzoek Reeuwijk FC 2015 Reeuwijk	CO-432500/360	gez.
FOTO BORING B01 bij S04 Type: Begemannboring 66 mm	BIJL. BFB1	form. A4

*) Vrijgegeven door Hsd op 2009-01-05 08:44

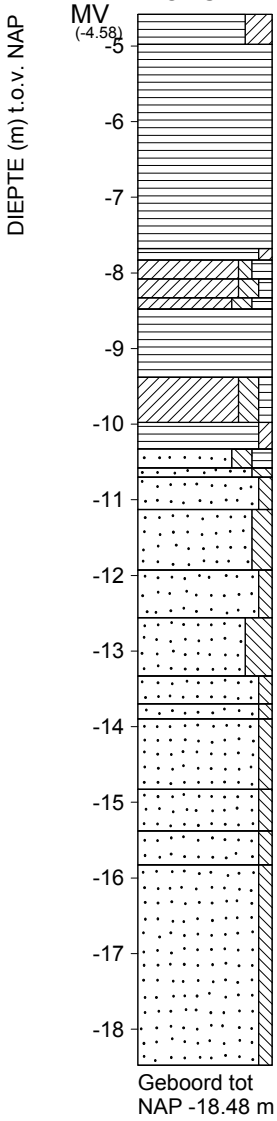

MONSTER	LAAG		VAN	TOT	BESCHRIJVING
1	1		-4.58	-4.98	VEEN, sterk kleiig
2	2		-4.98	-7.68	VEEN, mineraalarm
3 4 5 6	3		-7.68	-7.83	VEEN, zwak kleiig
	4		-7.83	-8.08	KLEI, zwak siltig, matig humeus
7	5		-8.08	-8.33	KLEI, matig siltig, zwak humeus Met plantenresten.
8 9	6		-8.33	-8.48	KLEI, matig siltig, matig humeus
10 11 12	7		-8.48	-9.38	VEEN, mineraalarm
13	8		-9.38	-9.98	KLEI, matig siltig, zwak humeus Met plantenresten en enkele veenlaagjes.
14	9		-9.98	-10.33	VEEN, zwak kleiig
15 16	10		-10.33	-10.58	ZAND, matig siltig, matig humeus ZM=0.150 mm
17 18	11		-10.58	-10.70	ZAND, matig siltig Enkele plantenrest. ZM=0.150 mm
19 20	12		-10.70	-11.13	ZAND, zwak siltig ZM=0.150 mm
	13		-11.13	-11.93	ZAND, matig siltig Met leemstukjes. ZM=0.125 mm
21	14		-11.93	-12.56	ZAND, zwak siltig Enkele grindstukjes, enkel leemstukje. ZM=0.350 mm
	15		-12.56	-13.33	ZAND, sterk siltig ZM=0.125 mm
	16		-13.33	-13.70	ZAND, zwak siltig ZM=0.210 mm
	17		-13.70	-13.90	ZAND, zwak siltig ZM=0.250 mm
	18		-13.90	-14.83	ZAND, zwak siltig ZM=0.300 mm
	19		-14.83	-15.38	ZAND, zwak siltig ZM=0.420 mm
	20		-15.38	-15.83	ZAND, zwak siltig ZM=0.175 mm
	21		-15.83	-18.48	ZAND, zwak siltig ZM=0.350 mm
					Einde Boring B01 bij S04 (Labbeschrijving)

X = 107238.38 m Y = 452370.59 m (RD)

Deltares Deltares
Stieltjesweg 2
2628 CK Delft
Telefoon +31-15-2693500
Telefax +31-15-2610821

datum 2008-08-26 | get. Hsd | gez.

Grondonderzoek Reeuwijk FC 2015
Reeuwijk

CO-432500/360

Begemannboring 66 mm B01 bij S04 (Labbeschrijving)

BIJL. BB1 | 24

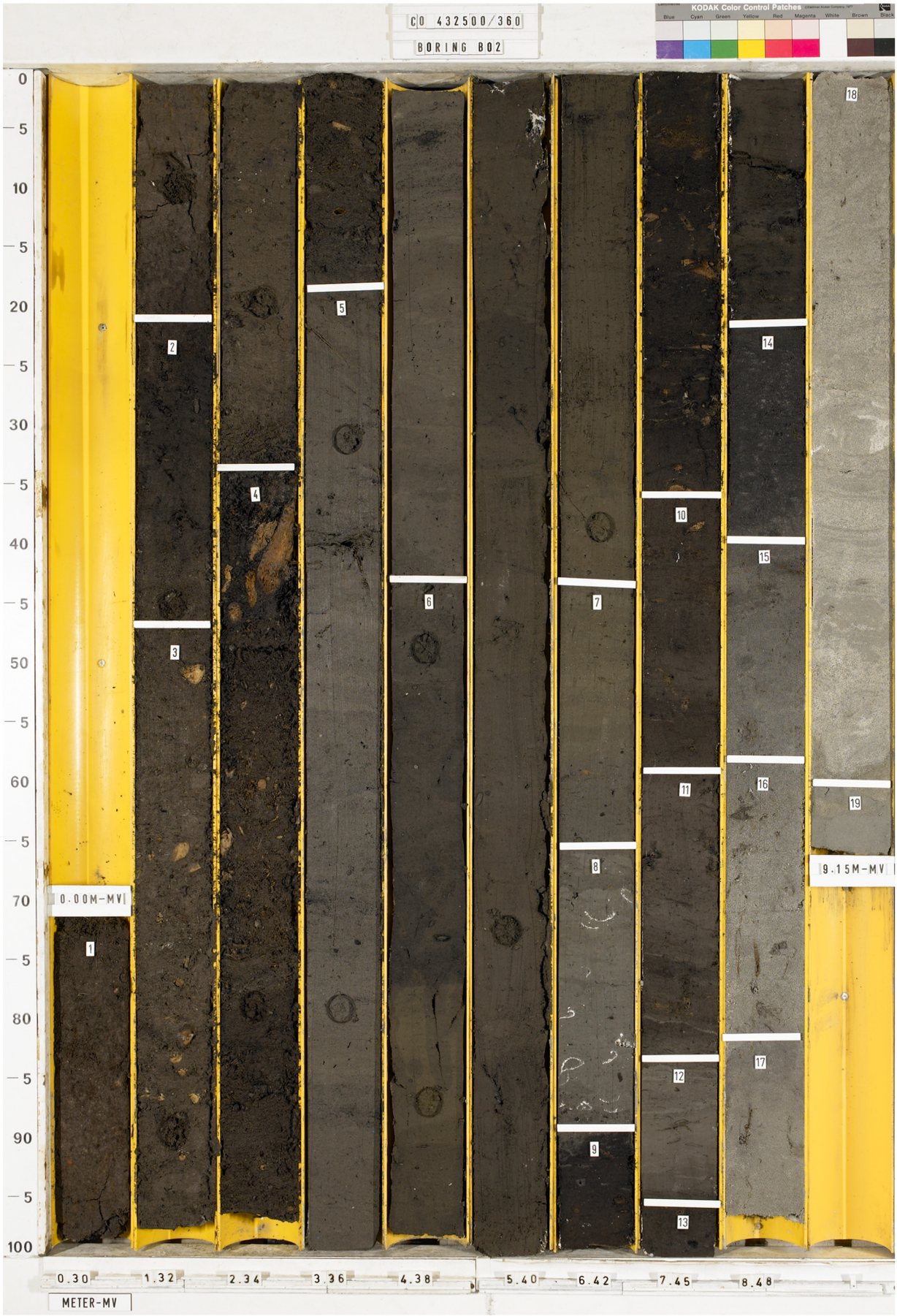

BESCHRIJVING: ZIE GETEKENDE VERSIE VAN BORING	Filenaam: B02bijS17	Gewijzigd: 2008-12-18	Blad 1/1

Deltares
Postbus 177 2600 MH Delft, Stieltjesweg 2, 2628 CK Delft
Telefoon (0)15 269 35 00 Telefax (0)15 261 08 21
www.deltares.nl info@deltares.nl

datum 2008-12-18	get. Mar	
Grondonderzoek Reeuwijk FC 2015 Reeuwijk	CO-432500/360	gez.
FOTO BORING B02 bij S17 Type: Begemannboring 66 mm	BIJL. BFB2	form. A4

*) Vrijgegeven door BjI op 2008-12-24 15:28

DIEPTE NAP [m]

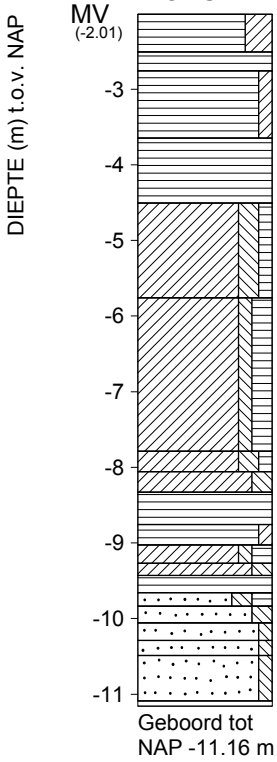

LAAG		VAN	TOT	BESCHRIJVING
1	1	-2.01	-2.51	VEEN, sterk kleiig Enkele puinstukjes.
2				
3	2	-2.51	-2.76	VEEN, mineraalarm
4	3	-2.76	-3.65	VEEN, zwak kleiig
	4	-3.65	-4.51	VEEN, mineraalarm
5	5	-4.51	-5.76	KLEI, matig siltig, zwak humeus Enkele plantenrest.
6	6	-5.76	-7.79	KLEI, zwak siltig, matig humeus Enkele plantenrest.
7	7	-7.79	-8.06	KLEI, matig siltig, zwak humeus Enkele plantenrest.
8				
9				
10	8	-8.06	-8.33	KLEI, matig siltig Met schelpresten.
11				
12				
13				
14	9	-8.33	-8.76	VEEN, mineraalarm
15				
16				
17	10	-8.76	-9.03	VEEN, zwak kleiig
18				
19	11	-9.03	-9.27	KLEI, zwak siltig, matig humeus Met plantenresten.
	12	-9.27	-9.43	KLEI, matig siltig Met plantenresten.
	13	-9.43	-9.66	VEEN, mineraalarm
	14	-9.66	-9.84	ZAND, matig siltig, matig humeus ZM=0.150 mm
	15	-9.84	-10.06	ZAND, matig siltig Enkele plantenrest ZM=0.150 mm
	16	-10.06	-10.29	ZAND, zwak siltig Enkele plantenrest. ZM=0.175 mm
	17	-10.29	-10.49	ZAND, zwak siltig ZM=0.125 mm
	18	-10.49	-11.09	ZAND, zwak siltig Enkele siltlaagjes. ZM=0.150 mm
	19	-11.09	-11.16	LEEM, zwak zandig
				Einde Boring B02 bij S17 (Labbeschrijving)

X = 107267.02 m Y = 452338.03 m (RD)

Deltares Deltares
Stieltjesweg 2
2628 CK Delft
Telefoon +31-15-2693500
Telefax +31-15-2610821

datum 2008-08-27 | get. Hsd | gez.

Grondonderzoek Reeuwijk FC 2015
Reeuwijk

CO-432500/360

Begemannboring 66 mm B02 bij S17 (Labbeschrijving)

BIJL. BB2 | A4

*) Vrijgegeven door Hsd op 2009-01-06 12:34

APPENDIX G

RSDYK2008 – THREE-DIMENSIONAL GROUND MODEL BASED ON BOREHOLES AND CPT

The borehole and cpt information has been used to develop a three-dimensional model of the subsurface of the Tempeldijk-South test area. Figure F-1 shows the location of the sections, and Figures 2 through 5 show the sections. Figure 6 shows the three-dimensional model. It should be noted that the reliability of the 3D model reduces significantly with a larger distance from boreholes and cpt's. On the following pages the surface grid is in UTM and the depth is with reference to NAP. The start and end points of the sections are given in UTM coordinates at the top of the section.

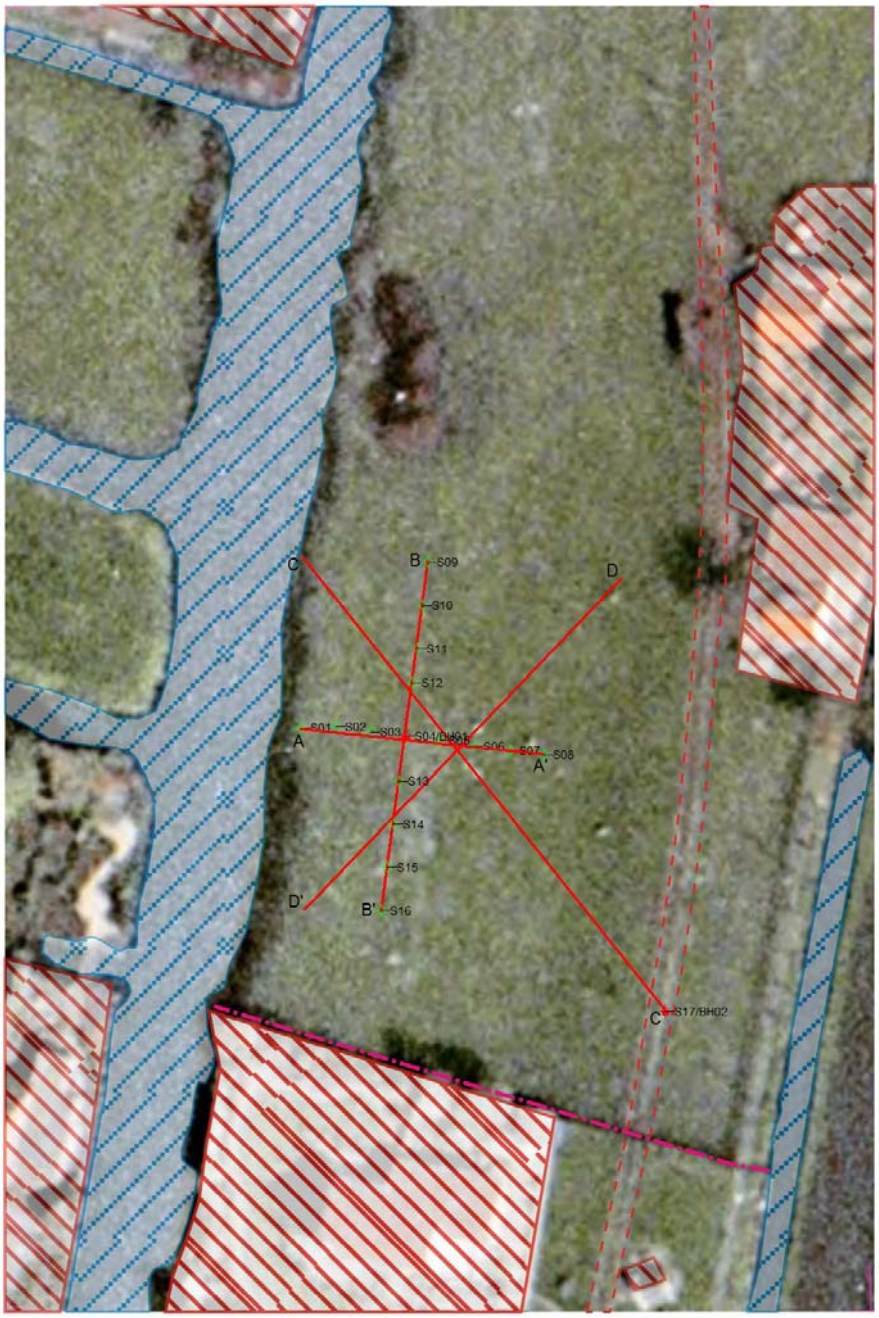

Figure 1. Location sections A-A', B-B'. C-C', and D-D'.

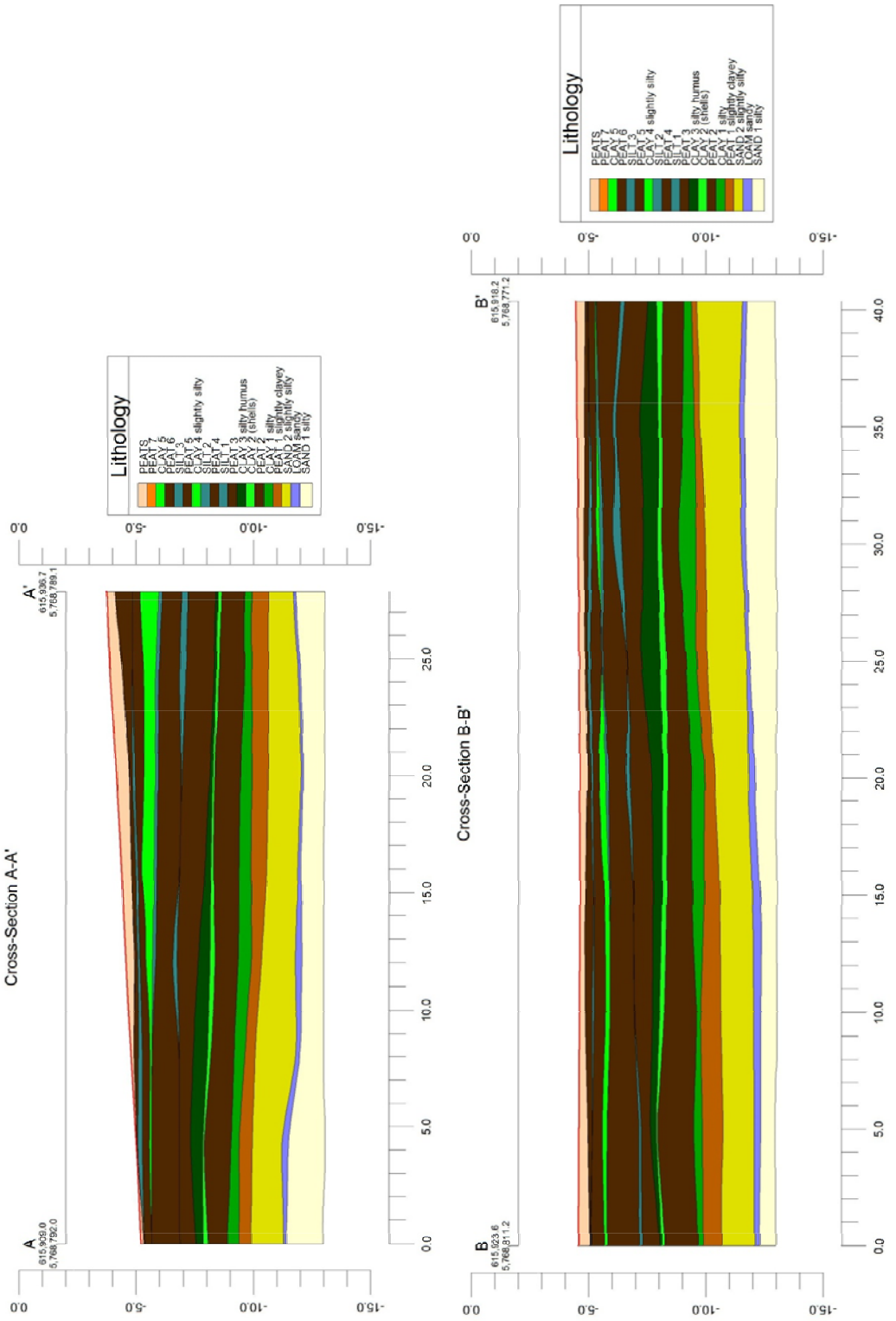

Figure 2. Sections A-A' (West-East) and B–B' (North-South).

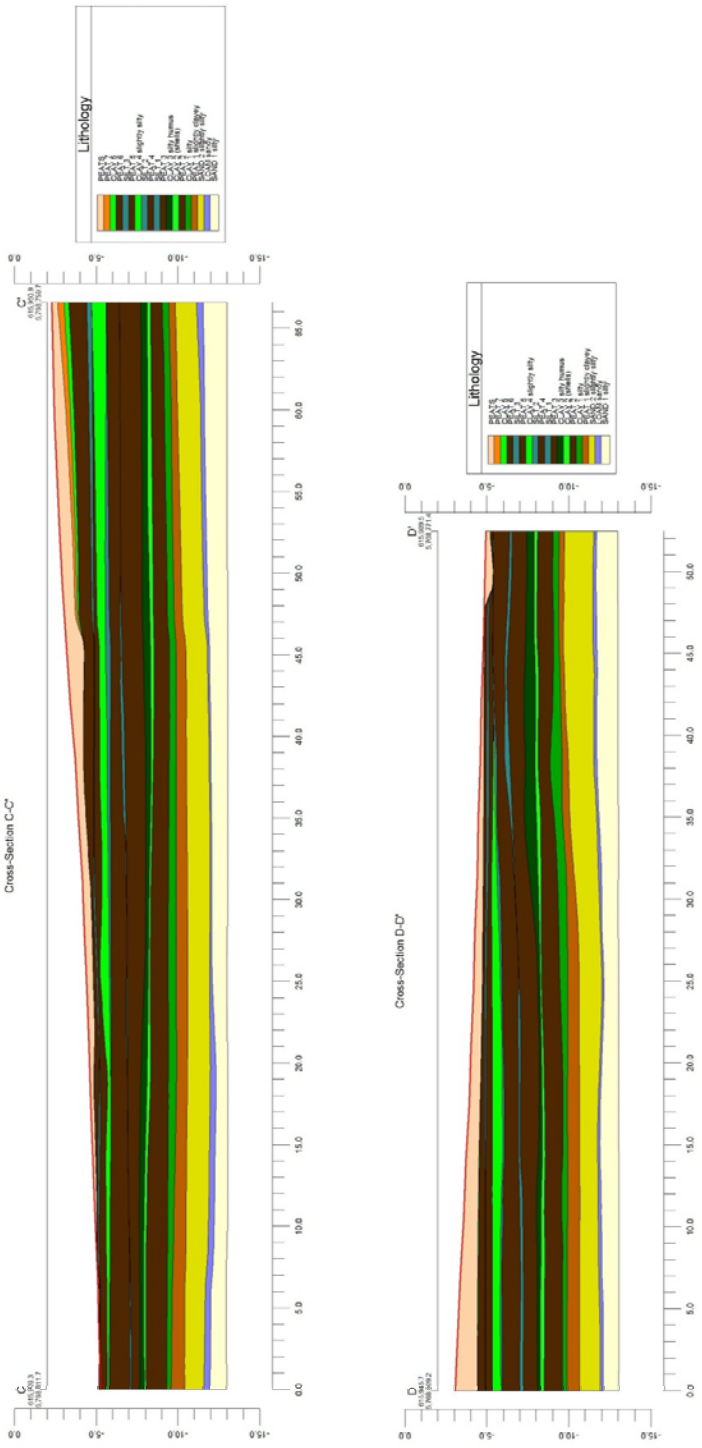

Figure 3. Sections C-C' (NNW-SSE) and D-D' (NNE-SSW)

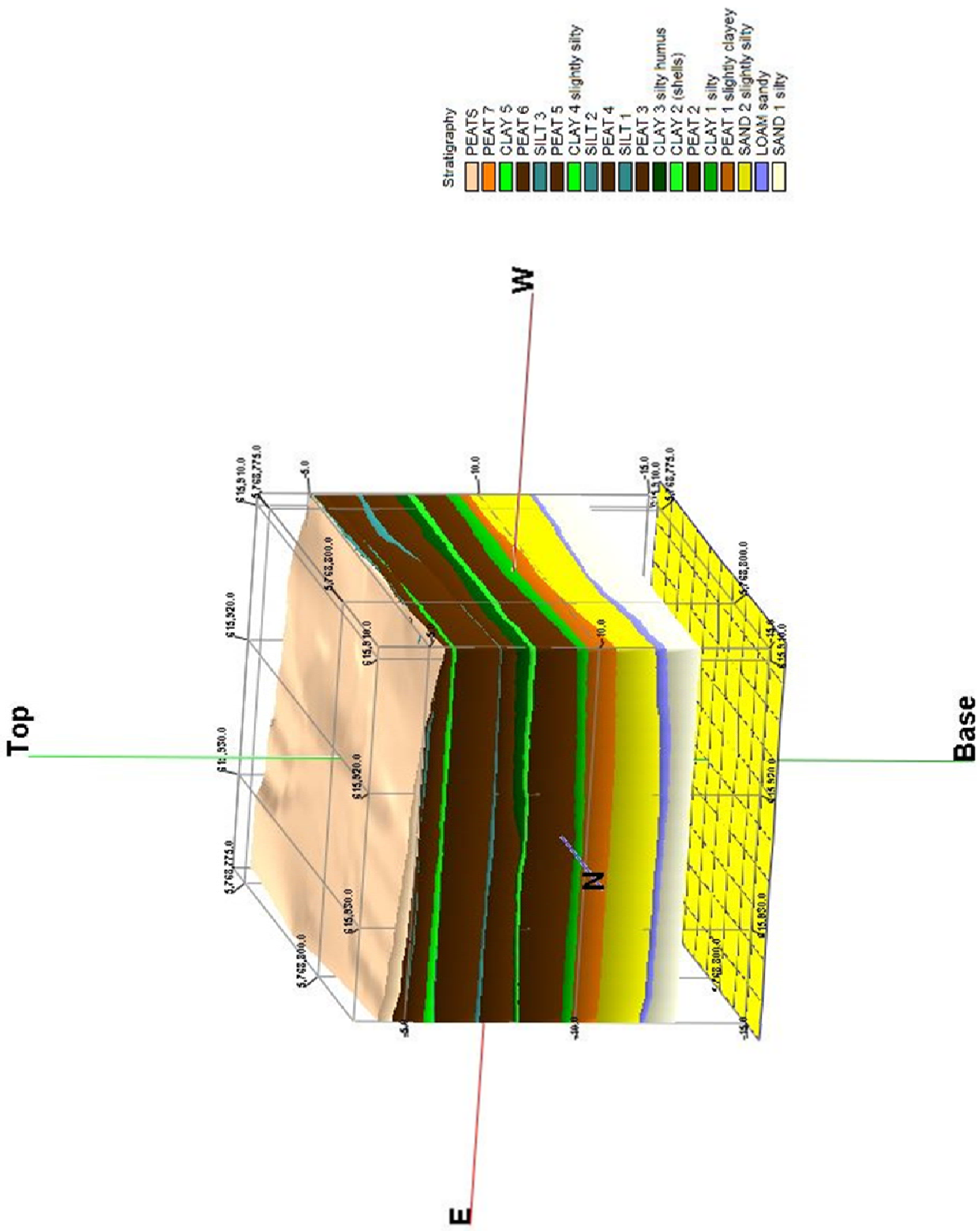

Figure 4. 3D model of the lithology

APPENDIX H

RSDYK2008 - ELECTRICAL RESISTIVITY IMAGING

Table of Contents

1 ELECTRICAL IMAGING

1.1 Introduction

In a uniform ground, there is no variation in the resistivity and it remains constant independent of electrode configuration. While if in-homogeneity exist in the subsurface, the resistivity will vary with the relative position of the electrodes. Heterogeneity of the resistivity in unconsolidated soils can be caused by:

- Different materials with a different resistivity in the subsurface (e.g. lithological variations, peat, clay, etc.),
- variation in the water content in the material in the subsurface, or
- non-homogeneity of the resistivity of the water (for example, salt or fresh water).

1.2 2D-measurements

A 2-D electrical imaging survey is usually carried out using a large number of electrodes connected to a multi-core cable. The typical setup for a 2-D survey with a number of electrodes along a straight line attached to a multi-core cable is illustrated in Figure 1. A computer operated "Sting R1/IP" has been used as measuring device. It is a single channel automatic resistivity imaging device with a multi-electrode system. It has a built-in set of command files for different electrode arrays. Typically, 28 electrodes are laid out in two strings of 14 electrodes, with electrodes connected by a multi core cable to a switching box and resistance meter (Figure 2). The electrode spacing has been 1 m.

1.2.1 TEMPELDIJK-NORTH

A 2-D electrical imaging survey was conducted. The survey line was along the crest of the dyke perpendicular to the imaging direction. The length of the survey line was 27 m, which is enough to obtain information down to about 3 m depth

1.3 Interpretation

Schlumberger, Wenner and dipole-dipole configuration arrays have been used to identify the best electrode configuration. The tests were done on the Tempeldijk-North and South locations. Figure 3 shows an example of the results. The upper 3-5m depth of the dyke consists of clay, peat and some thin more silty layers. Compared to clay, peat has a much higher porosity and ability to hold water under natural (unloaded) conditions. The higher fluid content of the peat causes the peat layer to be more conductive than the clay layer. Therefore, following the 2-D electrical imaging results, the top part of the dyke with a relatively high resistivity value is classified as clay and the lower resistivity in the lower part of the pseudo-section is classified as a peat.

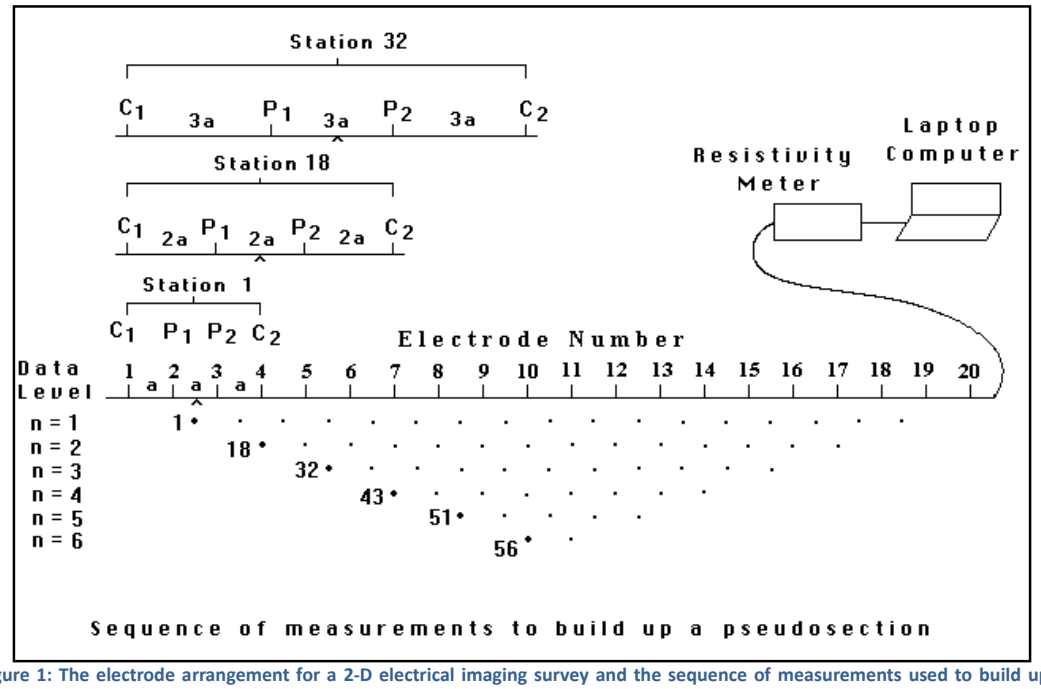

Figure 1: The electrode arrangement for a 2-D electrical imaging survey and the sequence of measurements used to build up a pseudo-section (Loke M.H., 2000).

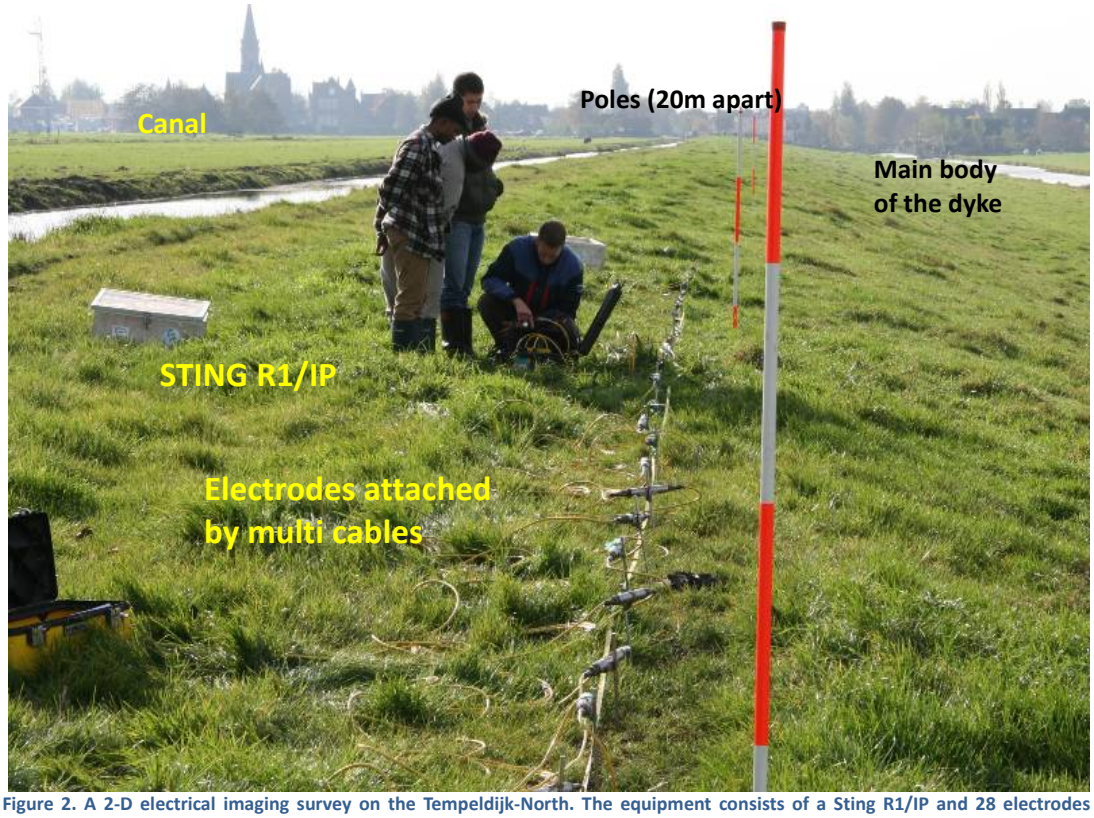

Figure 2. A 2-D electrical imaging survey on the Tempeldijk-North. The equipment consists of a Sting R1/IP and 28 electrodes having a 1 m spacing laid out in two strings of 14 electrodes.

1.4 Advantages and disadvantages of the three arrays

In 2-D imaging surveys, the electrode setups “Schlumberger”, “Wenner” and “dipole-dipole” are the electrode arrays that are the most commonly used. The choice of the “best” array for a field

survey depends on the type of structure to be mapped, the sensitivity of the resistivity meter and the background noise level. The Wenner array is relatively sensitive to vertical changes (i.e. horizontal structures) in the subsurface resistivity below the centre of the array. However, it is less sensitive to horizontal changes (i.e. narrow vertical structures) in the subsurface resistivity. The dipole-dipole array is most sensitive to resistivity changes between the electrodes in each dipole pair and the sensitivity contour pattern is almost vertical. This array is therefore very sensitive to horizontal changes in resistivity, but relatively insensitive to vertical changes in the resistivity. Unlike the above arrays, the Schlumberger array is moderately sensitive to both horizontal and vertical structures. In areas where both types of geological structures are expected, this array might be a good compromise between the Wenner and the dipole-dipole array.

1.5 3D Resistivity imaging

As the 2D surveys were suspected to be erroneous due to the three-dimensional variation of the surface and the layers in the subsurface, three-dimensional surveys have been done. In this pilot project only the survey for Tempeldijk-South section has been included. Two-dimensional sections based on a three-dimensional survey are shown in Figure 5 and 6. The location of the sections is indicated in Figure 4. The exact locations of the sections are indicated in the sections with the surface grid in UTM and depth is with reference to NAP.

The sections are plotted together with lithology sections based on the three-dimensional lithology model to allow comparison of the results. For a discussion on the results see the main text of this report.

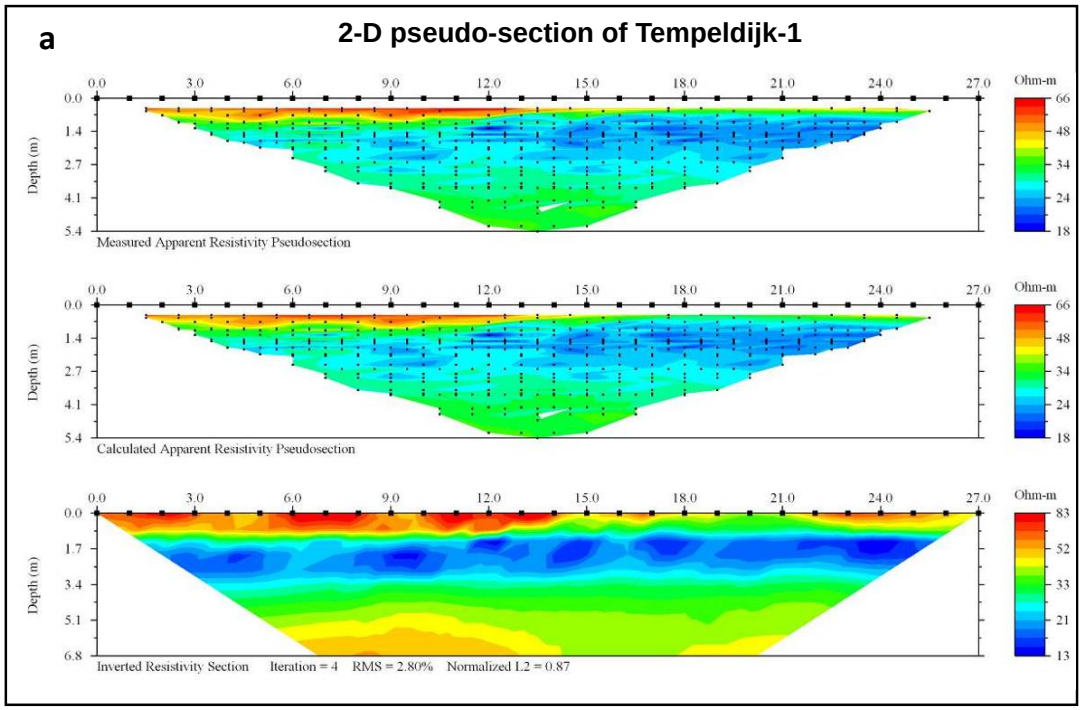

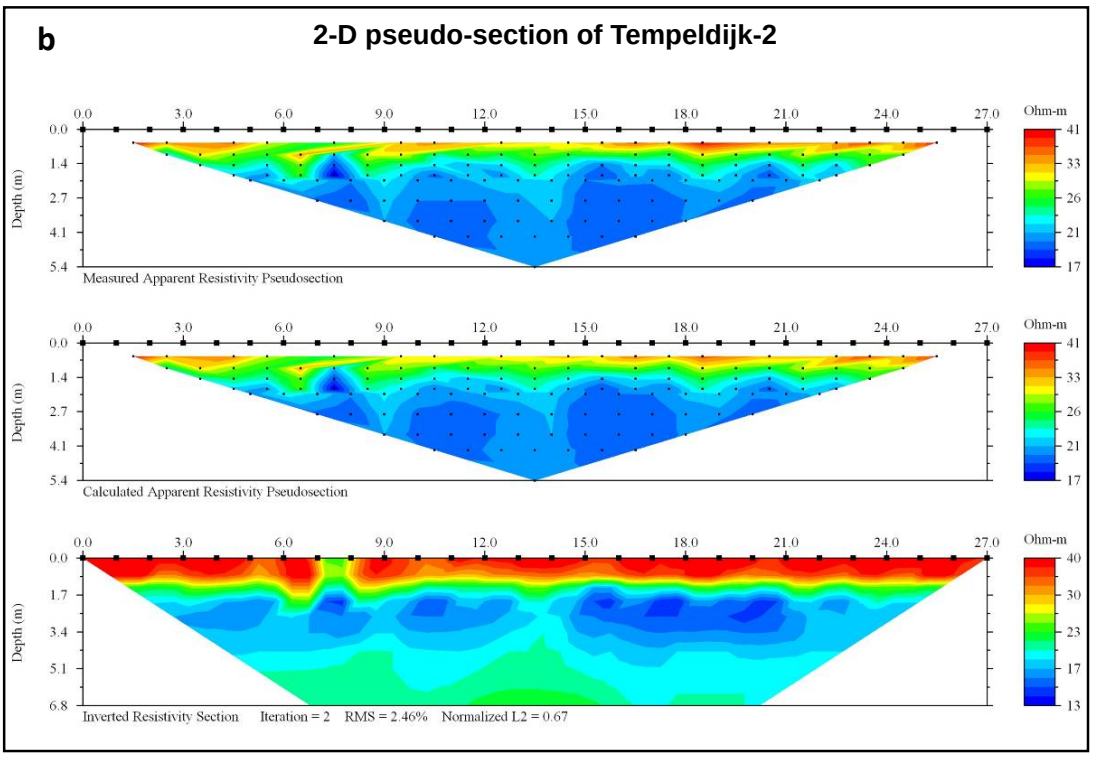

Figure 3. The 2-D pseudo-sections show the higher resistivity value of clay on the top of the peat layer for (a) Tempeldijk-1 and (b) Tempeldijk-2 (Tempeldijk 1 is Tempeldijk-North and Tempeldijk-2 is Tempeldijk-South location). The section for Tempeldijk-North is based on the combination of three configuration arrays and Tempeldijk-South is based only on the Schlumberger configuration array.

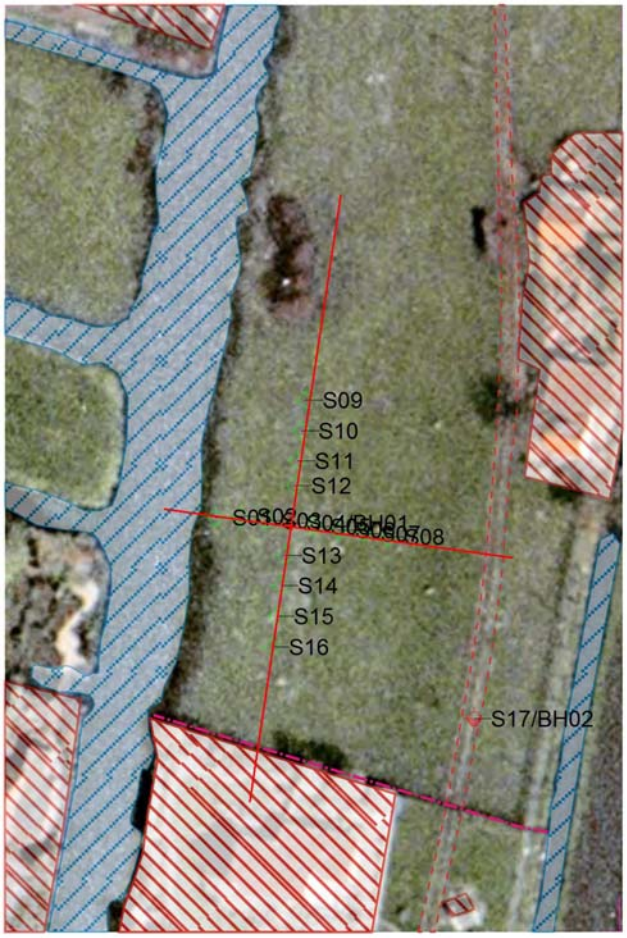

Figure 4. Tempeldijk-South location; electrical resistivity sections based on three-dimensional survey; North South (Figure 3) and West-East (Figure 4).

Tempeldijk-South three-dimensional resistivity sections

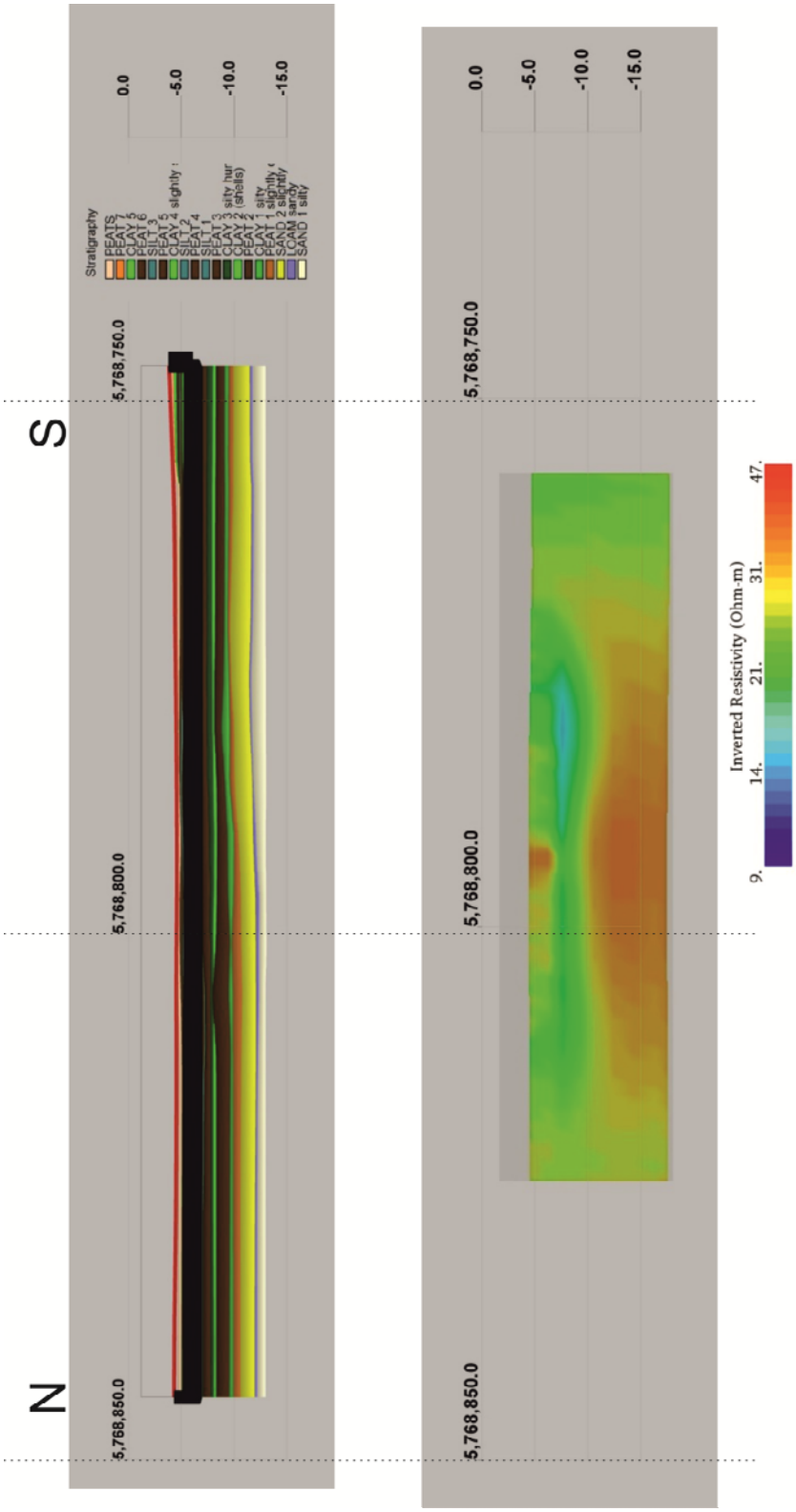

Figure 5. North-South lithology (left) and resistivity (right) sections.

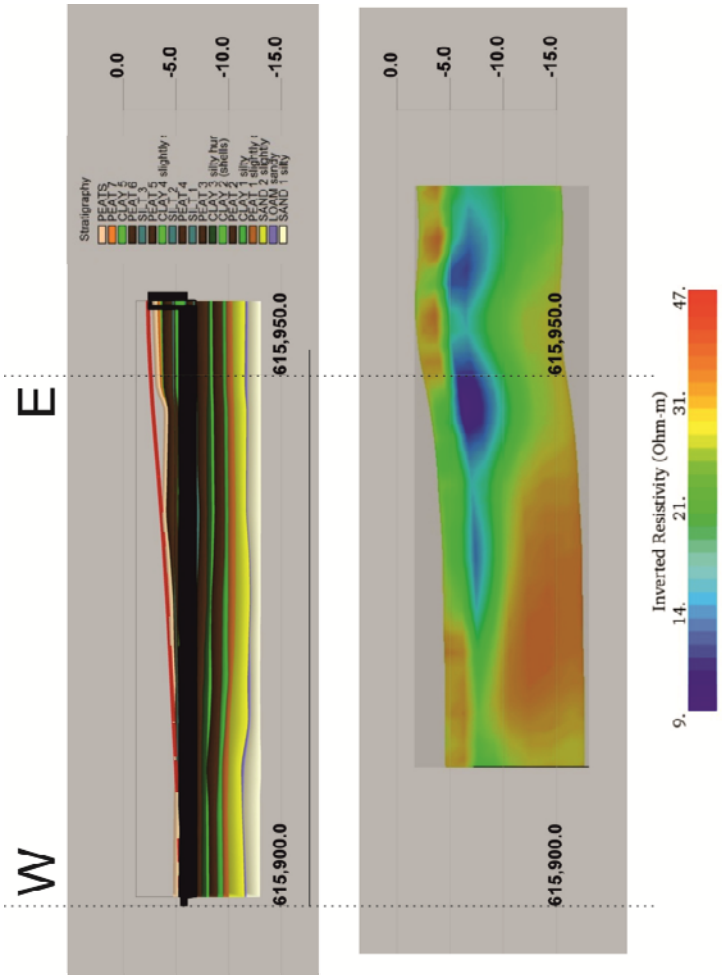

Figure 6. West-East lithology (left) and resistivity (right) sections.

APPENDIX I

RSDYK2008 – REMOTE SENSING

Contents

1 DATA COLLECTION

Terrestrial remote sensing is used to acquire field images of three selected sites on two dykes in Reeuwijk, The Netherlands. For this research, the locations are named Vreesterdijk, Tempeldijk-North and Tempeldijk-South (for location maps and images is referred to appendix D and Figure 1). Multi-temporal thermal infrared (TIR), near infrared (NIR) and visual images of the three sites have been collected in different seasons over 2007 and 2008. The physical condition of the sites during the field campaigns is described below.

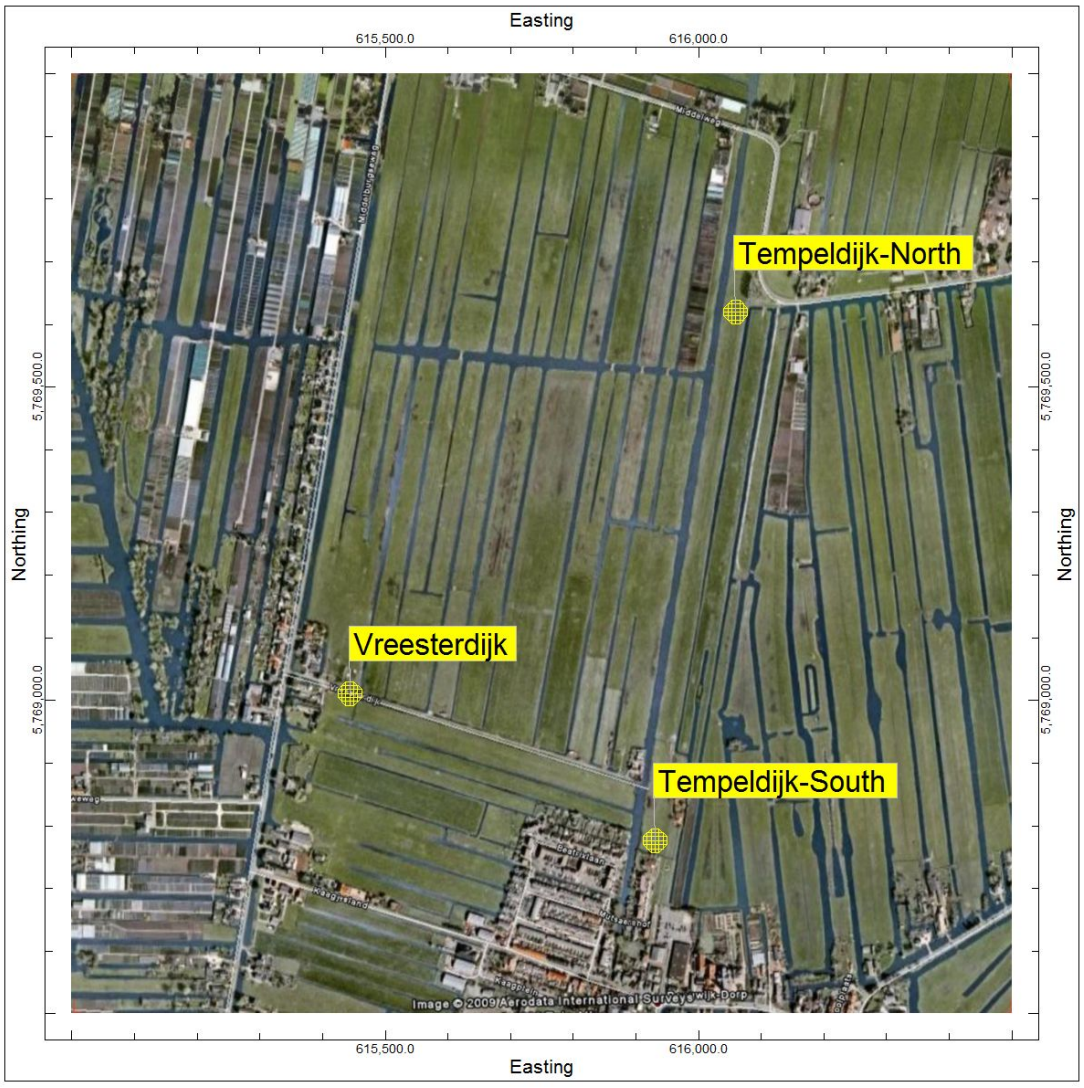

Figure 1. Location of the three dyke sites in Reeuwijk (from Google Earth)

1.1 Vreesterdijk

The Vreesterdijk is located in the area where peat has been excavated and consists of a road on an embankment of non-excavated peat. The structure of the dyke is not known in detail, but is assumed to consist of in-situ peat in the lower part. Likely, the dyke has been covered by road pavement materials many times and is covered by tar layers at present. The extent in depth of the layers is unknown. The dyke does not function as boundary for a water canal, but as a local division dyke (dam) in the excavated area, and as an access road to a farm.

1.1.1 REMOTE SENSING

Images of visual, Thermal InfraRed (TIR) and Near InfraRed (NIR) were taken oblique from a distance of about 50 m. Taking images perpendicular to the dyke was not possible due to cattle and a fence around a cattle field. The location where the images have been taken is above the top of the dyke. The dyke is about 200 m long and has a height of 1.5 m. Long grass fully covered the dyke materials as well as the water in the ditch during the first field campaign (Figure 3a). Some of the grass was dried out. The grass was removed a few days before the second field campaign. This exposed the topsoil of the outer layer materials of the dyke in parts of the dyke (Figure 3b). In December, the degree of exposed topsoil reduced due to the newly grown grass and due to the increase in the height of the grass as compared to the height of the grass in October (Figure 3c). During the first two field campaigns, the position of the sun was nearly perpendicular to the imaging direction while in December it was almost towards the lens of the camera.

1.2 Tempeldijk

The Tempeldijk is the boundary between a high-laying in-situ peat deposit area where the peat has not been excavated and a low-laying area where the peat layer has been excavated. The dyke functions as a dyke (e.g. dam – “boezem kade”) for a de-watering canal. Two test sites were selected; one on both ends, e.g. Tempeldijk-North and Tempeldijk-South (originally these were named Tempeldijk-1 and Tempeldijk-2. As this caused confusion names have changed to more location specific names of Tempeldijk North and Tempeldijk-South).

1.3 Tempeldijk-North

1.3.1 REMOTE SENSING

At Tempeldijk-North images were acquired over 80 m length. Poles for marking and referencing the images were set every 20 m. The images were acquired from the low-laying area, perpendicular to the dyke at a distance of 24 m from the top. The cameras were placed about every 10 m parallel to the poles. The images were taken about 1.65-1.75 m above the ground. In order to obtain directionally geo-referenced images, the imaging was taken from the same position in all survey campaigns.

In August images were taken with a clear sky. The grass was quit green with less apparent surface roughness (Figure 4a). In October, the sky was bright and the sun perpendicular to the imaging direction. The apparent roughness of the grass was larger than in August and in some areas the grass was dried out. Some of the grass was long enough to create its own shadow (Figure 4b). During the third field campaign in December, differences in the apparent roughness of the grass were observed. The position of the sun was towards the lens of the camera (Figure 4c). Direct sun was not allowed to enter the lens of the camera. The main part of the dyke was affected by its own shadow in December.

1.4 Tempeldijk-South

1.4.1 REMOTE SENSING

At Tempeldijk-South images were acquired over 100 m length. Poles for marking and referencing the images were set every 20 m. The images were acquired from the low-laying area, perpendicular to the dyke at a distance of 33 m from the top. The cameras were placed about every 10 m parallel to poles. The images were taken about 1.65-1.75 m above the ground. This is similar to the Tempeldijk-North location, only the larger distance increased the area covered by per image (Figure 2).

The apparent surface roughness of the grass was almost similar over the dyke during the first field campaign. Some dried out grasses were observed in the middle of the dyke (Figure 5a). Physical change especially in the apparent roughness of the grasses was noted in the second (Figure 5b) and third (Figure 5c) field campaigns. In all seasons, images were taken in sunshine. In December the position of the sun was at some angle to the lens of the camera and the topsoil of the dyke materials was exposed in some part of the dyke.

In Figure 6 a stitched photo mosaic is included showing the full length of the test site. Please note the presence of small yellow flowers in the center part of the image.

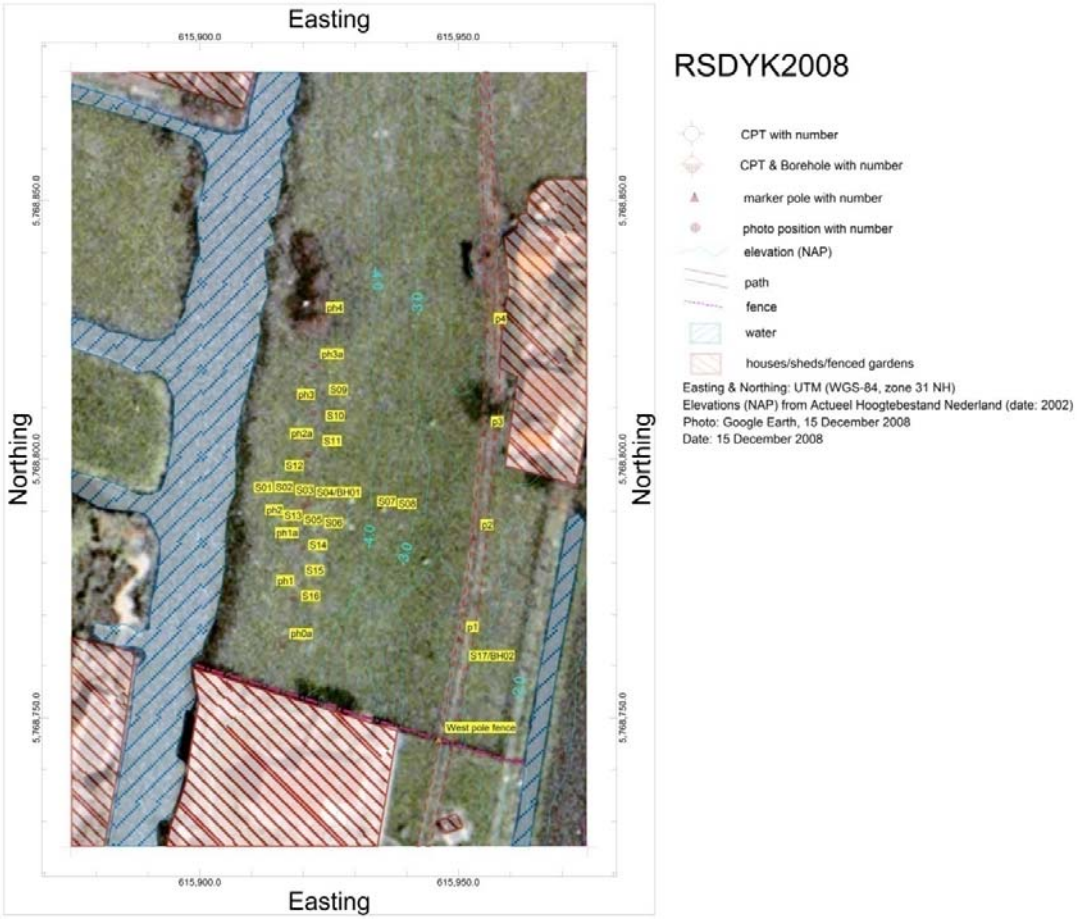

Figure 2. Tempeldijk-South location; layout of marker poles and photo positions.

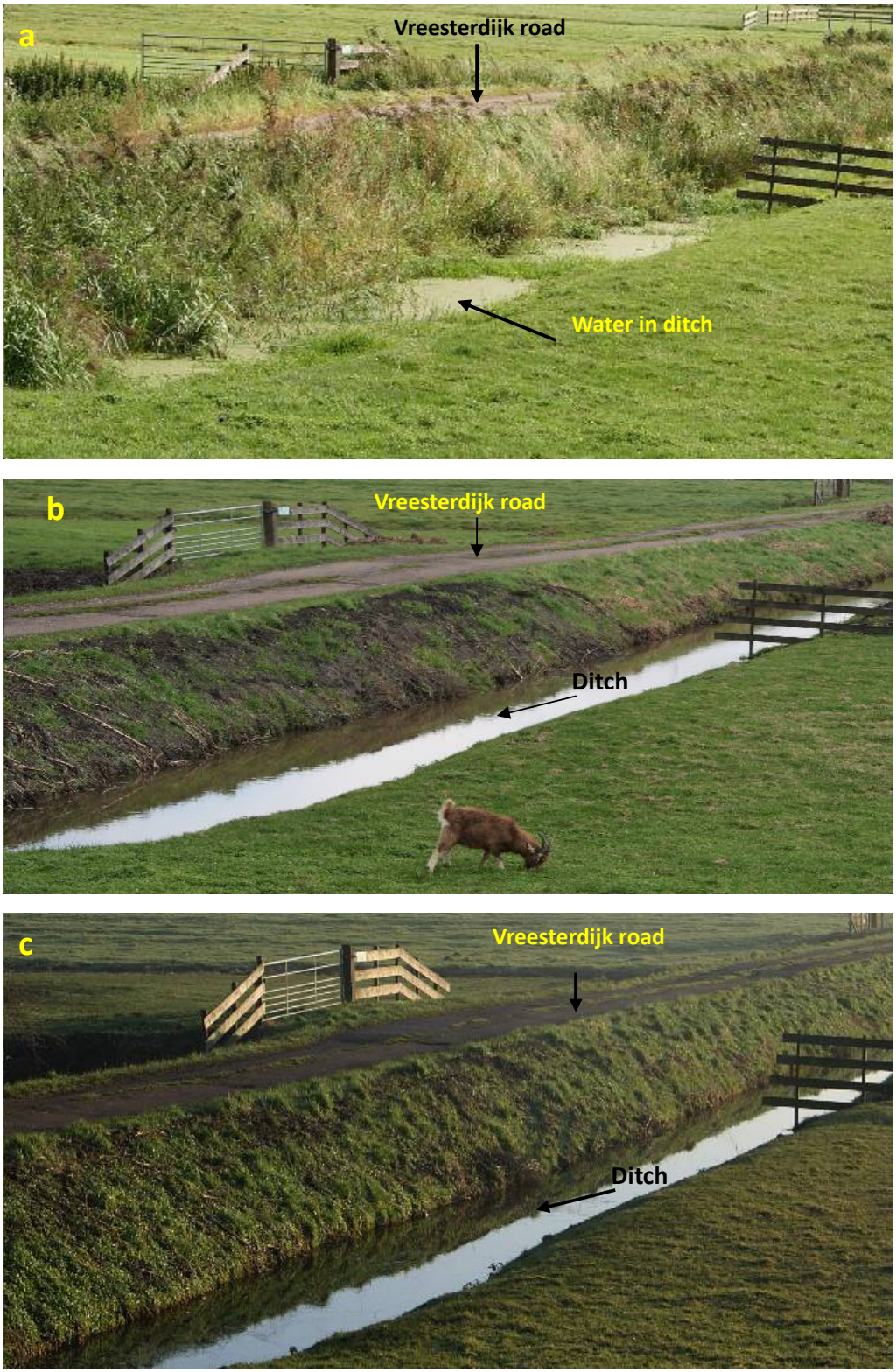

Figure 3. Visual images of Vreesterdijk shows the change in physical condition during the August 15, 2007 (a), October 31, 2007 (b) and December 13, 2007 (c) field campaigns.

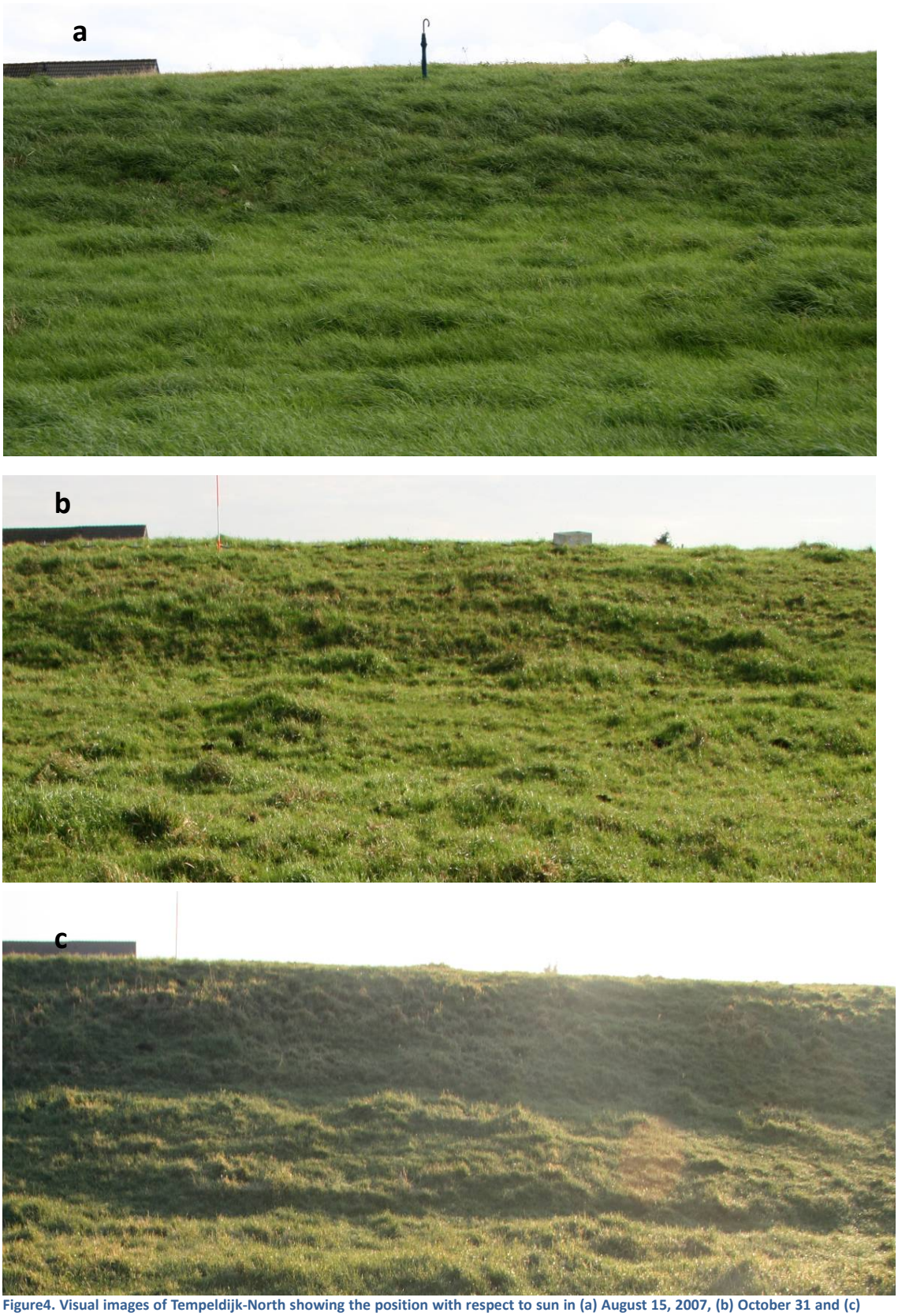

Figure4. Visual images of Tempeldijk-North showing the position with respect to sun in (a) August 15, 2007, (b) October 31 and (c) December 13, 2007 field campaigns.

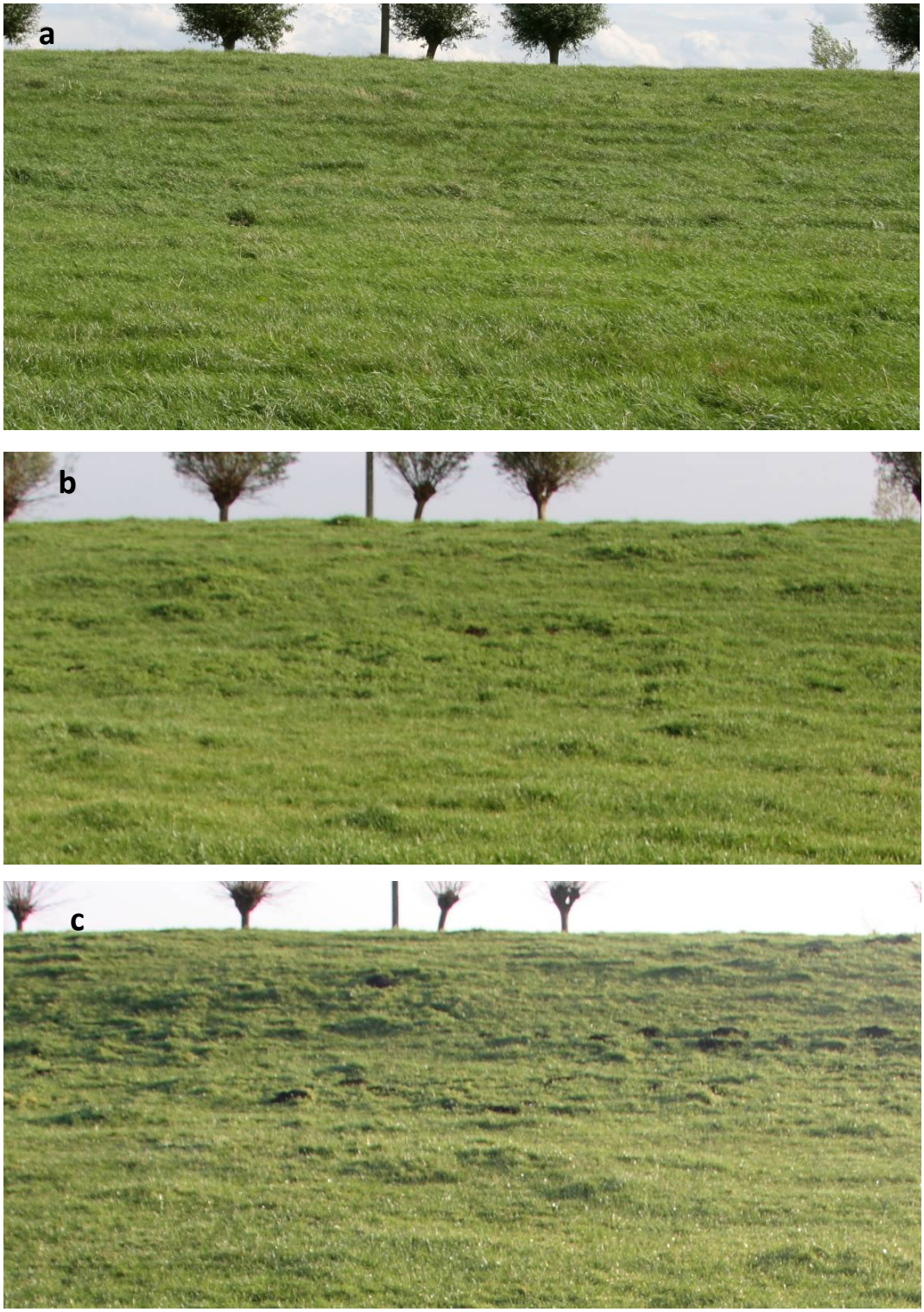

Figure 5. Visual images of Tempeldijk-South showing the difference in the apparent surface roughness in (a) August 15, 2007, (b) October 31, 2007 and (c) December 13, 2007 field campaigns.

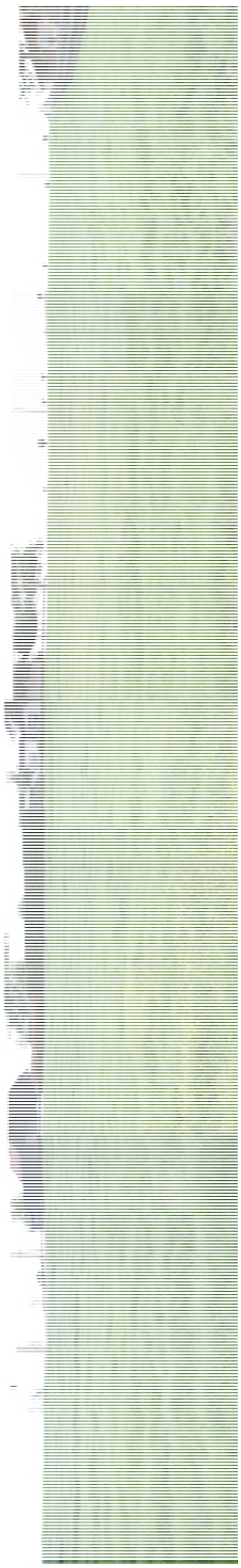

Figure 6. Stitched photo mosaic of Tempeldijk-South test site. Photo direction perpendicular to the dyke in about Eastern direction. The black lines indicate the pole positions (see location map Figure 2).

1.5 Terrestrial imaging using infrared remote sensing

1.5.1 THERMO TRACER TH9100PRO

The thermal camera that has been used for imaging the thermal radiation is a NEC Thermo Tracer TH9100Pro (Figure 7), which has a spectral range of 8 to 14 µm, a resolution of about 0.04^{o}C, and a focusing range from 30 cm to infinity. The pixel size of the thermal image is about 1.2 mm at a distance of 1 m and 1.2 cm at a distance of 10 m and the size of each image was 320 X 240 pixels (see Appendix-B for the specification of the camera). As described in section 4.1, the distance of imaging for the three sites is not the same, which means the images of these sites have different resolutions. For instant, the resolution for images of Tempeldijk-1 is 2.88cm while images of Tempeldijk-2 have 3.96cm.

On the screen of the camera, an image of the dyke surface is displayed with temperature values represented by different colours. In a grey-scale colour scheme the warmer areas becomes bright/white and colder areas become darker. The radiant flux emitted from a surface is received by the detector and converted into an image which pixel values are radiometric temperatures. This camera has a built-in automatic continuous calibration to a blackbody and the option to define emissivity values. The range of emissivity for ground components for soil and vegetation varies at a given wavelength according to their physical properties and water content (Fuchs and Tanner 1966, Van de Griend et al. 1991).

Figure 7. The thermo trace TH9100pro TIR camera used to map the emitted temperature of the dyke materials (photo taken during the summer field campaign).

1.5.2 ADC MULTISPECTRAL CAMERA

The Agricultural Digital Camera (ADC) (Figure 8) is a multispectral camera designed for agricultural and vegetation purposes. It takes images in the range of red to near-infrared of the electromagnetic spectrum (0.52 to 0.95 µm). The size of each image is 1280 x 1024 pixels.

Figure 8. ADC multispectral NIR camera used to map the reflectance variation of the grass that covers the dyke materials (source: the Tetra cam web site)

1.6 IMAGE PROCESSING

1.6.1 SAMPLING

Items such as trees, houses, main-power poles, the sky and roads are included in the images. These items have a great influence on establishing relationships between the multi-temporal TIR and NIR images. Figure 9 shows the distribution of the population in one of the near infrared images of the Tempeldijk-South dyke. The sky has the higher reflectance with DN-values of 100-200 and with a high number of pixels up to 20,000 (Figure 9a). For the dyke surface, the reflectance value ranges between 30 to 100 and the number of pixels is up to 9000. In order to avoid this influence and to make the images with one entity (e.g. the dyke material), sampling is very important. Sampling is obtained based on the best fitting and most changes were observed in both the NIR and TIR images of the dykes. The dimension of the sampling areas is not similar for all dykes. 271 X 62, 306 X 108, and 308 X 108 pixels with a 0.1-pixel size are used for the Vreesterdijk, Tempeldijk-North, and Tempeldijk-South sites respectively. After sampling the dyke material becomes normally distributed and stretched throughout the range between 0 and 255 (Figure 9b). The above sample areas are made for the whole dyke material; however, a further sampling was made on areas where most changes occur between the different survey campaigns. The pixel size is the same in all sample areas, which is 0.01. This was done in the GIS and MATLAB environment and the images are typically assigned a colour map emphasizing the difference in the objects temperature and reflectance value.

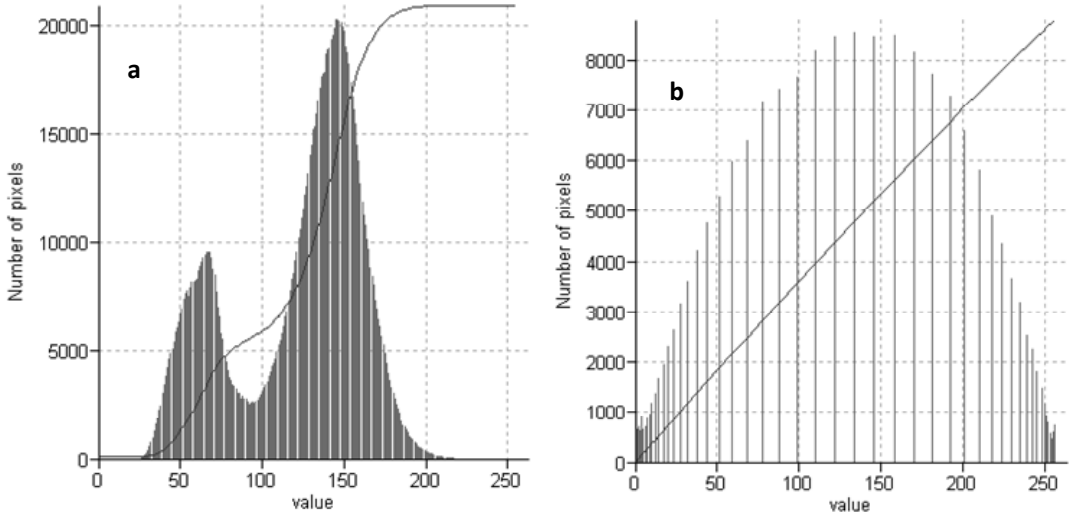

Figure 9. Histogram distribution of the near infrared image of Tempeldijk-South taken in October 2007 (a) the whole area and (b) the sampled area that is stretched to the 256 DN-value

2 IMAGE INTERPRETATION AND ANALYSES

This section describes the qualitative and quantitative analysis made on the remotely sensed images. The quantitative analysis is focusing on evaluating the relationship between the multi-temporal thermal infrared (TIR) as well as near infrared (NIR), which was done using MATLAB programming software.

2.1 Thermal imagery in different seasons

2.1.1 INTRODUCTION

The variation of the emitted temperature of any material is mainly depending on what is happening at its atomic level. Different materials can have widely different emissivity values within the range of 0 to 1. The pixels of the thermal images are represented by radiation temperature values of the ground. Unlike remote sensing of reflected light from surfaces in which only the topmost layer is involved, thermal remote sensing includes energy variations extending to varying shallow depths below the ground surface. During a single daily (diurnal) cycle, the near surface layer of unconsolidated soils experience alternate heating and cooling to depths typically between 0.5 and 1 m. Since, there is a limited difference in the absorbance and emissivity property of a homogenous material, the spatial distribution of the radiation temperature of such media is expected to be the same. However, the TIR images of all seasons show a variation in the spatial and temporal distribution of the radiation temperatures.

As discussed before the sites are covered by grass except in some part of the Vreesterdijk during October and December. This implies that the radiation temperature values are the resultant of emitted temperature from the topsoil of the dyke materials and the grass. It is difficult to establish how much of this resulted from the grass compared to that from the topsoil. The variation in the radiation temperature of the grass is mainly related to the accumulation of the rainfall water. The radiation is also influenced by fallen debris from the grass (dead leafs), the water content in the soil, the apparent roughness, variation in color, and the position with respect to the sun. For example, darker objects absorb and emit more than the lighter coloured objects. The same is true for the surface roughness: the greater the roughness (compared to λ), the greater the surface area, the greater the emission. Therefore, the darker and the higher the surface roughness can be indicated by higher temperature values in the thermal images. In this study the colour and the surface roughness are mainly related to the position of the sun angle, some exposed soils and to the grass that covers the dykes. The radiation temperature variation of the dyke materials is mainly related to the compositional variation of the soil, the seasonal variability of water content in the soil and to the presence of subsurface voids/cracks and therefore can probably be related to the geotechnical properties of the dyke materials.

The interpretation and analysis was done based on the spatial and temporal variations of the radiation temperature from the multi-temporal TIR images. These variations are further related to the geotechnical properties mainly to the distribution of moisture content of the topsoil. This is because soil moisture is one of the most important geotechnical parameter affecting surface stability in soil structures.

2.1.2 VREESTERDIJK

The images of this dyke have been acquired oblique. This angle was corrected by rotating the sample images of the TIR and NIR by 11.8^{o} (used this angle to rotate the dyke in to a horizontal position) to perform further statistical analysis. The original pixel information remains the same.

The material of the dyke is likely peat but details are not known. The removal of the grass between August and October makes the TIR images difficult to compare. The sampled images of the dyke are shown in Figure 10. During the summer field campaign, the height of the grasses that fully covered the dyke materials was above 0.5 m (Figure 10a). This implies that the radiation temperature resulted mainly from the emitted temperature of the grass rather than from the dyke material. The relatively dry grass (yellowish) show higher radiation temperatures than the green grass (Figure 10a). The TIR image of October shows high radiation temperatures for the exposed topsoil of the dyke and low on places that covered by grass (Figure 10b). The relatively dry part of the dyke materials are indicated by higher value (above 8^{o}C). The low values can be related to the moisture content of the grass as well as to the shadow effect of the grass on the dyke materials. In December a similar result was obtained from the TIR image (Figure 10c) as in October. The scatter plot (Figure 11) shows the radiation temperatures of October versus December. Establishing a relationship between the thermal images of August with the other two seasons is not useful due to the different grass heights. The range of the radiation temperature in relation to the atmospheric temperature is presented in Table 1.

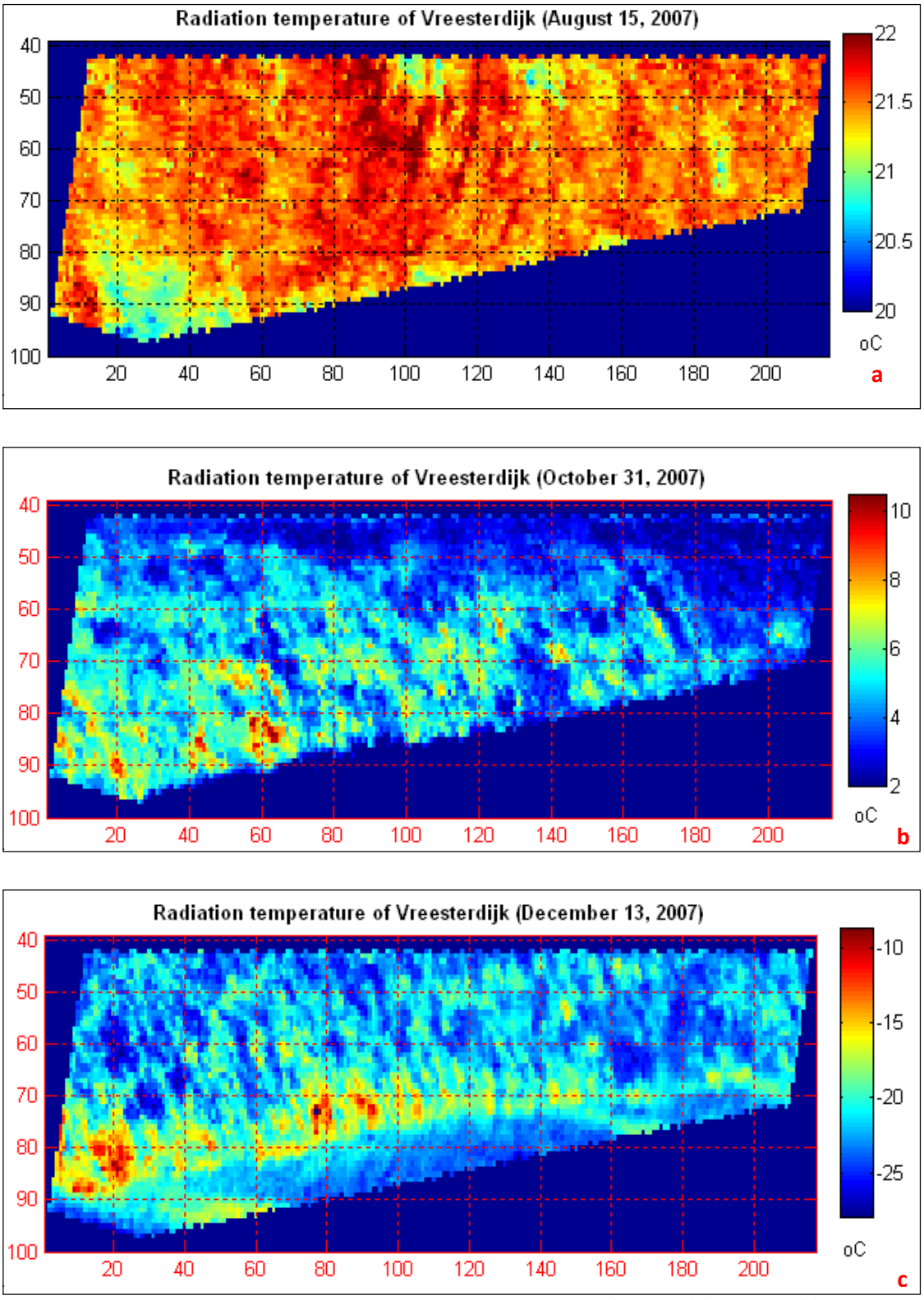

Figure 10. The spatial and temporal variation in the thermal images of the Vreesterdijk in (a) August, (b) October and (c) December. The gridding scale is based on the row and column number of the images.

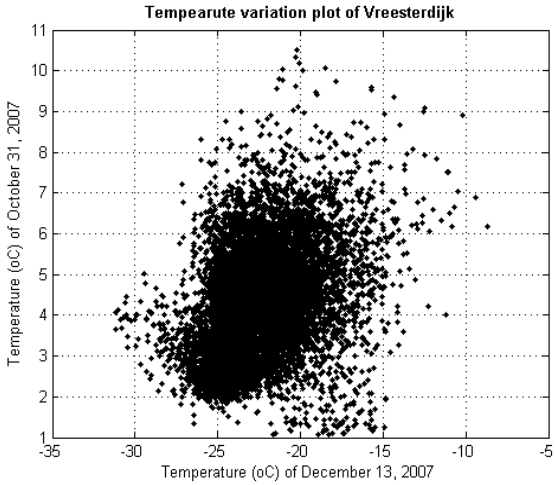

Figure 11. Scatter plot of the radiation temperature of October versus December.

Table 1. Surface and radiometric temperature of Vreesterdijk

Imaging period	Mean Atmospheric temperature	Radiation temperature of the dyke	Humidity
August 15, 2007	25°C	20 – 22°C	80%
October 31, 2007	12.5°C	1 – 8°C	87%
December 13, 2007	1°C	-31 – -15°C (*)	95%

(*) the temperatures do not reflect the real material temperature, but only a radiation temperature.

2.1.3 TEMPELDIJK-NORTH

The mean atmospheric temperature during the field campaigns was the same for all sites. However, the values of the radiation temperature of the other two sites are different from Tempeldijk-South. For the Tempeldijk-North, the radiation temperature of the dyke materials is lower than the mean atmospheric temperature in all field campaigns (Table 2). The temperature images are shown in Figure 12. These images show some similarities in certain areas. The high temperature (above 21.2^{o}C) for part of the August image indicated relatively dry areas of the dyke while the dark blue coloured areas show the relatively wet areas (Figure 12a). However, the general difference in the radiation temperature of this site is only 2^{o} C. In October, the upper part was dominated by relatively low temperature and the lower part has relatively high temperature (Figure 12b). That means the upper part can be identified as wet area while the areas with low temperatures observed in the lower part are due to the shadow effect of the grass or due to the presence of water. In December, the radiation temperatures are highly influenced with respect to the position of the sun. The middle part has low temperature due to the shadow effect of the dyke itself (Figure 5c) and hence the higher values are areas, which were exposed to the reflection of the sunshine (Figure 12c). The range of the radiation temperatures in December is very low. The multi-temporal TIR images of this site did not show similarities that can determine the composition of the dyke as compared to the Tempeldijk-South (see next chapter).

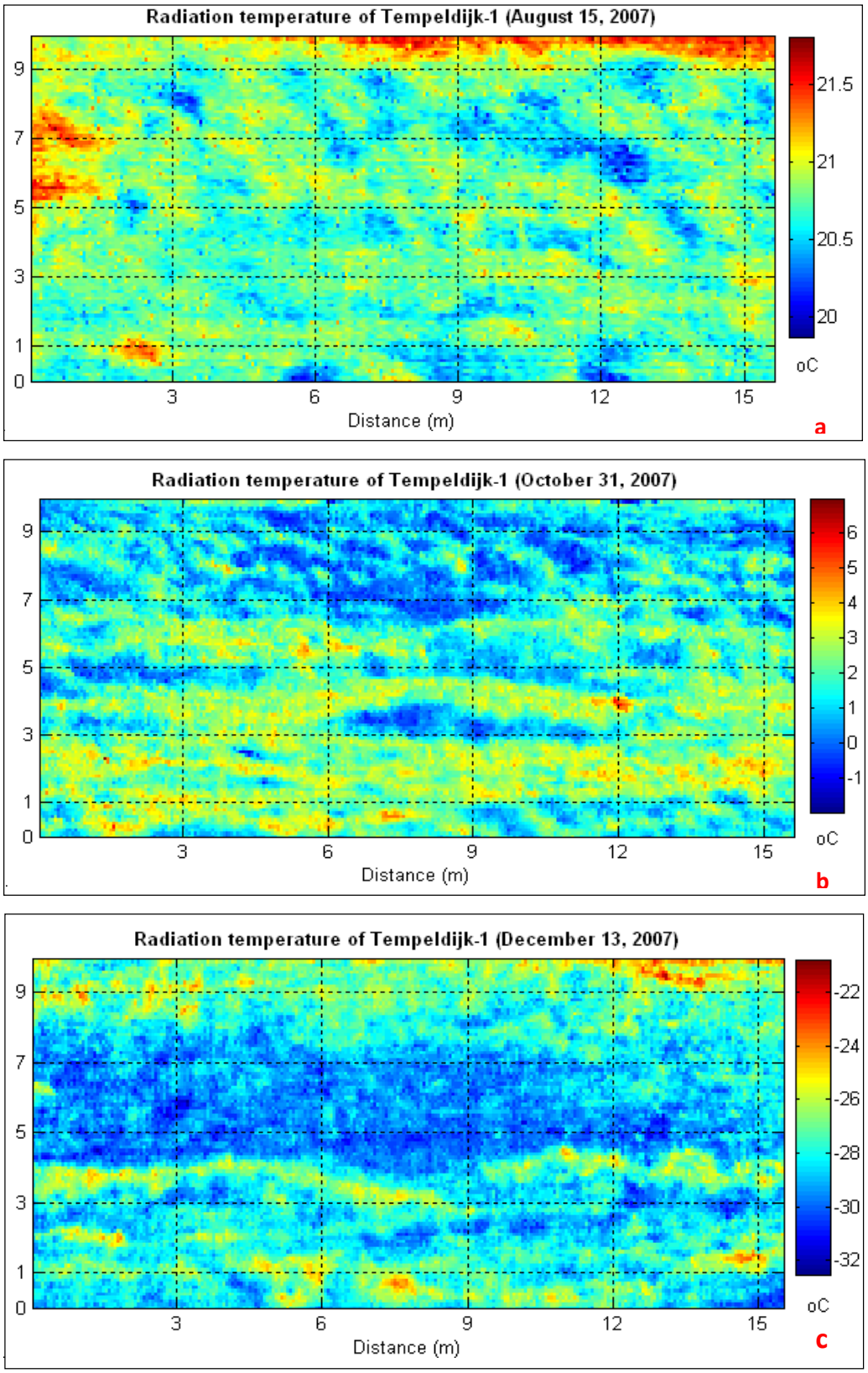

Figure 12. The spatial and temporal variation in the thermal radiation of the Tempeldijk-North in (a) August, (b) October shows relatively two layers and (c) December shows the influence of the shadow. (Tempeldijk-1 is Tempeldijk-North location)

Scatter plots are made to see the general trend of the possible correlations between the radiation temperature values of the three imaging periods. The plot between the radiation temperature of each pixel of August and October does not show any possible trend (Figure 13a). The sample points concentrate in the middle of the plot and extreme points are present everywhere. The same applies for correlation between October and December (Figure 13b). This is mainly due to the effect of the shadow during the December field campaign, which is shown in lower values. To some extent, the plot between August and December seems to show a weak positive correlation (Figure 13c) but in general, the correlation is very weak. The difference in temperature for the whole image of the dyke, is less than 2^{o}C for August, 7^{o}C for October and about 10^{o}C for December.

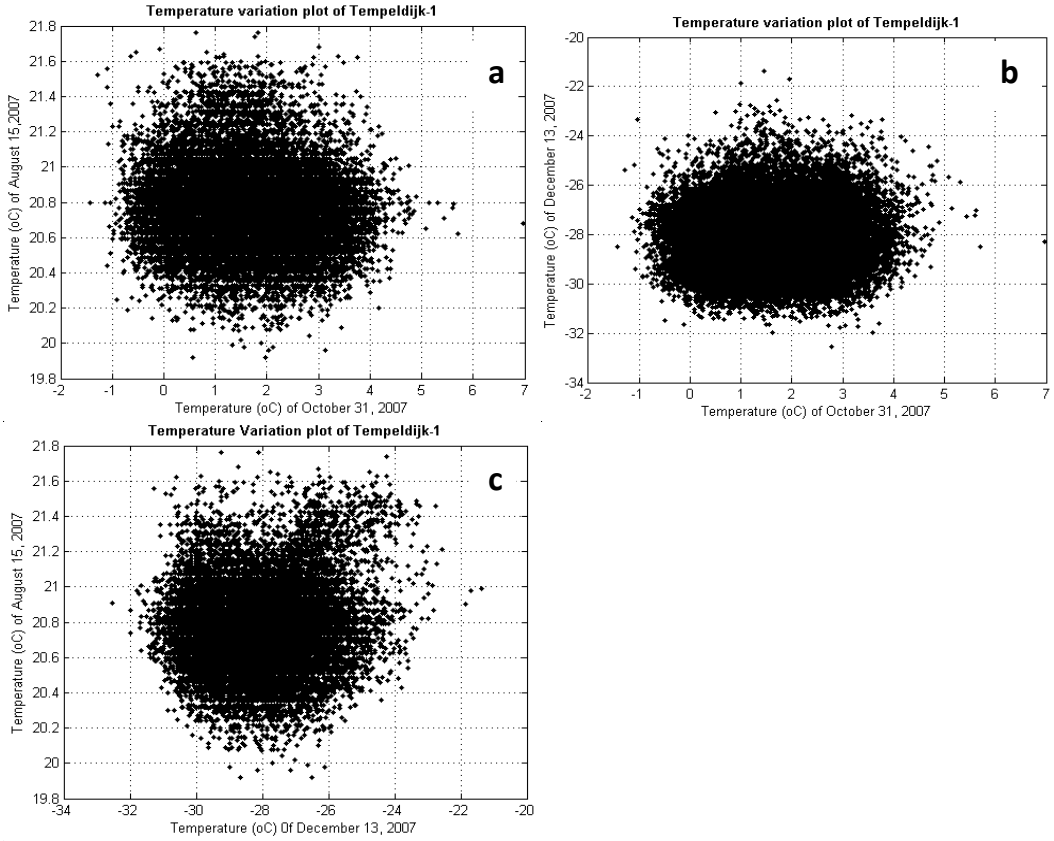

Figure 13. Scatter plots of the multi-temporal thermal images, which shows the radiation temperature of (a) August verses October, (b) December verses October and (c) August verses December (Tempeldijk-1 is Tempeldijk-North location)

Table 2. Surface and radiation temperature of Tempeldijk-North

Imaging period	Mean Atmospheric temperature	Radiation temperature of the site	Humidity
August 15, 2007	25°C	20 – 22°C	80%
October 31, 2007	12.5°C	-1 – 6°C	87%
December 13, 2007	1°C	-32 – -21°C	95%

2.1.4 TEMPELDIJK-SOUTH

The thermal image of the Tempeldijk-South made in August shows a low emitted temperature for the top and bottom part of the dyke (Figure 14a). The temperature value for this part is 25-26.5^{o}C which is nearly the same as the atmospheric temperature of that day. The middle part has

relatively higher radiation temperatures than the top and bottom parts. The higher values extend towards the upper part in the left side of the image. Depending on the values of the radiation temperature, the image shows three different layers. The boundary between the higher radiation and the lower radiation is not clearly determined (not horizontal). Also in October the same three layers can be distinguished. In this period, the top left part of the image was dominated by lower radiation temperatures as compared to August. In addition, the higher radiation values are scattered throughout the middle part of the image (Figure 14b). The range in the radiation temperature values of the dyke is below the mean atmospheric temperature of that day (Table 3). The TIR images of the December are different from the images made in August and October. The top and bottom part of the images, which are indicated by low temperatures in August and October, show a relatively high radiation temperature while the middle part has low radiation temperatures (Figure 14c). The range of the radiation temperature in this period is -29 to -18^{o}C.

In all of the TIR images of the Tempeldijk-South site, the radiation temperature is influenced by the emissivity of the topsoil of the dyke beyond the emissivity of the grass on the surface. The basic variation between the top and the middle part of the images is mainly due to the difference in the soil properties of the dyke materials. Based on this, the top part can be classified as clay and the middle part as peat. This implies that the peat layer has high radiation temperature in the August and October TIR images while it has a low temperature in the December TIR images. This temporal difference in the radiation temperature of the peat unit can be explained by the characteristics of the atmospheric interference and their change with time. In the field, wet areas were cooler because these take a longer time to warm than dry areas. During the summer following the reduction of moisture content due to evaporation and evapo-transpiration from the topsoil, the middle part becomes dry and has high temperatures whereas during the winter it becomes wet and has low temperatures.

Scatter plots of this site are made between the pixel values of the multi-temporal TIR images to see the possible correlations. The plot between August and October shows a vague positive correlation (Figure 15a). While the correlations between August and December as well as between October and December have a vague negative correlation. The negative correlation is much stronger between August and December (Figure 15b) than between October and December (Figure 15c). These plots can indicate the seasonal variability of the water content in the topsoil of the dyke materials.

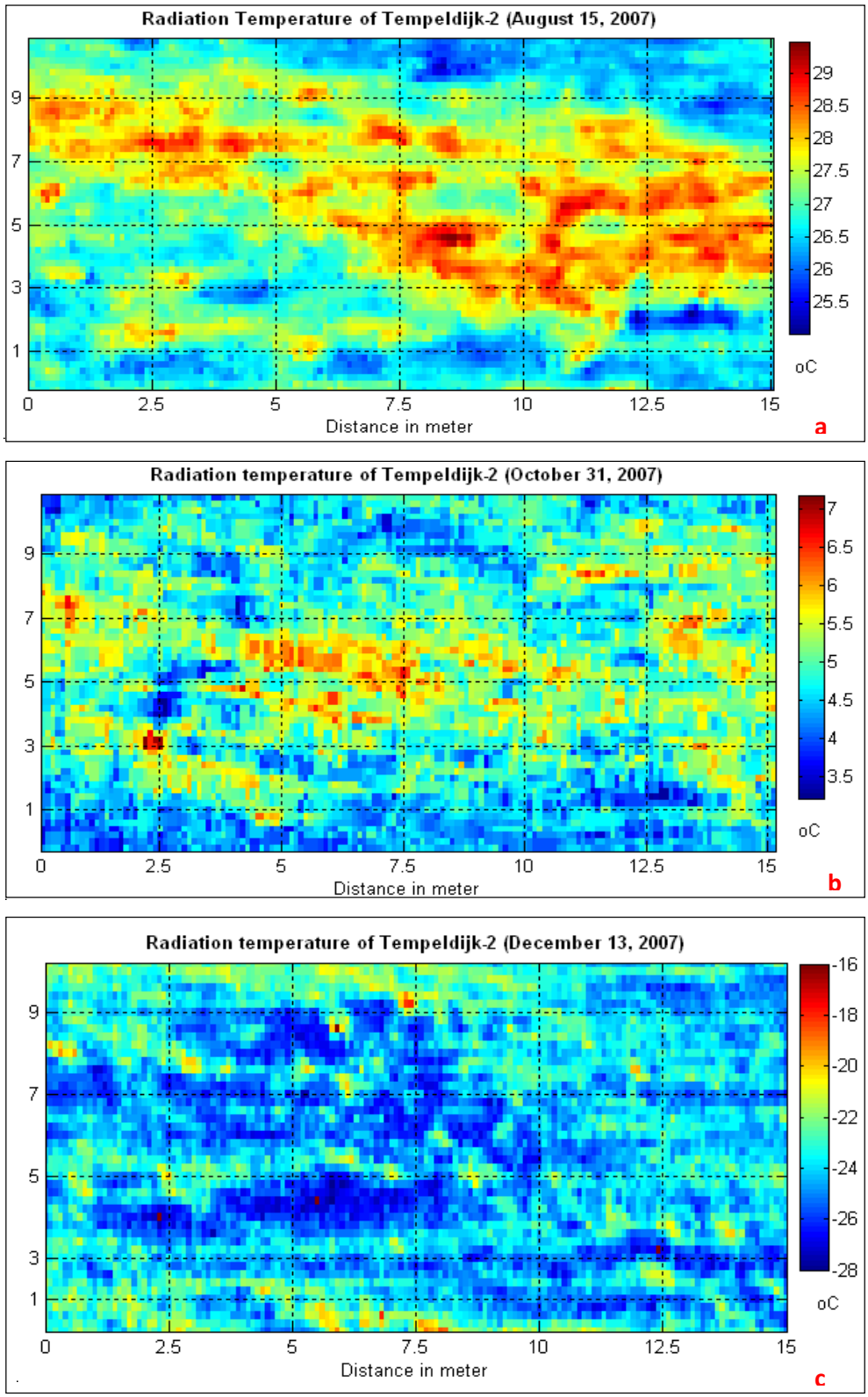

Figure 14. The spatial and temporal variation in the thermal radiation of the Tempeldijk-South, which has relatively high radiation temperature for peat layer in (a) August 15, 2007 and (b) October 31, 2007. While low temperature was acquired in(c) December 13, 2007 field campaigns (Tempeldijk-2 is Tempeldijk-South).

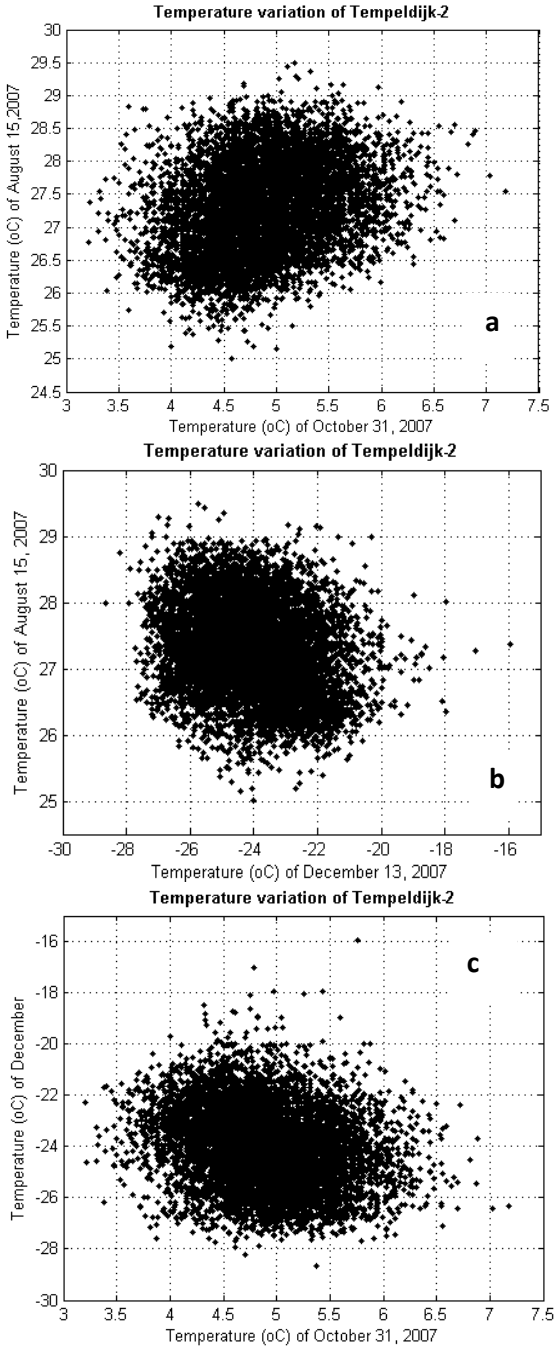

Figure 15. Scatter plots of the thermal images, which shows the radiation temperature of (a) August verses October, (b) August verses December and (c) October verses December (Tempeldijk-2 is Tempeldijk-South).

Table 3. Surface and radiation temperature of Tempeldijk-South

Imaging period	Mean Atmospheric temperature	Radiation temperature of the dyke	Humidity
August 15, 2007	25°C	25 - 29.5°C	80%
October 31, 2007	12.5°C	2 - 8°C	87%
December 13, 2007	1°C	- 29 - -18°C	95%

2.1.5 LOW RADIATION TEMPERATURES

The radiation temperature acquired in December for Tempeldijk-South is very low compared to the mean atmospheric temperature. This can be related to the following reasons:

- In the rainy season, when the topsoil water content is high, the heat capacity of the topsoil is also high and as a result, more energy is needed to increase its temperature. In consequence, the surface temperature response to the solar radiation and air temperature is slower and weaker. However, during the dry season following the reduction of the water content from the topsoil, surface temperature responds quicker to solar radiation and air temperatures (Katra et. al, 2006).
- In addition, the thermal conductivity depends on the water/ice content in soil. When the temperature drops below 0^{o}C the energy storage in the soil is changed such that liquid water is converted to ice, this implies that the latent heat will change simultaneous with decreasing temperature.
- The other possible reason is related to the detecting sensor of the thermal imaging cameras. The thermal imaging cameras do not determine the true temperature of any material from its emissivity. They can only compute the apparent temperature of the material. Thus, the apparent temperature is a function of both temperature and emissivity. This apparent temperature of an object may be substantially different from its true temperature.

2.2 Near infrared images in different seasons

The near infrared multispectral images provide only the surface information depending on the greenness of the grass that covers the dyke sites (Quiroz et. al, 2001). The greenness is mainly related to the stress due to the evaporation of water from the topsoil which may cause the grass to come yellowish. Hence, the near infrared images may deliver supplementary information on the condition of the dykes. In the original images (Figure 16), it is difficult to see any difference in reflectance of the grasses except for some dark spots.

Figure 16. The raw NIR image in near and red bands acquired using the ADC multispectral camera of Tempeldijk-2 in August (upper) and the shadow effect in the Tempeldijk-1 in December (lower).

Since the ADC (Agricultural Digital Camera) multispectral camera gives the reflectance value in the red and near infrared band, it was tried to emphasize the absorbance and reflectance property of the grass in separate bands (hence in different wavelength). Considering the response to light energy, natural surfaces are about equally bright in the red and near infrared. That means the areas of topsoil having a little or no green grass will appear similar in both red and near infrared wavelengths. Whereas areas with much green grass will be very bright in the near infrared and very dark in the red part of the spectrum. This is because red light is strongly absorbed by photosynthetic pigment (chlorophyll) while near infrared light is highly reflected. Therefore, the NIR wavelength of the camera was used to determine the variation in the reflectance of the grass. As a result, differences in the reflectance were noted in this portion of the spectrum. In this portion, the green grasses and the shining surface of the dyke appear with a high reflectance value. The low reflectance values are mainly related to the dried out grass, leafs with accumulated rainfall, shadows and dark objects (exposed dyke materials). However, it is difficult to discriminate the stressed grass from the healthy grass.

The difference in the reflectance value is highly dependent on a large number of vegetation properties such as the leaf area, biomass, chlorophyll concentration in leaves, plant productivity, vegetation cover, accumulated rainfall, etc. These properties vary with the seasonal variation and influence the reflectance value of the grass. On the other hand, external factors such as apparent roughness, wind direction and position with respect to the sun also influence the true reflectance values of the grass. The physical appearance of the grass changes from season to season. The tall grass has higher possibility to bend with minor influence for example the wind, which affects the apparent roughness of the dykes, and hence the true reflectance value of the grass. The position of the sun angle is also one of the factors that influence the reflectance values. For instance, in the December field campaign the reflectance value of Tempeldijk-North was highly affected by the shadow due to the position of the sun, which was behind the imaging surface of the dyke and directly towards the lens of the camera. As a result, areas covered by shadow show a low reflectance value (Figure 5.8 lower and Figure 5.11c) while the grass exposed to the sunshine had a higher reflectance. Comparing to the other two field campaign seasons, images of this season did not reflect the actual condition of the dyke. This is because the green grass with a high concentration of chlorophyll are expected to show high reflectance value in the

near infrared as the others but they show low reflectance value due the presence of shadow. This has high impact on the possible correlation that can have with the other imaging seasons. Sampled images of all sites are shown below (Figure 17, 18, and 19).

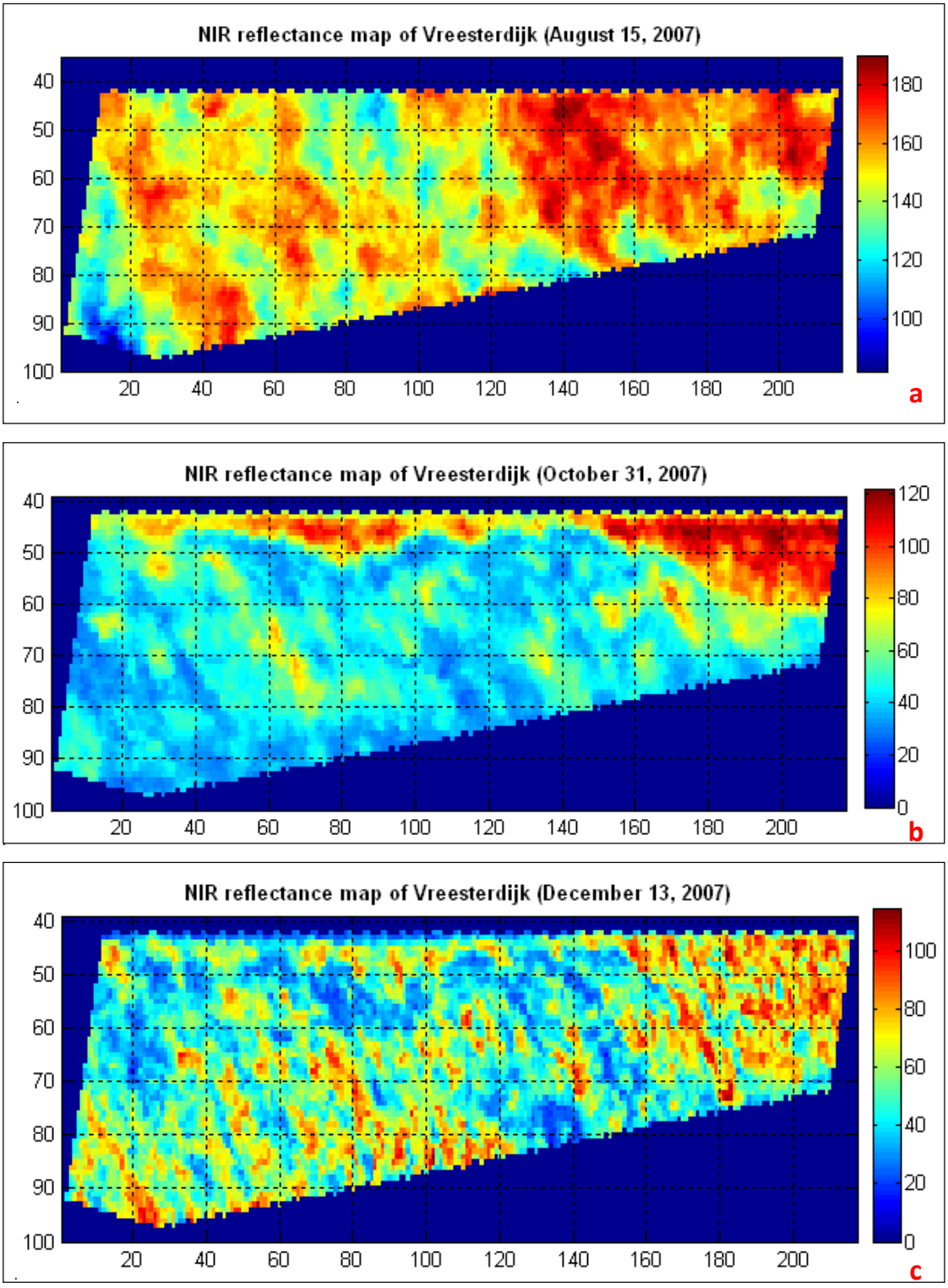

Figure 17. The multi-temporal near infrared images of Vreesterdijk shows high reflectance for the long green grasses in August (a). Low reflectance values in October (b) and December (c) are typically the reflectance from the exposed topsoil.

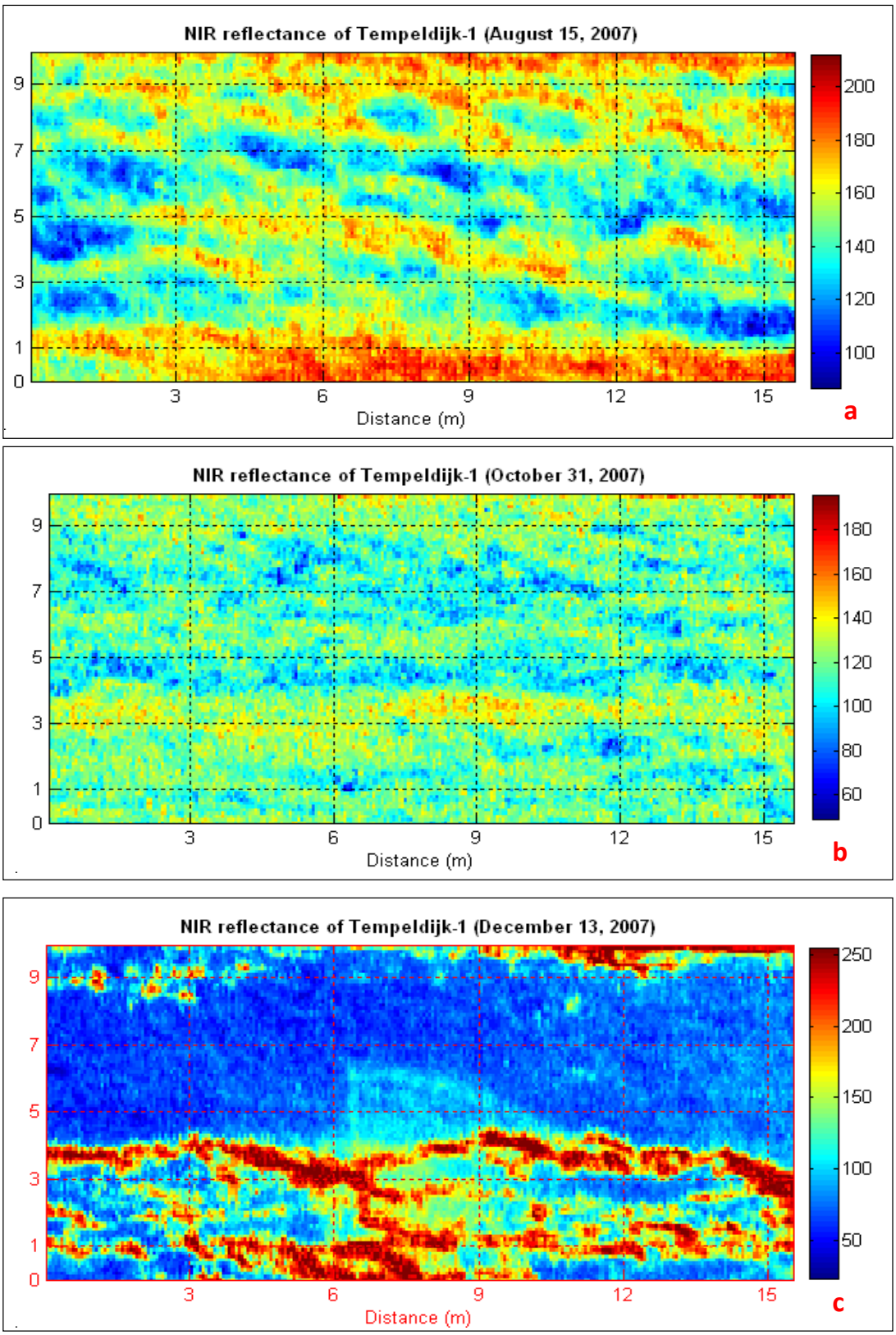

Figure 18. The spatial and temporal variation in reflectance of Tempeldijk-North in (a) August, (b) October and (c) December (which is highly influenced by the position of the sun angle) field campaign (Tempeldijk-1 is Tempeldijk-North).

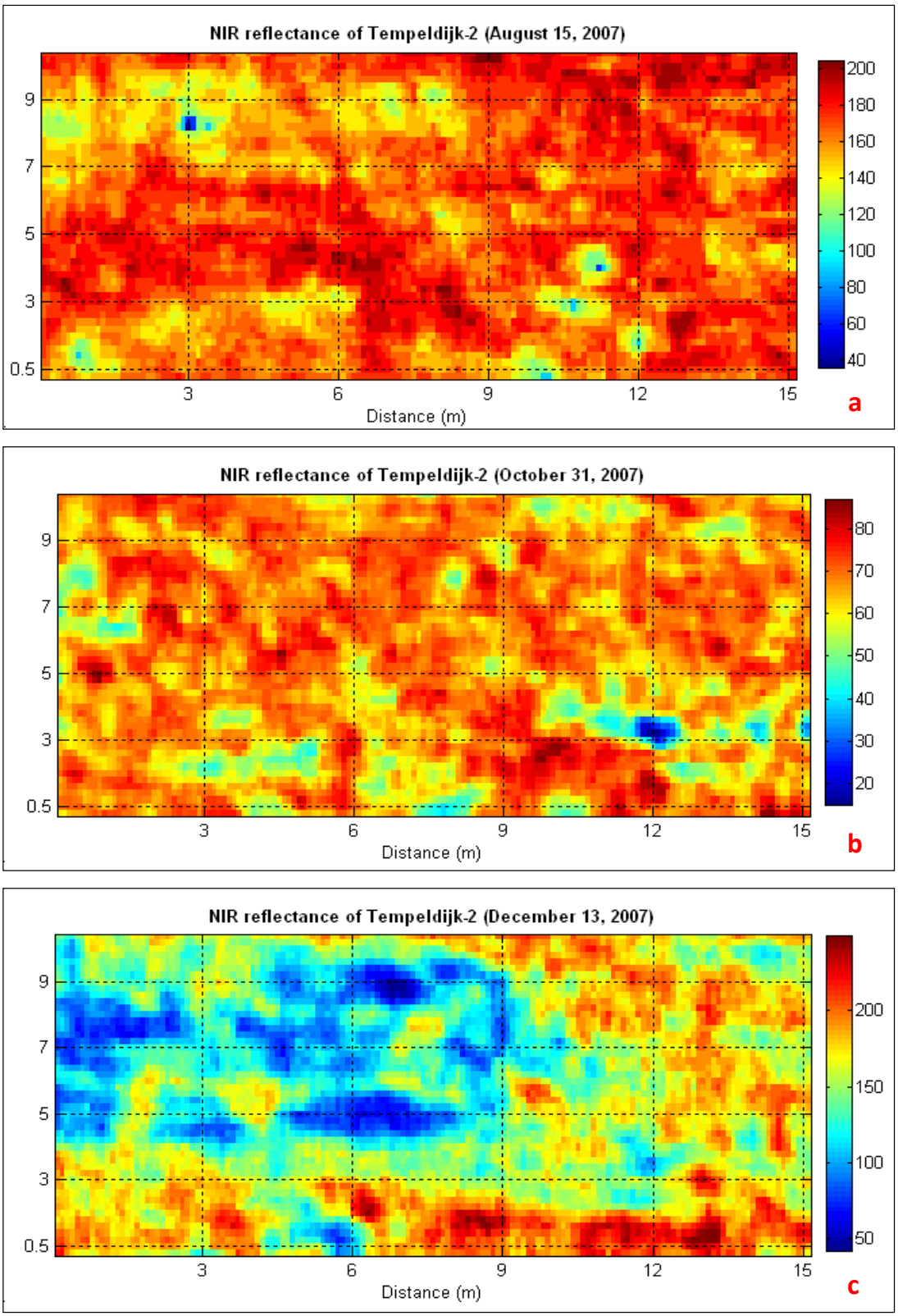

Figure 19. The spatial and temporal variations in reflectance of Tempeldijk-2 showing minor variations in (a) August and (b) October NIR images while in December the variation is high due to the presence of exposed topsoil (c) (Tempeldijk-2 is Tempeldijk-South).

The plot of October versus August for the Vreesterdijk (Figure 20 left) shows clustering at the lower right part of the graph, which indicates the high reflectance during the summer (presence

of grass) and low during the October (absence of grass). However, the clustering in the scatter plot between October and December (Figure 20 right) is in the lower left corner and sample points extend towards the upper right corner. This might show the only weak positive correlation of the images. The clustering extends towards the lower right, which indicates the increment of the reflectance in some areas due to the growth of grass.

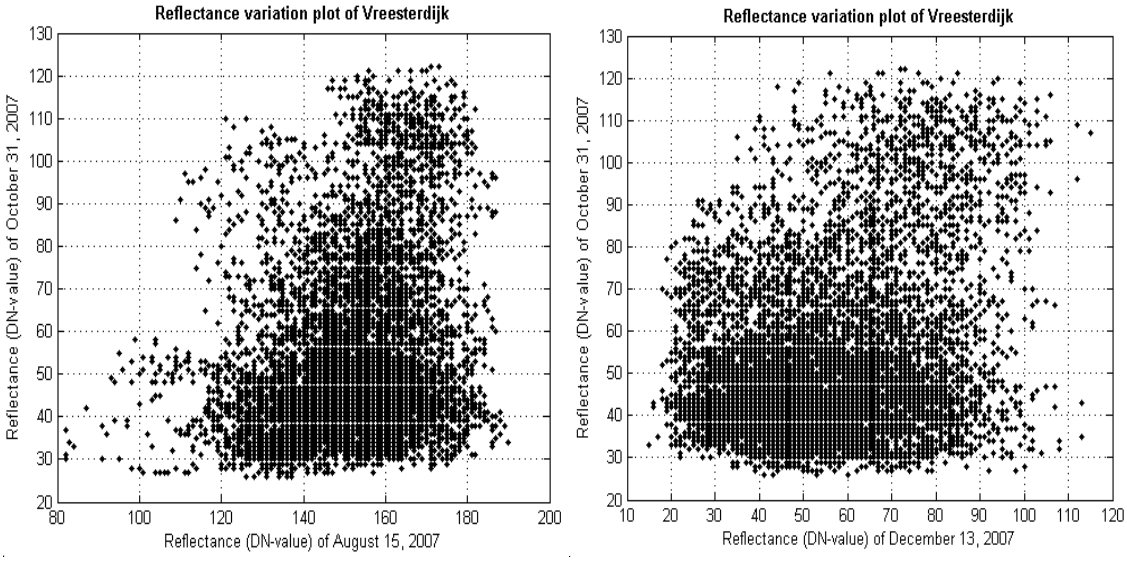

Figure 20. Scatter plots of the multi-temporal near infrared images of Vreesterdijk, which shows the correlation in the reflectance of August verses October (left) and October verses December (right)

The plots of Tempeldijk-North do not show any trend that can possibly indicate the correlation of the multi-temporal images. Many sample points are concentrated in cluster (Figure 21). The shadow effect (during the December field campaign of this site) is clear in the relation between the images of October and December, for different reflectance values of the October show the same value in the December. There is also no indication of correlation in the scatter plots of the Tempeldijk-South (Figure 22). This might show the change in the reflectance of the grass with respect to the seasonal variation. Thus, for all the sites the correlation between the NIR images of the different seasons is poor.

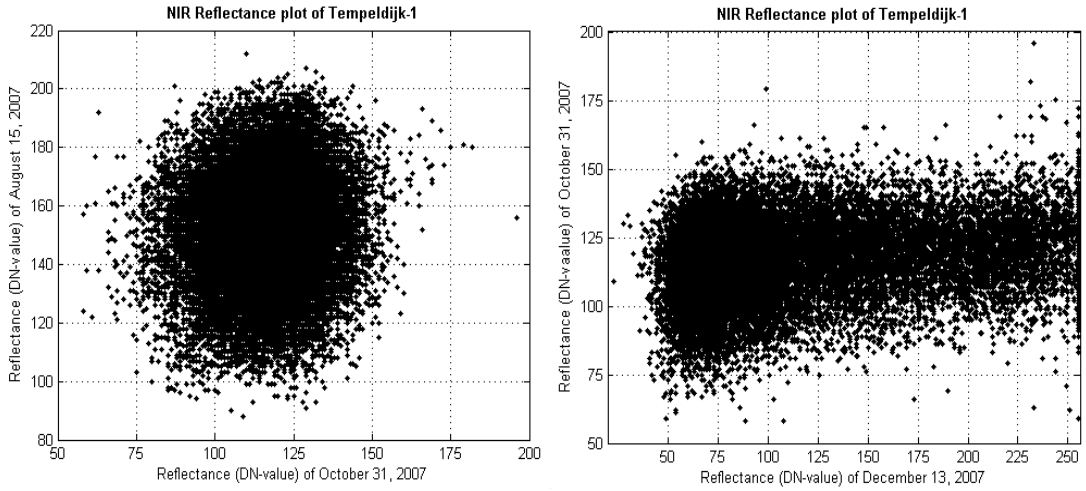

Figure 21. Scatter plots of the multi-temporal near infrared images of Tempeldijk-North, which shows the relationship in the reflectance (DN-value) of August verses October (left) and October verses December (right) (Tempeldijk-1 is Tempeldijk-North).

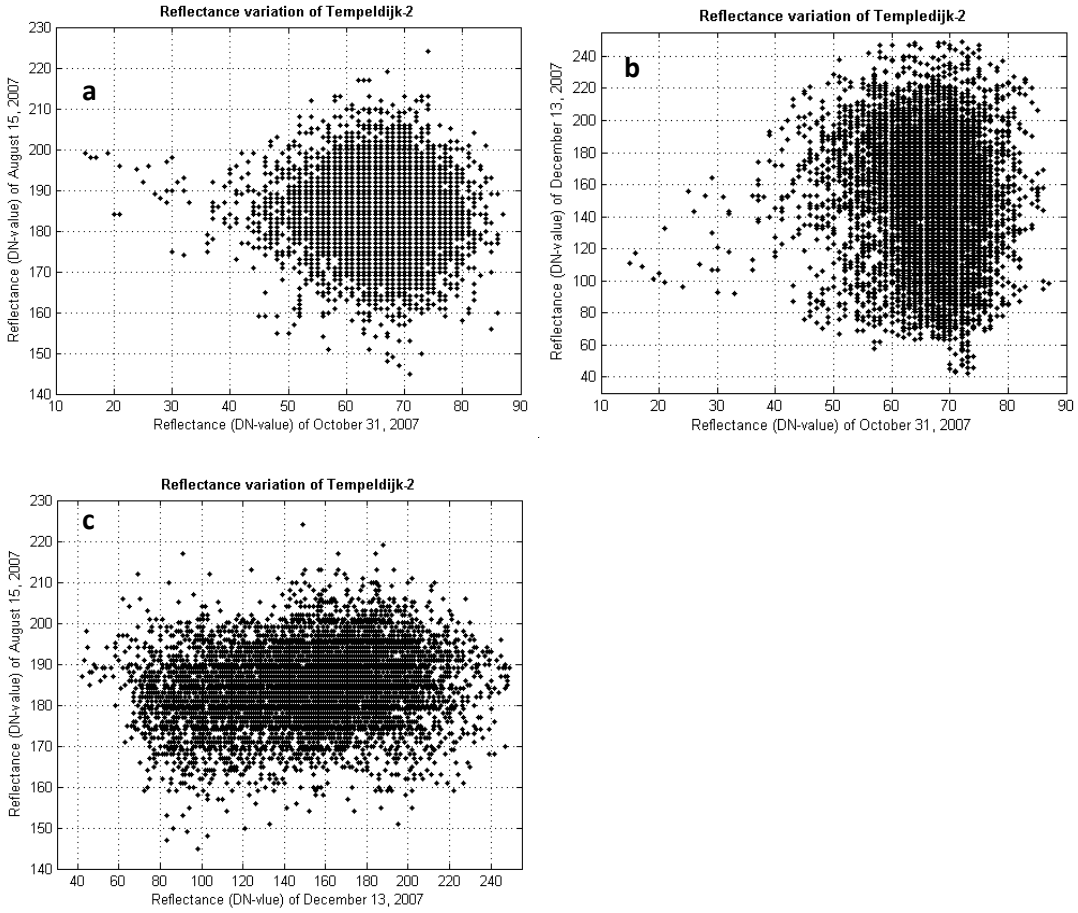

Figure 22. Scatter plots of the multi-temporal near infrared images of Tempeldijk-South showing the correlation in the reflectance of (a) August verses October, (b) October verses December and (c) August verses December (Tempeldijk-2 is Tempeldijk-South).

APPENDIX K

RSDYK2008 – GAMMA RAY SURVEY

1 GAMMA RAY SURVEY

A terrestrial gamma ray survey was done to investigate the options for using gamma ray for dyke inspection.

The location Tempeldijk-2 refers to Tempeldijk-North and Tempeldijk-3 refers to Tempeldijk-South.

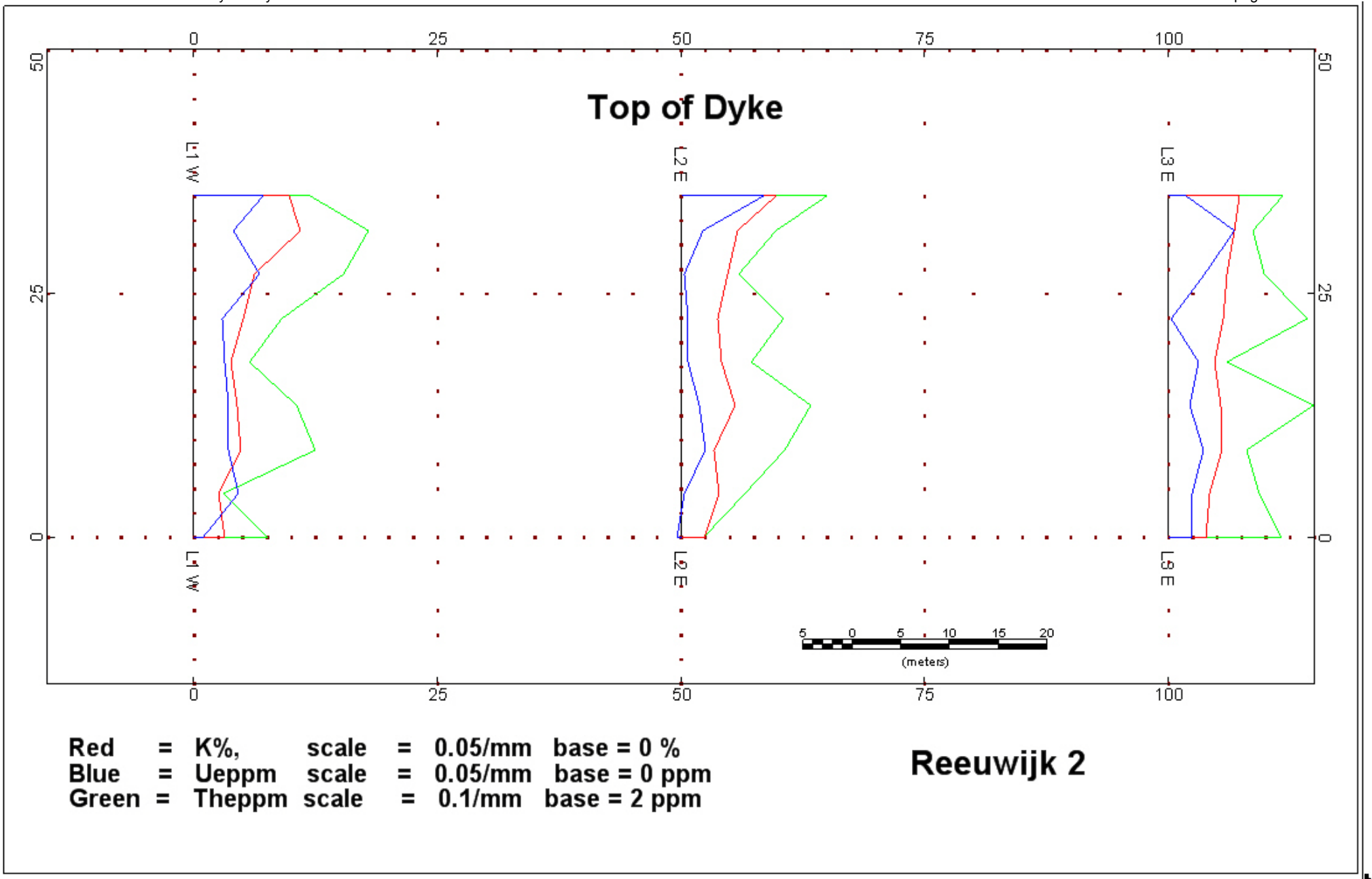
Top of Dyke
L1 W
L2 E
L3 E
L1 W
L2 E
L3 E
0
25
50
75
100
5 0 5 10 15 20
(meters)
Red = K%, scale = 0.05/mm base = 0 %
Blue = Ueppm scale = 0.05/mm base = 0 ppm
Green = Theppm scale = 0.1/mm base = 2 ppm
Reeuwijk 2

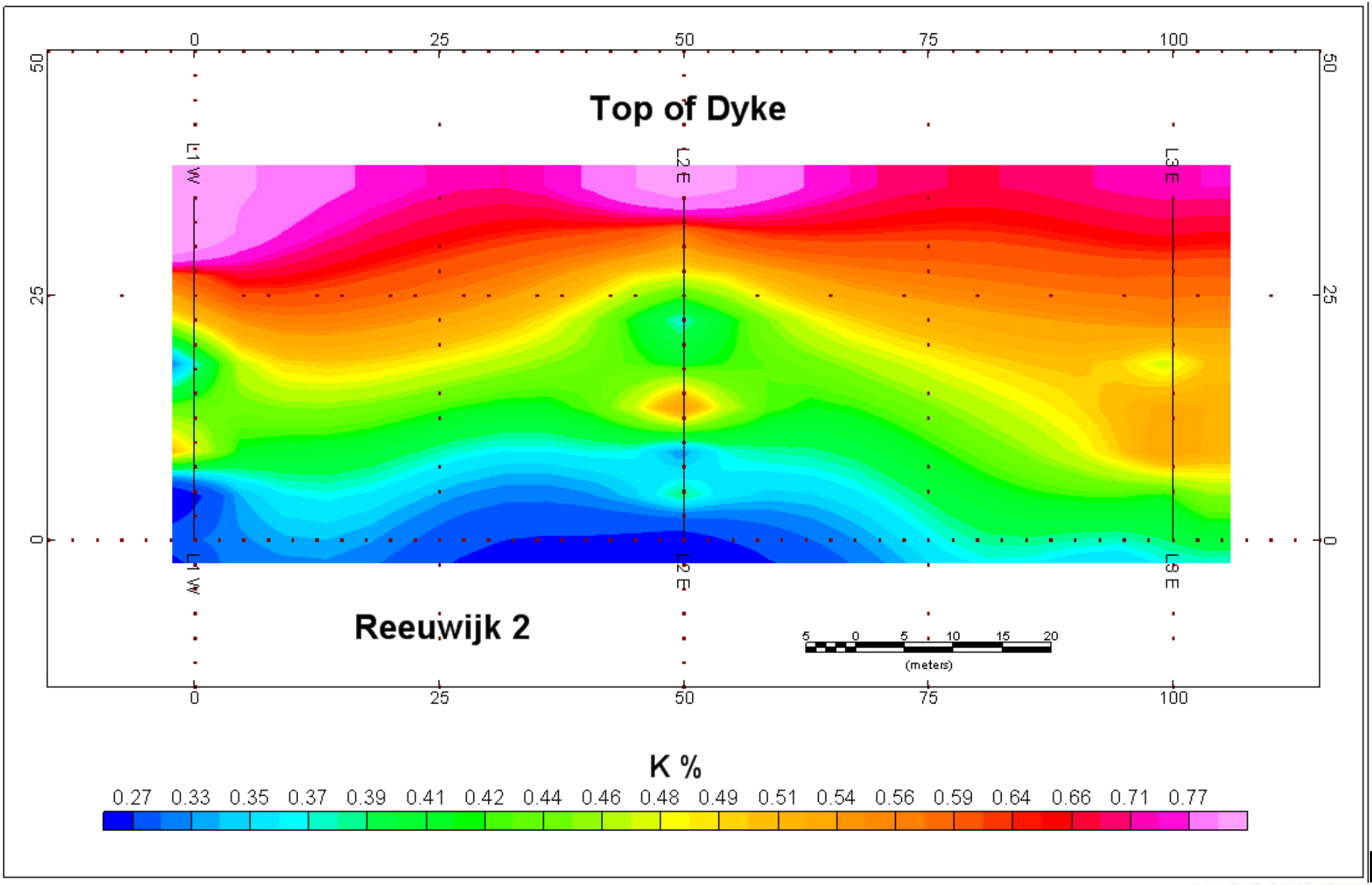
Top of Dyke
L1 W
L2 E
L3 E
L1 W
L2 E
L3 E
Reeuwijk 2
5 0 5 10 15 20
(meters)
0 25 50 75 100
50
25
0
K %
0.27 0.33 0.35 0.37 0.39 0.41 0.42 0.44 0.46 0.48 0.49 0.51 0.54 0.56 0.59 0.64 0.66 0.71 0.77

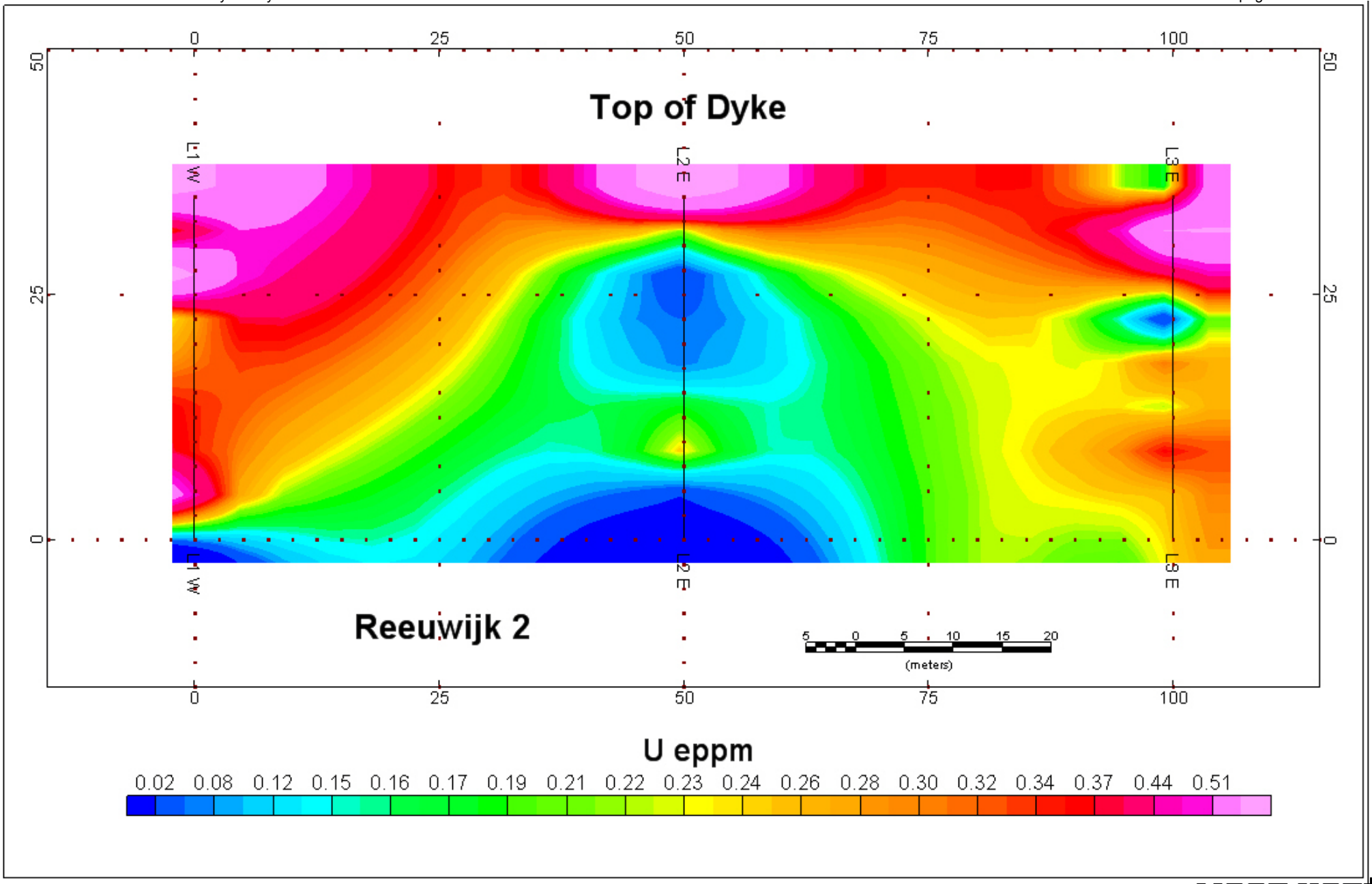
Top of Dyke
L1 W
L2 E
L3 E
L4 W
L5 E
L6 E
Reeuwijk 2
5 0 5 10 15 20
(meters)
0 25 50 75 100
U eppm
0.02 0.08 0.12 0.15 0.16 0.17 0.19 0.21 0.22 0.23 0.24 0.26 0.28 0.30 0.32 0.34 0.37 0.44 0.51

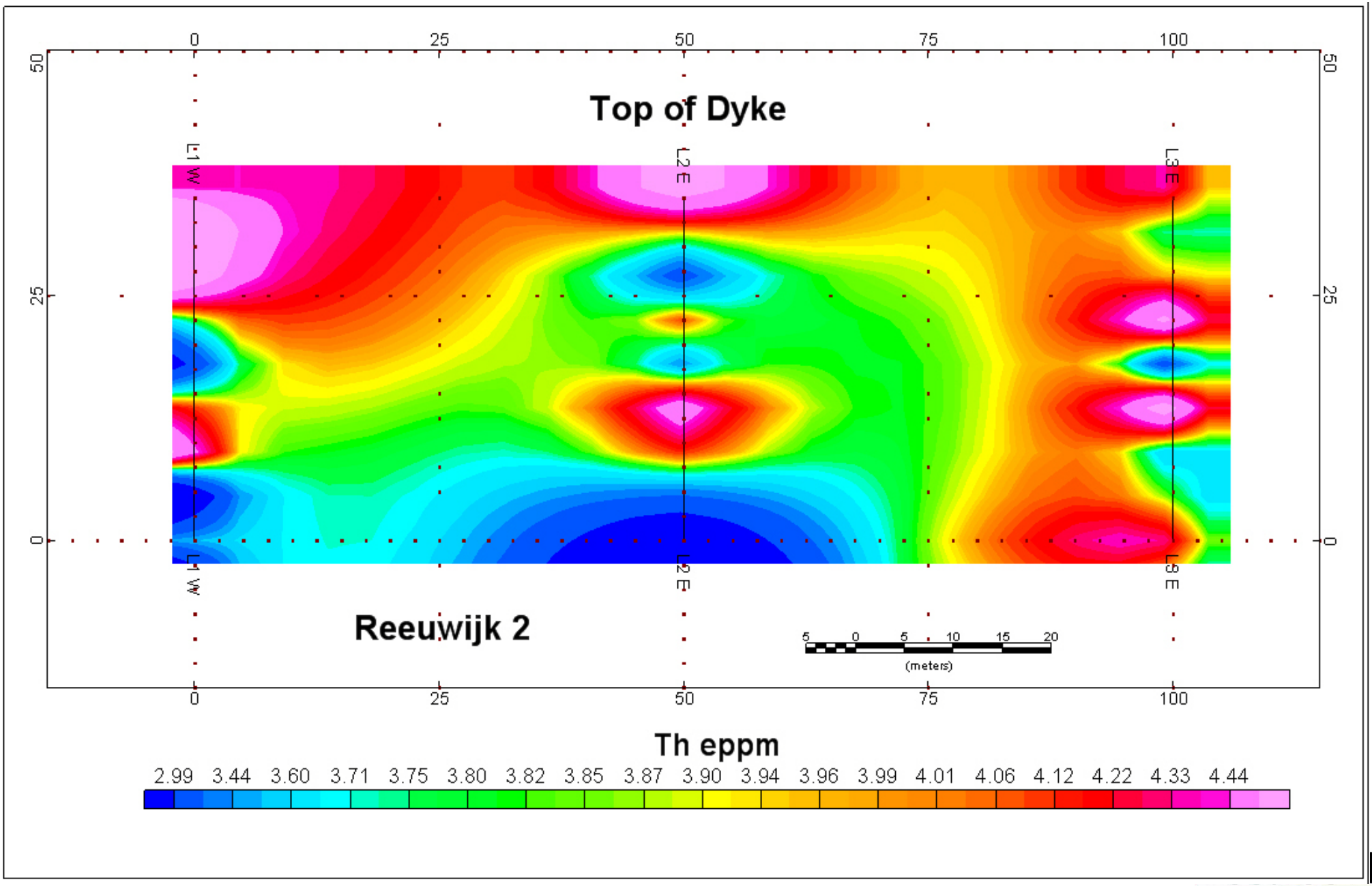
Top of Dyke
L1 W
L2 E
L3 E
L1 W
L2 E
L3 E
Reeuwijk 2
5 0 5 10 15 20
(meters)
0 25 50 75 100
50
25
0
Th eppm
2.99 3.44 3.60 3.71 3.75 3.80 3.82 3.85 3.87 3.90 3.94 3.96 3.99 4.01 4.06 4.12 4.22 4.33 4.44

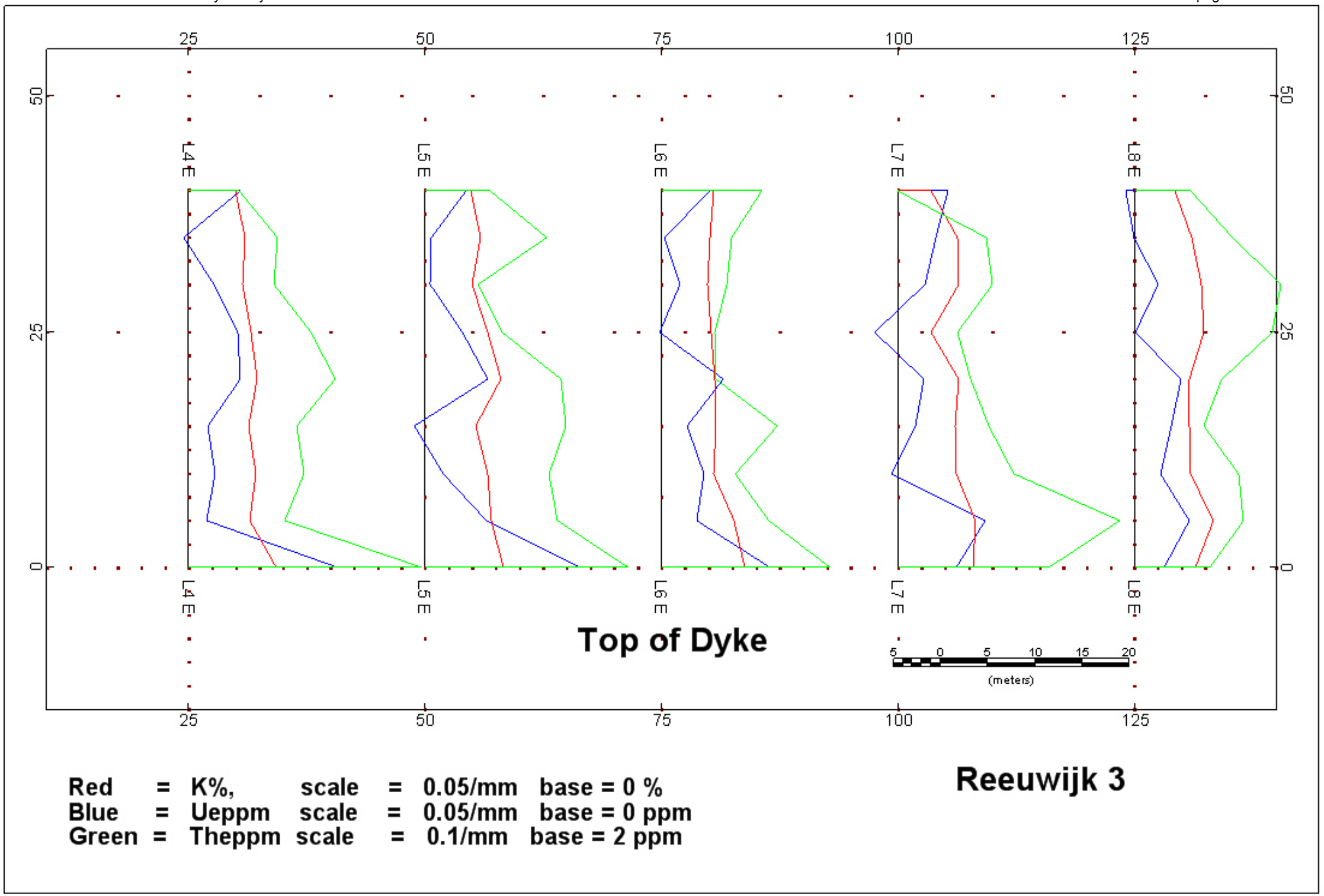
25
50
75
100
125
50
25
0
L4 E
L5 E
L6 E
L7 E
L8 E
Top of Dyke
5 0 5 10 15 20
(meters)
Red = K%, scale = 0.05/mm base = 0 %
Blue = Ueppm scale = 0.05/mm base = 0 ppm
Green = Theppm scale = 0.1/mm base = 2 ppm
Reeuwijk 3

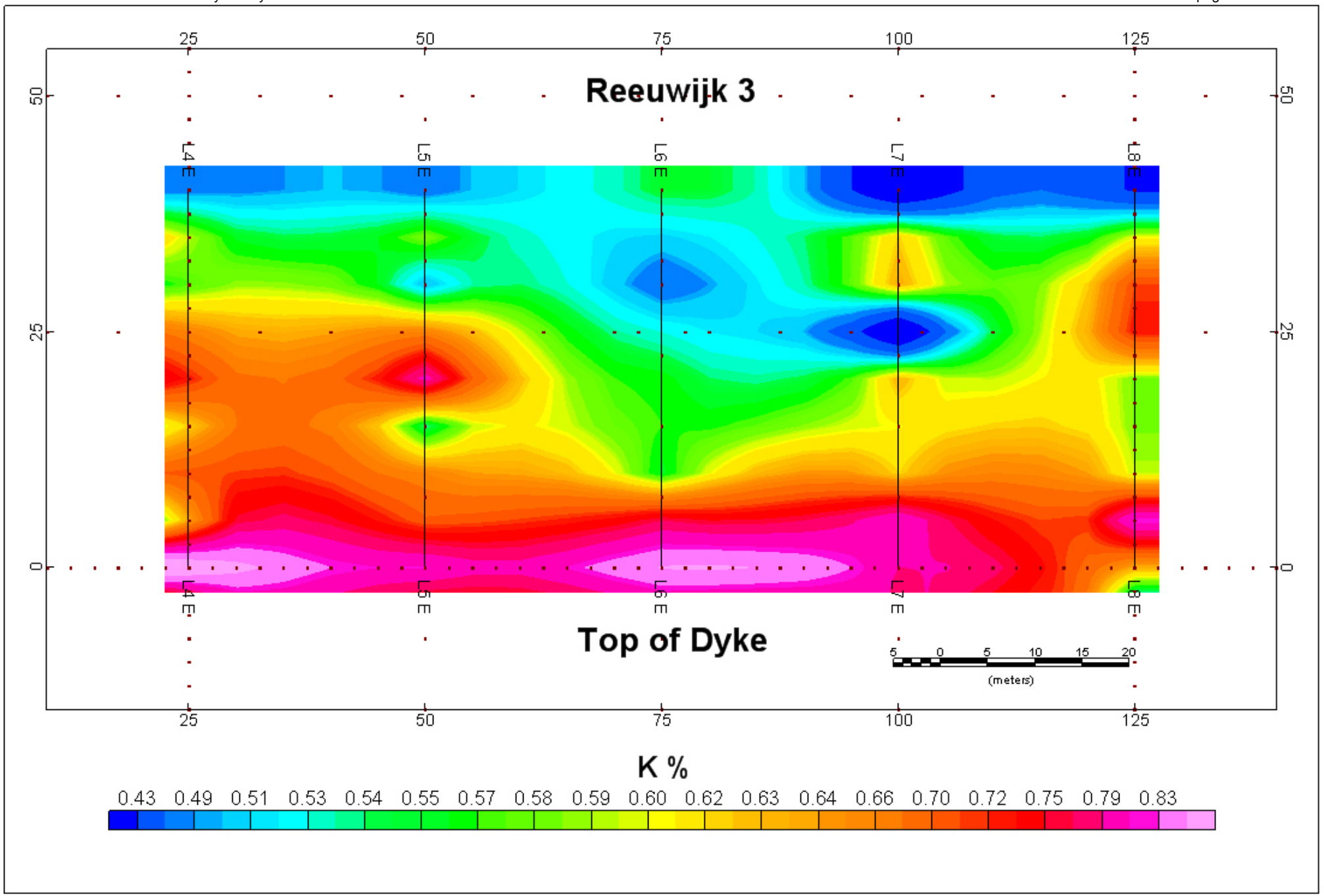
Reeuwijk 3
25
50
75
100
125
50
25
0
L4 E
L5 E
L6 E
L7 E
L8 E
Top of Dyke
5 0 5 10 15 20
(meters)
K %
0.43 0.49 0.51 0.53 0.54 0.55 0.57 0.58 0.59 0.60 0.62 0.63 0.64 0.66 0.70 0.72 0.75 0.79 0.83

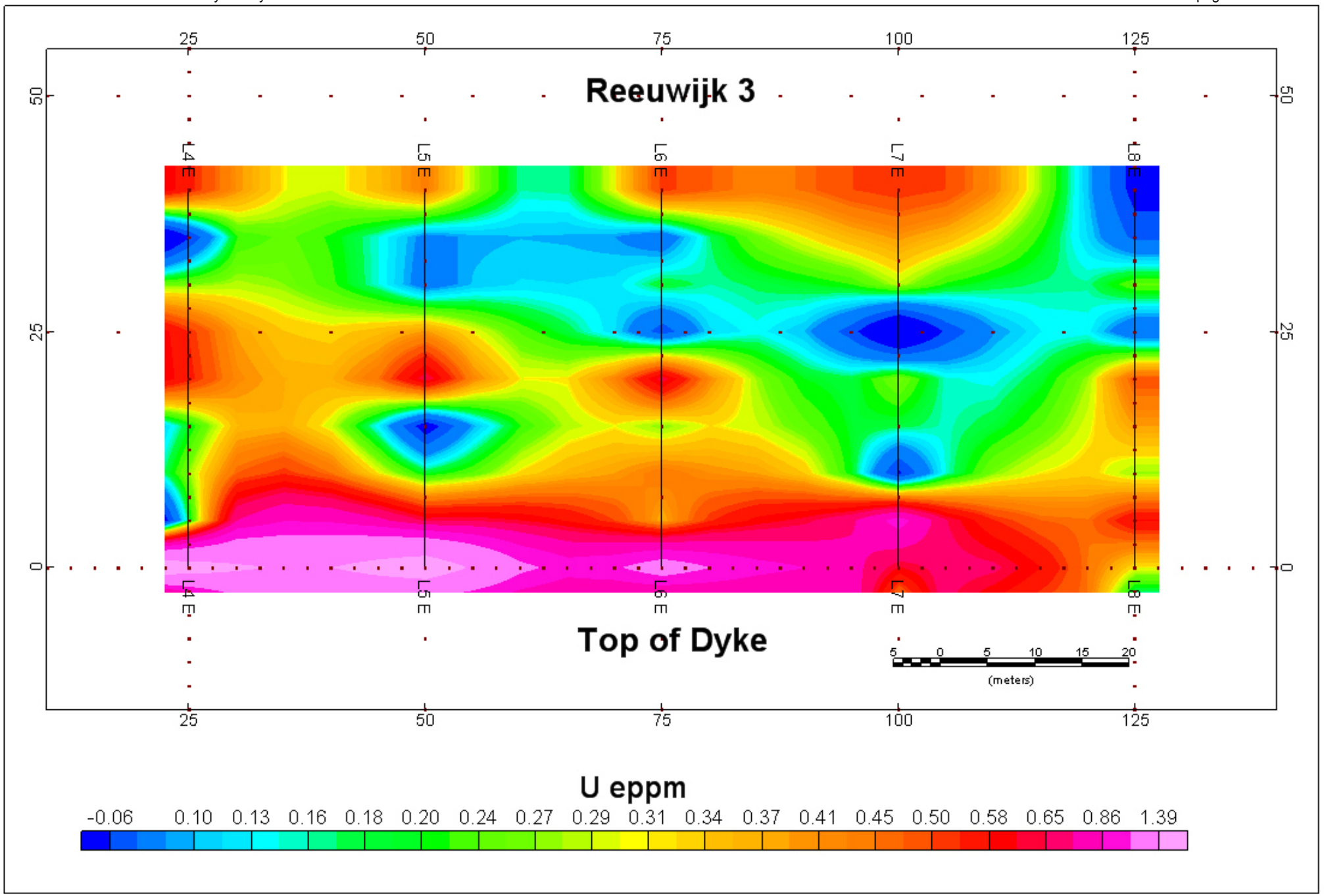
Reeuwijk 3
25
50
75
100
125
0
25
50
L4 E
L5 E
L6 E
L7 E
L8 E
Top of Dyke
5 0 5 10 15 20
(meters)
U eppm
-0.06 0.10 0.13 0.16 0.18 0.20 0.24 0.27 0.29 0.31 0.34 0.37 0.41 0.45 0.50 0.58 0.65 0.86 1.39

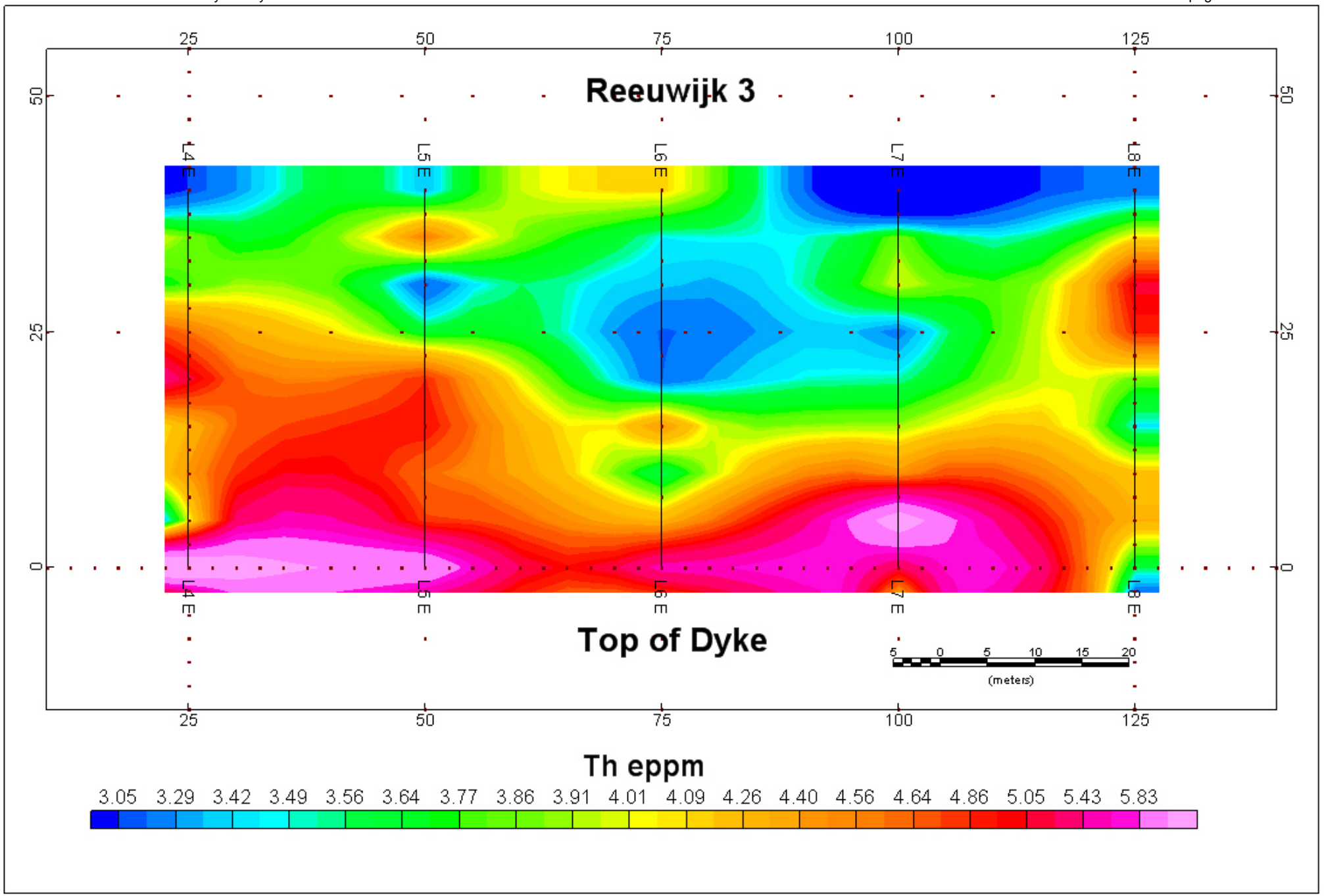
Reeuwijk 3
25
50
75
100
125
0
25
50
L4 E
L5 E
L6 E
L7 E
L8 E
Top of Dyke
5 0 5 10 15 20
(meters)
Th eppm
3.05 3.29 3.42 3.49 3.56 3.64 3.77 3.86 3.91 4.01 4.09 4.26 4.40 4.56 4.64 4.86 5.05 5.43 5.83

APPENDIX L

RSDYK2008 – HYPER SPECTRAL SURVEY

1 GAMMA RAY SURVEY

A terrestrial hyper spectral survey was done to investigate the options for using hyper spectral surveys for dyke inspection.

Dike measurements

- Measurements procedure
- The spectrometer is situated at a distance of approximately 25m of the dike, measuring on a line its vertical profile.

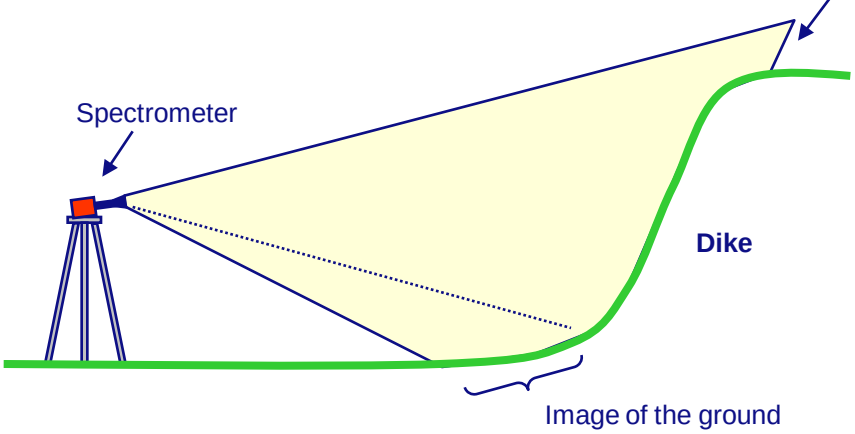

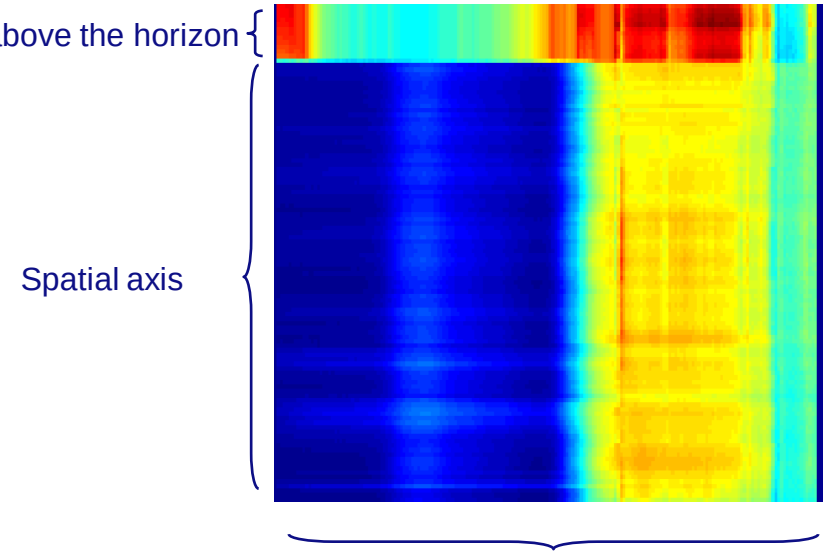

Equipment

Imspector spectrometer

- Spectral range: 400-100nm
- Spectral resolution: 6nm

Dolphin CCD

- High sensitivity
- Low noise

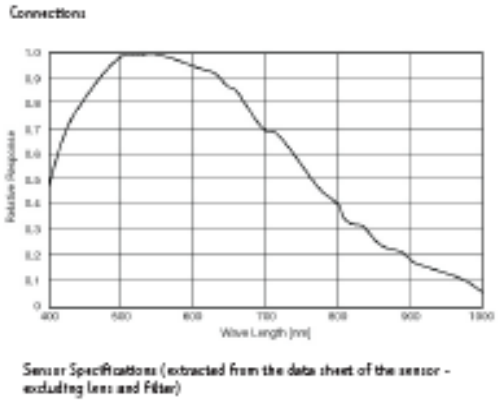

Sensor Specifications (extracted from the data sheet of the sensor - excluding lens and filter)

Front optics

25mm optical system.

20° Aperture

Measured Area

The measured area is divided in 3 different Sectors.

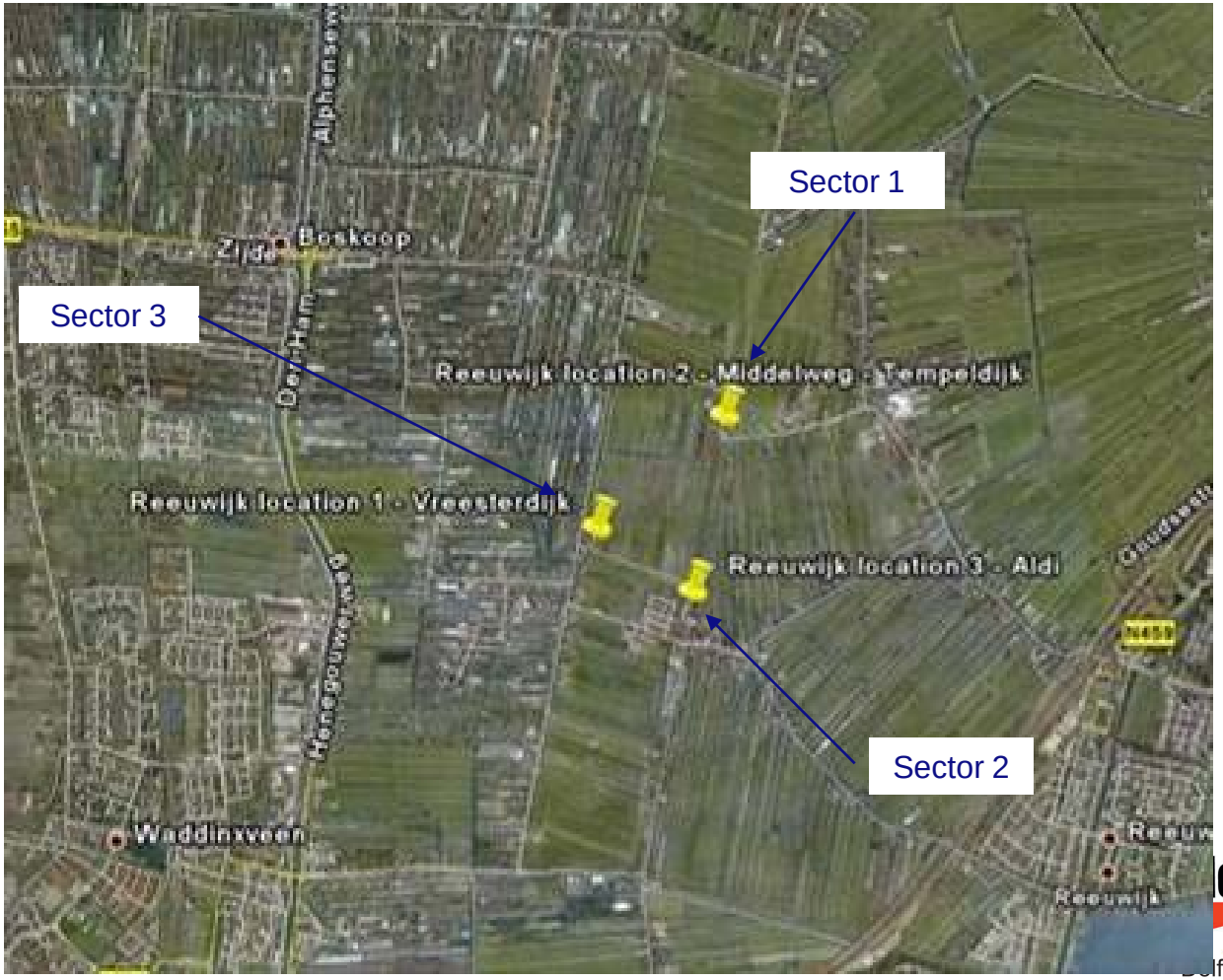

Sector1

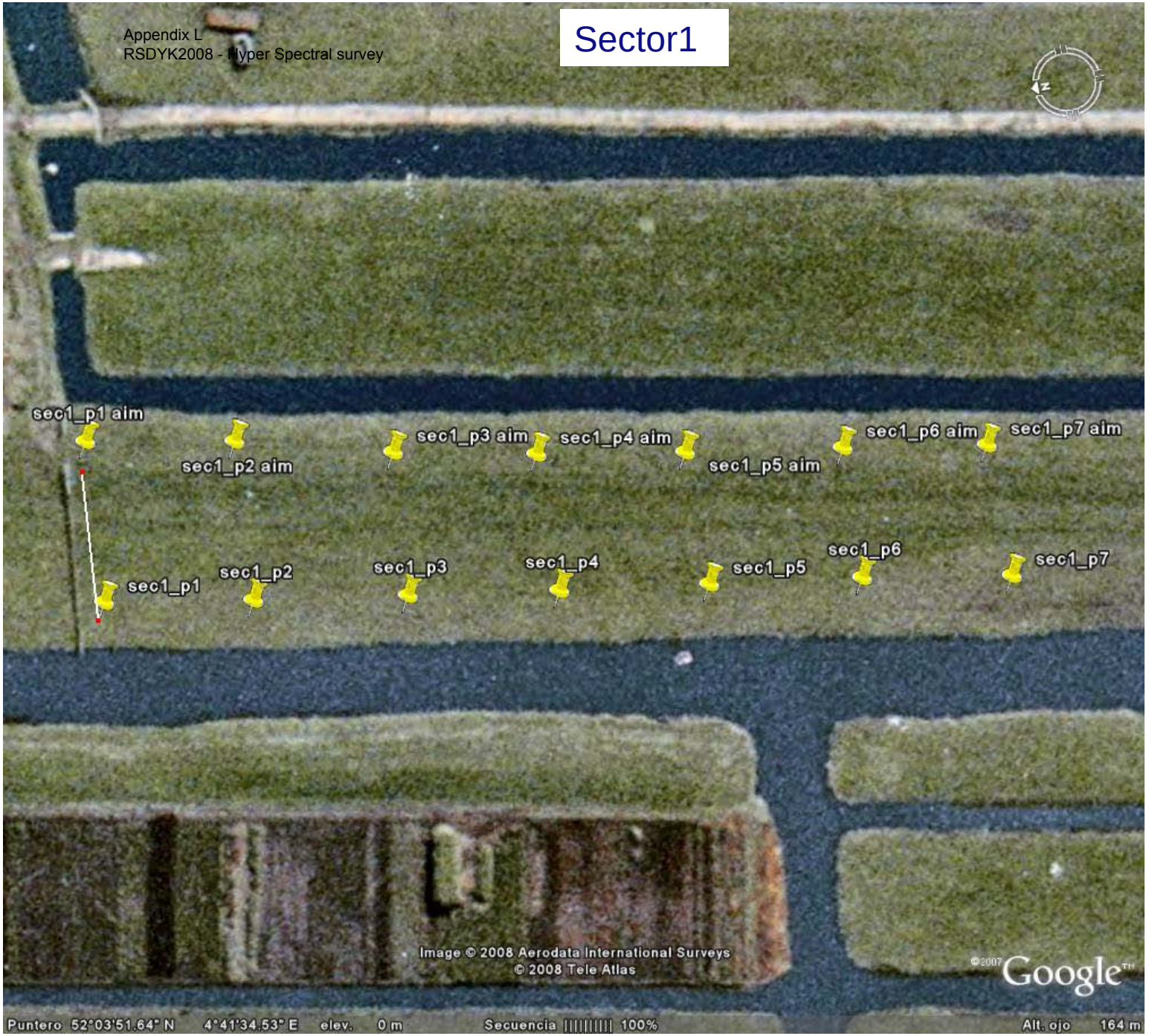

sec1_p1: 24.82m

sec1_p2:25.5m

sec2_p3: 23.47m

sec2_p4: 22.81m

sec1_p5: 21.75m

sec1_p6: 22.68

sec1_p7: 22.06

Sector2

sec2_p1: 32.98m
sec2_p2: 32.03m
sec2_p3: 32.20m
sec2_p4: 33.11

Sector3

sec3_p1: 62.8m

$\Delta\alpha$ per pixel 0.1724°

Data Process

Measurement of the dike

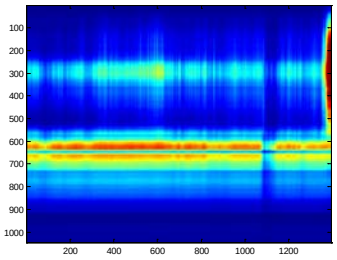

Incident light spectrum obtained from a diffuser

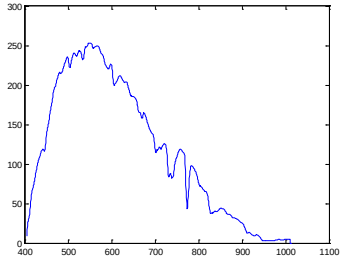

Reflectivity

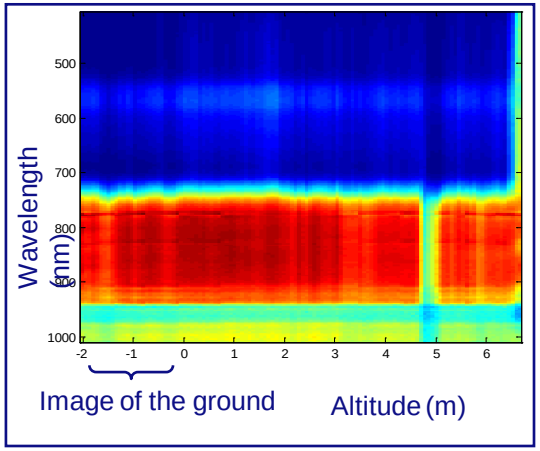

Output format

- Results are save in Matlab files with the following denomination:

Secx_py_total.mat

With x: Sector measured.
y: point in the sector.

Each line of the file corresponds to a wavelength

Each column corresponds to an altitude on the dike.

The first column indicates the reference Wavelength. The first line indicates the altitude.

An exception is the file sec3_p1_total, where the first line indicates the distance from the spectrometer.

Altitude (m)

Wavelength (nm)

Reflectivity

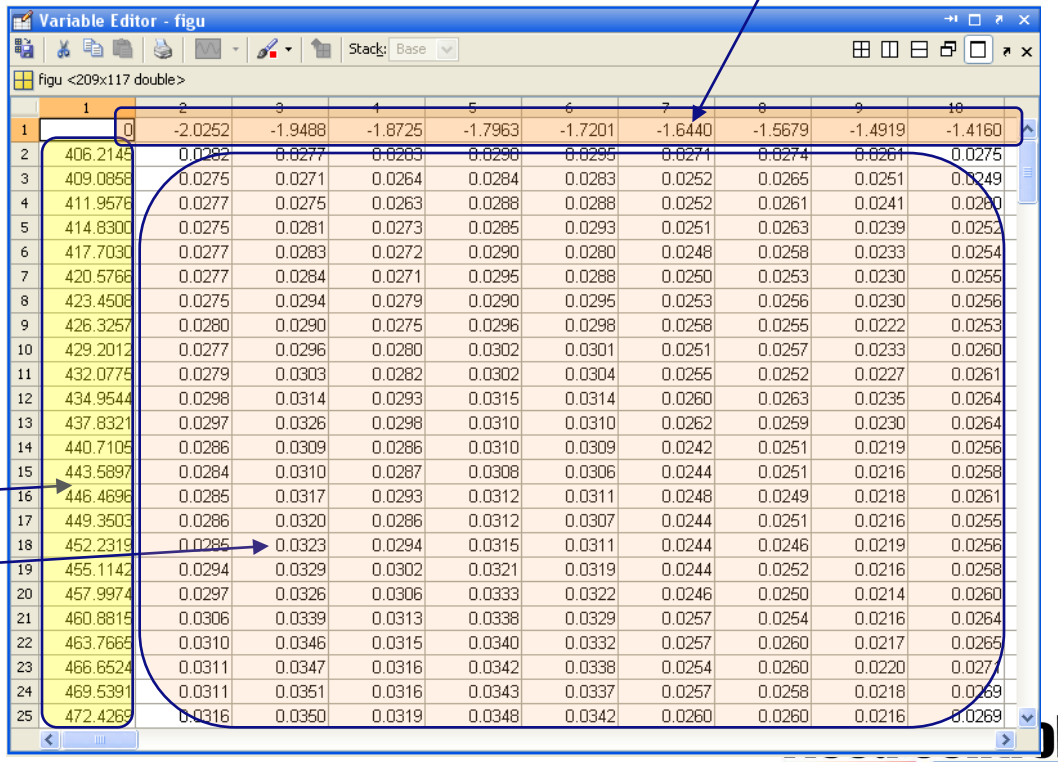

	1	2	3	4	5	6	7	8	9	10
1	0	-2.0252	-1.9488	-1.8725	-1.7963	-1.7201	-1.6440	-1.5679	-1.4919	-1.4160
2	406.2145	0.0282	0.0277	0.0263	0.0296	0.0295	0.0271	0.0274	0.0261	0.0275
3	409.0858	0.0275	0.0271	0.0264	0.0284	0.0283	0.0252	0.0265	0.0251	0.0249
4	411.9576	0.0277	0.0275	0.0263	0.0288	0.0288	0.0252	0.0261	0.0241	0.0260
5	414.8300	0.0275	0.0281	0.0273	0.0285	0.0293	0.0251	0.0263	0.0239	0.0252
6	417.7030	0.0277	0.0283	0.0272	0.0290	0.0280	0.0248	0.0258	0.0233	0.0254
7	420.5766	0.0277	0.0284	0.0271	0.0295	0.0288	0.0250	0.0253	0.0230	0.0255
8	423.4508	0.0275	0.0294	0.0279	0.0290	0.0295	0.0253	0.0256	0.0230	0.0256
9	426.3257	0.0280	0.0290	0.0275	0.0296	0.0298	0.0258	0.0255	0.0222	0.0253
10	429.2012	0.0277	0.0296	0.0280	0.0302	0.0301	0.0251	0.0257	0.0233	0.0260
11	432.0775	0.0279	0.0303	0.0282	0.0302	0.0304	0.0255	0.0252	0.0227	0.0261
12	434.9544	0.0298	0.0314	0.0293	0.0315	0.0314	0.0260	0.0263	0.0235	0.0264
13	437.8321	0.0297	0.0326	0.0298	0.0310	0.0310	0.0262	0.0259	0.0230	0.0264
14	440.7105	0.0286	0.0309	0.0286	0.0310	0.0309	0.0242	0.0251	0.0219	0.0256
15	443.5897	0.0284	0.0310	0.0287	0.0308	0.0306	0.0244	0.0251	0.0216	0.0258
16	446.4696	0.0285	0.0317	0.0293	0.0312	0.0311	0.0248	0.0249	0.0218	0.0261
17	449.3503	0.0286	0.0320	0.0286	0.0312	0.0307	0.0244	0.0251	0.0216	0.0255
18	452.2319	0.0285	0.0323	0.0294	0.0315	0.0311	0.0244	0.0246	0.0219	0.0256
19	455.1142	0.0294	0.0329	0.0302	0.0321	0.0319	0.0244	0.0252	0.0216	0.0258
20	457.9974	0.0297	0.0326	0.0306	0.0333	0.0322	0.0246	0.0250	0.0214	0.0260
21	460.8815	0.0306	0.0339	0.0313	0.0338	0.0329	0.0257	0.0254	0.0216	0.0264
22	463.7665	0.0310	0.0346	0.0315	0.0340	0.0332	0.0257	0.0260	0.0217	0.0265
23	466.6524	0.0311	0.0347	0.0316	0.0342	0.0338	0.0254	0.0260	0.0220	0.0271
24	469.5391	0.0311	0.0351	0.0316	0.0343	0.0337	0.0257	0.0258	0.0218	0.0269
25	472.4269	0.0316	0.0350	0.0319	0.0348	0.0342	0.0260	0.0260	0.0216	0.0269

Output format (II)

Example case: sec2_p4_total

Spatial data is divided in 3 different areas:

1. Position coordinates with negative values corresponds to a section of the ground situated before the dike. It can be seen in slide number 2
2. Altitude on the dike. It has been assumed that the dikes are 6.5m tall.
3. Light from above the horizon line. It is diffused light from the sky. It can be seen that the spectrum is slightly different to the reference one as the incident light is oblique

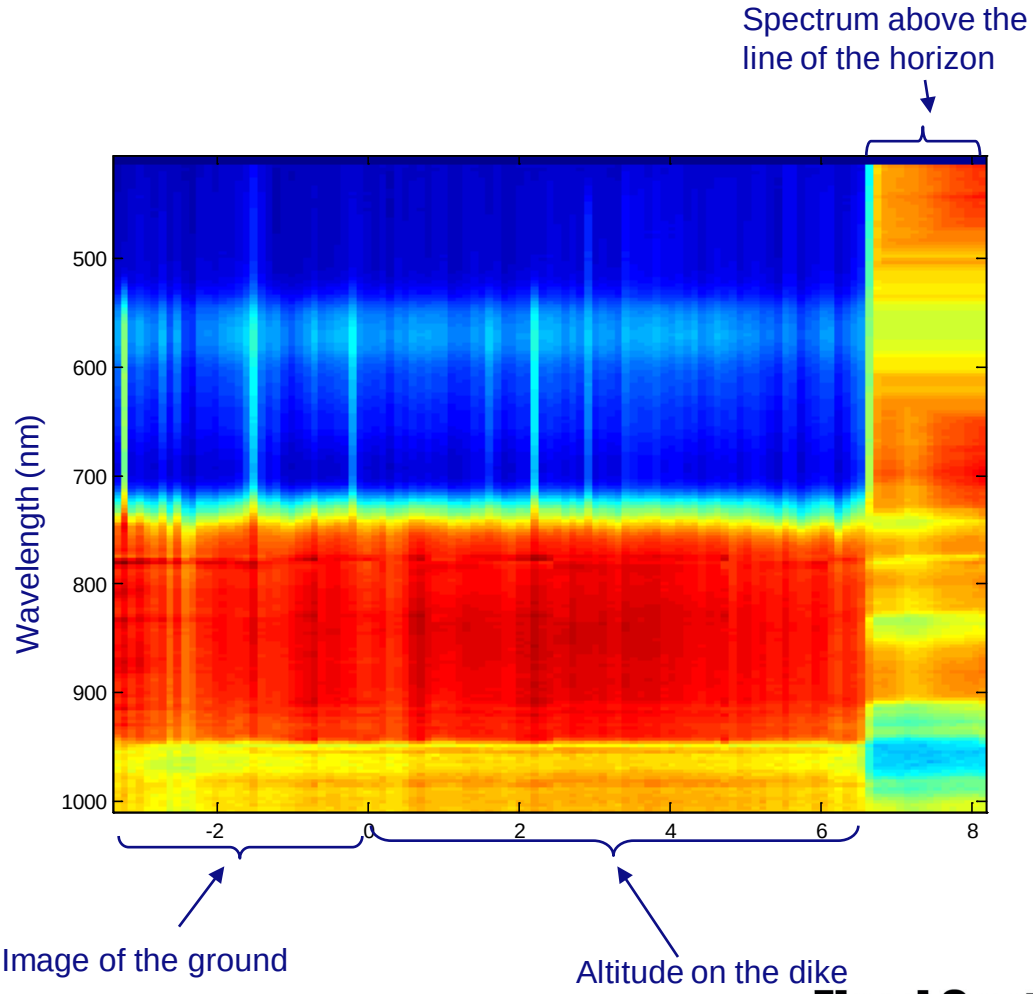

APPENDIX M

RSDYK2008 – SPECIFICATION OF THE THERMAL INFRARED CAMERA

SPECIFICATION OF THE THERMAL INFRARED IMAGERY USED TO ACQUIRE RADIATION TEMPERATURE OF THE DYKES.

Specifications

		TH9100PMV	TH9100PWV
Measuring range	Range 1	–20 to 100°C	–40 to 120°C
	Range 2	0 to 250°C	0 to 500°C
	Range 3 (option)	100 to 800°C	200 to 2000°C
	Range 4 (option)	200 to 2000°C	–
Resolution	Range 1	0.06°C (at 30°C 60Hz) 0.02°C (at 30°CΣ64)	0.08°C (at 30°C 60Hz) 0.03°C (at 30°CΣ64)
Accuracy	±2°C or ±2% of reading whichever greater		
Detector	Uncooled focal plane array (microbolometer)		
Spectral range	8 to 14μm		
I.F.O.V.	1.2mrad		
Focusing range	30cm to infinity		
Field of view	21.7°(H) x 16.4°(V)		
Frame time	60 frames/sec		
Display	View finder and 3.5 inch LCD monitor with auto switch		
Thermal image pixels	320 (H) x 240 (V) pixels		
A/D resolution	14 bits		
Measuring functions	Run/Freeze		
S/N improvement	Σ2, Σ8, Σ16, Σ32, Σ64 and spatial filter ON/OFF		
Alarm	Screen display and alarm sound (ON/OFF)		
Interval measurement	Recording on built in real time memory : 1/60 to 3600 sec interval Recording on memory card : 5 to 3600 sec interval (thermal image) 30 to 3600 sec. (thermal & visual image) Trigger function provided		
Emissivity correction	0.10 to 1.00 (at 0.01 step), Emissivity table provided		
Env. temp. correction	Provided (including interval NUC)		
User setup	Pre-registration of environmental setup (max. 10 setups)		
Background comp.	Provided		
Auto functions	Full automatic (level, sense, focus) Level trace, auto-gain control		
Display functions	Thermal/visual composite image display Display color : color/monochrome, positive/negative Gradation : 16, 32, 64, 128, 256 Color pallette : rainbow, brightness, shine, hot-iron, medical, fine Isothermal band display : max. 4 bands Thumbnail display : 12 thermal images replay Multi-sense display, Battery life indicator Line-profile : X, Y line profile (waveform display) Multilingual menu		
Image processing functions	Variable level/sense Multi-point temperature display (10pts) Multi-point emissivity display (10pts) Δt display Max/Min (peak hold) temperature display Alarm (full screen or specified box) Digital zoom : 2, 4 times (Run/Freeze) Box setting (max. 5 boxes)		
Annotation	Text and voice annotation (30 sec per image)		
Storage device	Compact flash memory card for; Thermal image in SIT or BMP file format Visual image in SIT or JPEG file format Thermal/visual composite image in BMP file format		
Movie recording	Real-time memory : 1664 images (max. 60Hz)		
Video signal output	NTSC/PAL composite video signal, S-video		
Interface	IEEE1394, RS-232C		
Operating temp/humidity	–15 to 50°C, 90% RH or less (not condensed)		
Storage temp./humidity	–40 to 70°C, 90% RH or less (not condensed)		
Power supply	AC adaptor : 100V to 240V, DC 7.2V (nominal)		
Power consumption	Approx. 6W (typ)		
Shock and vibration	294m/sec² (IEC60068-2-27), 29.4m/sec² (IEC60068-2-6)		
Environmental protection	IP54 (IEC60529)		
Dimensions	Approx.108 (W) x 113 (H) x 189 (D) mm (excluding projection)		
Weight	Approx. 1.4kg (excluding LCD & battery) Approx. 1.7kg (including LCD & battery)		
Standard accessories	AC adaptor, battery pack (2pcs), battery charger, compact flash memory card, grip belt, neck strap, lens cap, carrying case, viewer software, operation manual		

Specifications are subject to change without prior notice.

Visual Camera

Pixels	0.41Mega pixels
Effective image pixels	752 (H) x 480 (V) pixels
Field of view	30.1° (H) x 22.7° (V)
Sensitivity	1 lux
Focusing distance	30cm to infinity
Auto exposure	Provided
Video signal	NTSC/PAL

Viewer Software

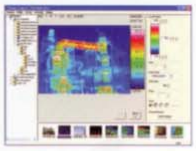

- Thermal image display :
  - Thermal image thumbnail (Windows Explorer)
  - Thermal image replay
  - Image preview
- Setup & Functions :
  Level, Sense, Span, Voice replay, Selection of thermal or visual image, Color bars, Gradation, Page
- Edit :
  Image save (BMP or JPEG)
  Select folder

Options

TH91-390	High temperature range for TH9100PMV *1 R3: 100 to 800°C, R4: 200 to 2000°C
TH91-392	High temperature range for TH9100PWV *1 R3: 200 to 2000°C
TH91-313	USB Interface with TH91-737 remote program *1
TH91-382	Telephoto lens (x2) 10.9°(H) x 8.2°(V) with visual camera
TH91-383	Wide angle lens 42.0°(H) x 32.1°(V) with visual camera
TH91-386	Close-up lens, 95μm, 30mm(H) x 22mm(V) W.D. 75mm
TH91-385	Close-up lens, 37μm, 11mm(H) x 8mm(V) W.D. 13mm
TH91-387	External lens adaptor for TH71-344A wide angle lens, TH71-377/378 close up lenses
TH71-464	Rechargeable battery pack (Li-ion) 7.2V 1800mAh
TH71-340	Battery charger for 100/110V (2 battery slots)
TH71-339	Battery charger for 220/240V (2 battery slots)
TH71-334	AC adaptor (100/110V AC)
TH71-360	AC adaptor (110V AC) UL
TH71-359	AC adaptor (220/240V AC) CE
TH91-375	Remote controller
TH91-398-L05	5m cable for remote controller TH91-375
TH71-347	LCD remote controller (TH91-347-L connecting cable is required)
TH91-347-L05	5m cable for LCD remote controller TH71-347
TH91-347-L10	10m cable for LCD remote controller TH71-347
TH91-347-L15	15m cable for LCD remote controller TH71-347
TH91-347-L20	20m cable for LCD remote controller TH71-347
TH91-349	RS232C Cable
TH91-348	S-video cable
TH91-713	Report Generator Software *2
TH91-711	Image Processor Software (TH91-713 is required) *2
TH91-712	Image Processor Pro Software *2
TH71-717	IEEE1394 Data Capture Software *2
MikroSpec	Thermal Imaging Software *2
MikroSpec R/T	Real-Time Thermal Data Acquisition & Analysis Software *2
irMotion	Recorder, Trigger and Measurement Software *2
Trigger Box	Trigger box for irMotion

*1 Specify these options when ordering the main unit (TH9100PMV/PWV)
*2 Compatible with the Microsoft Windows 2000 professional, Windows XP

Field of View Diagram (Thermal image)

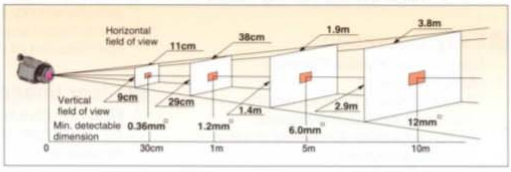

CAUTION FOR SAFETY

Please read "WARNING" & "CAUTION" in the operation manual attached to the product carefully for proper operation before using the product.

ebs **Automatisierte Thermographie und Systemtechnik GmbH**
Kienzestrasse 1
85737 Ismaning - **Germany**
Telefon: +49 (0)89 9230 687-10
Telefax: +49 (0)89 9230 687-29
e-Mail: info@irPOD.net
Internet: www.irPOD.net

NEC San-ei Instruments, Ltd.
1-25-12, Akebono-cho, Tachikawa-shi,
Tokyo 190-8537, Japan
Phone: +81-42-522-0529
Fax : +81-42-522-0538
E-mail: osd@necsan-ei.co.jp
Web : http://www.necsan-ei.co.jp/osd/

Catalog ref : 048
I0506A3 Printed in Japan

APPENDIX N

RSDYK2008 - REFERENCES

References

Abu-Farsakh, M. Y., Zhang, Z., Tumay, M., & Morvant, M. (2008). Development of MS-Windows CPT Soil Classification Software. TRB 2008 Annual Meeting., CD-Rom.

Adams, M. L., Philpot, W. G., & Norvell, W. A. (1999). Yellowness index: an application of spectral second derivatives to estimate chlorosis of leaves in stressed vegetation. International Journal of Remote Sensing , 20 (18), 3663-3675.

Amurane, D.P. (2003). Decision support system to assess settlement in a peaty Holocene deltaic environment, the Netherlands. M.Sc thesis, ITC (International Institute for Geo-Information Science and Earth Observation), The Netherlands.

Bijlsma, S. 1982. Geology of Holocene in the Western part of the Netherlands, In: de Bakker, H. and van der Berg, M.W.[ed], Procedings of the symposium on peatlands below the sea level, International Institute for Land Reclamation and Improvement ILRI, Wageningen, The Netherlands.

Blumberg, D.G., Freilikher, V., Kaganovskii, Y., and Maradudin, A.A. 2002. Subsurface microwave remote sensing of soil-water content: Field studies in Negev Desert and optical modelling. International Journal of Remote Sensing, 23, pp. 4039-4054.

Blumberg, D.G., Freilikher, V., Lyalko, I.V., Vulfson, L.D., Kotlyar, A.L., Shevchenko, V.N., and Ryabokonenko, A.D. 2000. Soil moisture (water-content) assessment by an airborne scatterometer: the Chernobyl disaster area and the Negev desert. Remote Sensing of Environment, 71, pp. 309-319.

Bosch, J.H.A., and Kok, H. 1994. Toelichtingen bij de Geologische kaart van Nederland 1:50.000 (38W) - Rijks Geologische Dienst, Haarlem, The Netherlands.

Carling, P. 1986. Peat slides in Teesdale and Weardale, northern Pennines, July 1983: description and failure mechanisms. Earth Surface Processes and Landforms 11: 193-206.

Carlson, T.N., Gillies, R.R., and Schmugge, T.J. (1995). An interpretation of methodologies for indirect measurement of soil water content. Agricultural and Forest Meteorology, 77, 191-205.

Esch van, J.M. 2007. Geo-hydrologic design procedure for peat dykes under drying conditions. Delft.

Dykes AP, and KJ., K. 2001. Initiation of a multiple peat slide on Cuilcagh Mountain, Northern Ireland. Earth Surface Processes and Landforms 26: 395-408.

Evans MG, Burt TP, Holden J, and JK., A. 1999. Runoff generation and water table fluctuations in blanket peat: evidence from UK data spanning the dry summer of 1995. Journal of Hydrology 221: 141-160.

Famiglietti, J.S., Davereaux, J.A., Laymon, C.A., Tsegaye, T., Houser, P.R., Jackson, T.J., Graham, S.T., Rodell, M., and P.J., V.O. 1999. Ground based investigationof soil moisture variability within remote sensing footprints during the Southern Great Plains 1977 (SGP97) Hydrology experiment. Water Resources Research, 35: 1839 - 1851.

Fredlund D.G., H.V.Q. (2001). Prediction of volume change in an expansive soil as a result of vegetation and environmental changes.

Fuchs, M., and Tanner, C.B. 1966. Infrared thermometry of vegetation. Agronomy Journal, 58, pp. 597-601.

Gausman, H.W., and . 1974. Leaf reflectance of near-infrared. Photogrammetric Engineering. 10: 183-191.

Griffiths, D.H., and Barker, R.D. 1993. Two-dimensional resistivity imaging and modelling in areas of complex geology. Journal of Applied Geophysics. 29: 211-226.

I. Katra, D.G.B., H. Lavee, P. Sarah. 2006. A method for estimating the spatial distribution of soil moisture of arid microenvironments by close range thermal infrared imaging. International Journal of Remote Sensing. vol.27, No.12, pp.2599-2611.

Idso, S.B., Schmugge, T.J., Jackson, R.D., and Reginato, R.J. 1975. The utility of surface temperature measurements for the remote sensing of surface soil water status. Journal of Geophysical Research, 80, pp. 3044-3049.

Jackson, R.D., Idso, S.B., Reginato, R.J., and Pinter, P.J. 1981. Canopy temperature as a crop water stress indicator. Water Resource Research 17, 1133-1138.

Li, J., and Islam, S. 1999. On the estimation of soil moisture profile and surface fluxes partitioning from sequential assimilation of surface layer soil moisture. Journal of Hydrology 220 (1999) 86-103.

Loke, M.H. (2000). Electrical imaging surveys for environmental and engineering studies, A practical guide to 2-D and 3-D surveys. 5-15.

Long M., J.P. 2006 Analysis of the peat slide at Pollatomish, County Mayo, Ireland

McCahon CP, Carling PA, and D., P. 1987. Chemical and ecological effects of a Pennine peat slide. Environmental Pollution 45: 275-289.

Mahabubur, R.K. 2007. Settlement Prediction on the Basis of a 3D Subsurface Model, Case study Reeuwijk area, the Netherlands, M.Sc thesis, ITC (International Institute for Geo-Information Science and Earth Observation), The Netherlands

P.Mora, M.Berti, and A.Simoni. 2007. Observations of soil moisture from thermal infrared data, Geophysical Research Abstracts, Vol. 9, 04157, SRef-ID: 1607-7962/gra/EGU2007-A-04157,European Geosciences Union 2007.

Price, J.C. 1980. The potential of remotely sensed thermal infrared data to infer surface soil moisture and evaporation. Water Resources Research, 16, pp. 787-795.

Reineck, H.E., and Singh, I.B. 1973. Depositional Sedimentary Environments: with reference to terrigenous clastics. Springer-Verlag, Berlin.

R. Quiroz, Ji Qiumei, P. Zorogastúa, C. León-Velarde, and Cañas, R. 2001. Assessing Dry Matter Availability in Tibetan Grasslands Using Ground-Level Remotely Sensed Data.

Reginato, R.J., Idso, S.B., Vedder, J.F., Jackson, R.D., Blanchard, M.B., and Goettelman, R. 1976. Soil water content and evaporation by thermal parameters obtained from ground-based and remote measurements. Journal of Geophysical Research, 81, pp. 1617-1620.

Robertson, P. K. (1990). “Soil Classification using the Cone Penetration Test,” Canadian Geotechnical Journal, Vol. 1, No. 27, pp. 151-158.

Saiyid Hassan, S. (1994). Variability of geotechnical properties of peat. Delft: ITC.

Swart, L.M.Th. (2007) Remote sensing voor inspectie van waterkeringen. publ. Rijswaterstaat, The Netherlands. ISBN: 978-90-79331-01-7 (paperback), 978-90-79331-02-4 (pdf). (in Dutch)

Tallis JH, Meade R, and (eds)., H.P. 1997. Blanket mire degradation: causes, consequences and challenges. In Proceedings of the Mires. Research Group, University of Manchester, 9-11 April 1997 . The Macaulay Land Use Research Institute: Aberdeen.

Tansey, K.J.A.C., Millington, A.C., A.M., Battikhi, A.M., and White, K.H. 1999. Monitoring soil moisture dynamics using satellite imaging radar in northeastern Jordan. Applied Geography 19 (1999) 325-344.

Ten Cate, J.A.M. (1982). The River and Coastal Plains of The Netherlands. In: ten Cate (ed.) Report of the working group from September 13, 1981 till May 31, 1982 - IGU working

Group on Geomorphology of River and Coastal Plains, Wageningen, The Netherlands. 4-11.

Tucker, C.J. 1979. Red and photographic infrared linear combinations for monitoring vegetation. Remote Sensing of Environment. 8: 127-150.

Van Baars, S. (2005). The horizontal failure mechanism of the Wilms peat dyke Delft.

Van de Griend, A.A., Owe, M., Groen, M., and Stoll, M.P. 1991. Measurement and spatial variation of thermal infrared surface emissivity in a savannah environment. Water Resources Research, 27, pp. 371-379.

Van der Meijde, M., van der Werff, H.M.A., and van der Meer, F.D. (2006). Detection of anomalous vegetation related to pipeline leakages using airborne hyperspectral measurements : final report. 25. Enschede: ITC.

van Staalduinen, C.J.e.a. 1979a. Toelichtingen bij de Geologische kaart van Nederland 1:50.000 (38W) - Rijks Geologische Dienst, Haarlem, The Netherlands.

van Staalduinen, C.J.e.a. 1979b. The Geology of the Netherlands - Mededelingen Rijks Geologische Dienst vol. 31-2.

Van der Werff, H.M.A., Noomen, M.F., van der Meijde, M., and van der Meer, F.D. 2007. Remote sensing of onshore hydrocarbon seepage: problems and solutions. Geological Society, London, Special Publications. 283(1): 125-133.

Warburton J, Holden J, and AJ., M. 2004. Hydrological controls of surficial mass movements in peat. Earth Science Reviews 67: 139-156.

Xavier Comas, L.S., Andrew Reeve. 2004. Geophysical evidence for peat basin morphology and stratigraphic controls on vegetation observed in a Northern Peatland. Journal of Hydrology 295, 173–184

Yang, H. (1995). Detection of areas of spontaneous combustion of coal by using airborne and TM data in Xinjiang, China. Enschede: ITC.